DEVELOPMENT OF NON-ENZYMATIC GLUCOSE BIOSENSOR BASED ON CONDUCTING POLYMER NANOCOMPOSITE FILMS FABRICATED BY ELECTROCHEMICAL TECHNIQUE

ALI MOHAMAD ALI ABDUL AMIR

FACULTY OF SCIENCE
UNIVERSITY OF MALAYA
KUALA LUMPUR

2017

DEVELOPMENT OF NON-ENZYMATIC GLUCOSE BIOSENSOR BASED ON CONDUCTING POLYMER NANOCOMPOSITE FILMS FABRICATED BY ELECTROCHEMICAL TECHNIQUE

ALI MOHAMAD ALI ABDUL AMIR

THESIS SUBMITTED IN FULFILMENT OF THE REQUIREMENTS FOR THE DEGREE OF DOCTOR OF PHILOSOPHY

FACULTY OF SCIENCE
UNIVERSITY OF MALAYA
KUALA LUMPUR

2017

UNIVERSITY OF MALAYA

ORIGINAL LITERARY WORK DECLARATION

Name of Candidate: **Ali Mohamad Ali Abdul Amir**

Registration/Matric No: **SHC120039**

Name of Degree: **DOCTOR OF PHOLOSOPY**

Title of Project Paper/Research Report/Dissertation/Thesis (~~"t~~his Work"):

DEVELOPMENT OF NON-ENZYMATIC GLUCOSE BIOSENSOR BASED ON CONDUCTING POLYMER NANOCOMPOSITE FILMS FABRICATED BY ELECTROCHEMICAL TECHNIQUE

Field of Study: **Polymer Chemistry**

I do solemnly and sincerely declare that:

(1) I am the sole author/writer of this Work;
(2) This Work is original;
(3) Any use of any work in which copyright exists was done by way of fair dealing and for permitted purposes and any excerpt or extract from, or reference to or reproduction of any copyright work has been disclosed expressly and sufficiently and the title of the Work and its authorship have been acknowledged in this Work;
(4) I do not have any actual knowledge nor do I ought reasonably to know that the making of this work constitutes an infringement of any copyright work;
(5) I hereby assign all and every rights in the copyright to this Work to the University of Malaya (~~"U~~M"), who henceforth shall be owner of the copyright in this Work and that any reproduction or use in any form or by any means whatsoever is prohibited without the written consent of UM having been first had and obtained;
(6) I am fully aware that if in the course of making this Work I have infringed any copyright whether intentionally or otherwise, I may be subject to legal action or any other action as may be determined by UM.

Candidate's Signature Date:

Subscribed and solemnly declared before,

Witness's Signature Date:

Name:

Designation:

ABSTRACT

Different analytical principles have been adopted for monitoring blood glucose levels which include spectrophotometry and electrochemical methods. Out of these, electrochemical methods are highly reliable, simple and sensitive. Non-enzymatic procedures are preferred over enzymatic methods since it overcomes the serious problem of storage stability of enzyme based sensors. Non-enzymatic method utilizes direct electrooxidation of glucose on the surface of electrodes. Nanomaterials are used as electrocatalysts to modify sensor electrodes and achieve greater electrochemical response. In the present work, polypyrrole conducting polymer/chitosan-based non-enzymatic glucose biosensors using Fe_3O_4 and TiO_2 as nanomaterials in one-step electrodeposition technique have been developed. Conducting polymer nanocomposite films prepared on ITO glass electrode by cyclic voltammetry were characterized by FTIR, XRD, SEM, HR-TEM, and XPS. All these characterizations confirm the formation of Ppy-CS-metal oxide nanocomposite films. The oxidation potential of +0.18V (vs Ag/AgCl) and +0.13V (vs Ag/AgCl) as determined from cyclic voltammetry were applied on the sensor electrode of Ppy-CS-Fe_3O_4 and Ppy-CS-TiO_2, respectively, for the amperometric determination of glucose in 0.1 M NaOH. A highly selective and sensitive non-enzymatic glucose sensor with wide detection range were fabricated with the detection range of 1 mM to 16 mM, and 1 mM to 14 mM for (Ppy-CS-Fe_3O_4/ITO) and (Ppy-CS-TiO_2/ITO), respectively, with a fast response time of 3 seconds. This work has presented the role of nanomaterials and described the easy process of their homogenous distribution in the Ppy-CS composite films by one-step electrochemical process where all the components are taken in one solution in the electrochemical cell. The vital role of the nanomaterials is well realized in the glucose sensor due to the homogenous distribution of nanomaterials in the polymer films from this one-step deposition technique. Glucose was detected in common physiological

interfering biomolecules such as uric acid, ascorbic acid, and cholesterol where the biomolecules were found to have no interference. The results exposed that the present sensor possesses a good selectivity and sensitivity towards the glucose detection. Additionally, the modified electrode has showed an excellent stability towards glucose sensing upon exposure in the environment for several days.

ABSTRAK

Prinsip analisis yang berbeza telah digunakan untuk memantau tahap glukosa darah termasuk spektrofotometri dan kaedah elektrokimia. Daripada jumlah itu, kaedah elektrokimia adalah sangat dipercayai, mudah dan sensitif. Prosedur bukan enzim lebih digemari berbanding kaedah enzim kerana ia mengatasi masalah yang serius mengenai kestabilan penyimpanan sensor berasaskan enzim. Kaedah bukan enzim menggunakan electrooxidation langsung glukosa pada permukaan elektrod. Bahan nano digunakan sebagai mangkin-elektro untuk mengubahsuai elektrod sensor dan mencapai respons elektrokimia yang lebih besar. Dalam kajian ini, biosemsor glukosa bukan enzim berasaskan polimer pengkondukisan polypirrol/chitosan menggunakan Fe_3O_4 dan TiO_2 sebagai bahan nano dalam teknik pengelektroenapan satu-langkah telah dibangunkan. Filem nano komposit polimer pengkonduksian yang disediakan pada elektrod kaca ITO melalui voltammetri berkitar telah dicirikan dengan FTIR, XRD, SEM, HR-TEM dan XPS. Semua pencirian ini mengesahkan pembentukan filem nano komposit Ppy-CS-logam oksida. Potensi pengoksidaan sebanyak +0.18 V (vs Ag/AgCl) dan +0.13 V (vs Ag/AgCl) seperti ditentukan daripada voltammetri berkitar telah digunakan pada elektrod sensor daripada Ppy-CS-Fe_3O_4 dan Ppy-CS-TiO_2, masing-masing, untuk penentuan amperometric bagi glukosa dalam 0.1 M NaOH. Sensor glukosa bukan enzim yang sangat selektif dan sensitif dengan jarak pengesanan luas telah difabrikasi dengan julat pengesanan dari 1 mM ke 16 mM, dan 1 mM ke 14 mM untuk (Ppy-CS-Fe_3O_4/ITO) dan (Ppy-CS-TiO_2/ITO), masing-masing, dengan masa respons yang cepat sebanyak 3 saat. Kerja ini telah menunjukkan peranan bahan nano dan menjelaskan proses mudah bagi taburan homogen bahan ini dalam filem komposit Ppy-CS melalui proses elektrokimia satu-langkah di mana semua komponen diambil dalam satu larutan dalam sel elektrokimia. Peranan penting bagi bahan nano telah begitu direalisasikan dalam sensor glukosa disebabakan oleh taburan homogen bahan nano dalam filem

polimer daripada teknik pemendapan satu-langkah ini.Glukosa dikesan dalam biomolekul gangguan fisiologi yang biasa seperti asid urik, asid askorbik, dan kolesterol dimana biomolekul tersebut didapati tidak mempunyai sebarang gangguan. Keputusan kajian ini mendedahkan bahawa sensor ini mempunyai pemilihan dan sensitiviti yang baik terhadap pengesanan glukosa. Selain itu, elektrod diubahsuai ini telah menunjukkan kestabilan yang sangat unggul terhadap pengesanan glukosa apabila terdedah dalam persekitaran selama beberapa hari.

ACKNOWLEDGEMENTS

Alhamdulillah, under the graceful blessing of the Loving God, the unending love of my father, my brother, my wife, lecturers and friends, this thesis has been successfully completed. I would like to take this opportunity to thank a group of people who have given me the greatest support during my PhD study at the University Malaya. I extend my sincere gratitude with most grateful and appreciation to the supervisory committee, Prof. Dr. Rosiyah Yahya, Assoc Prof. Dr. Habibun Nabi Muhammad Ekramul Mahmud and Dr. Mahnaz M Abdi for their excellent guidance throughout the entire course of this work. I would like to express my earnest appreciation for their valuable advices and motivation ever since my PhD days in University of Malaya. Likewise, I would like to acknowledge the financial support from the University of Malaya during my candidature. A part of that I am very much appreciative of the assistance given to me by the all staff member of chemistry department, University of Malaya for their help in the necessary equipment's. Also, my gratitude goes to Al-Mustansiriya University, chemistry department, in Iraq for supporting me and sponsoring me during my PhD study. Next, I am also thankful to all of my friend, and my PhD. colleagues; Obidul Huq, Hammeed Wasiu, Wisam Almehana, Tamar Husein, Shahid Mehmood, Nouman Arshid, Mickel Adekunle Olatunji, Md. Shafiqur Rahman and my entire friend throughout my life for support and cooperation during the period of this endeavour.

At last and most importantly, I dedicate my gratefulness and respect without limits to my beloved family members as my father, my brother, my lovely wife and my kids for their unconditional support and encouragement throughout the period of my research. Their companionship from afar during the difficulty times I faced is indeed a cherishing moment for me. I would like to express my most sincere and warmest gratitude to them for their prayers, loving, generous, endless support and moral inputs during my study. They are always close to my heart.

To the soul of my deeply love (**Mother**) whose always want to be proud on me.

To my beloved **(Father)** whose patience, and pray always to me.

To my beloved brother **(Mazin)** for his love, and encouragement.

To my beloved **(Wife and my Kids)** for their love, and encouragement and made my life enjoyable.

To my beloved country people and bleeding country **(Iraq)**, May Allah grant you peace.

TABLE OF CONTENTS

LIST OF FIGURES

LIST OF TABLES

LIST OF SYMBOLS AND ABBREVIATIONS

CS	Chitosan
Ppy	Polypyrrole
Fe_3O_4 Np	Iron oxide manoparticles
TiO_2 Np	Titanium dioxide nanoparticles
Ppy-CS	Polypyrrole-chitosan composite
Ppy-CS-Fe_3O_4	Polypyrrole-chitosan- iron oxide nanocomposite
Ppy-CS-TiO_2	Polypyrrole-chitosan- titanium dioxide nanocomposite
NaOH	Sodium Hydroxide
ITO	Indium tin oxide
AA	Ascorbic acid
UA	Uric acid
CH	Cholesterol
P-TS	*p*-Toluene Sulfonate
CV	Cyclic voltammetry
Ag/AgCl	Ag/AgCl Silver/silver chloride
MWCNT	Multi walled carbon nanotubes
GCE	Glassy carbon electrode
WE	Working electrode
RE	Reference electrode
CE	Counter electrode
RSD	Relative standard deviation
LOD	Limit of detection
XPS	X-ray photoelectron spectroscopy
PBS	Phosphate buffered saline
FT-IR	Fourier transform infrared spectroscopy
HR-TEM	High resolution transmission electron microscopy
FE-SEM	Field-emission scanning electron microscopy
XRD	X-ray diffraction
EDX	Energy dispersive X-ray
HZ	Hertz
Ev	electron volt
EIS	Electrochemical impedance spectroscopy
Eq.	Equation
E	Potential
$m.Vs^{-1}$	Millivolt per second
mM	Mill molar
mL	Millilitre
S	Second
S/N	Signal-to-noise ratio
SD	Standard Deviation
Rct	Charge transfer resistance
I	Current
W	Warburg diffusion
vs.	Versus.

CHAPTER 1: INTRODUCTION

1.1 Overview

The purpose of the current thesis is to explore conducting polymer nanocomposite films as non-enzymatic glucose sensors. This was accomplished by developing polypyrrole conducting polymer-chitosan nanocomposites using iron oxide or titanium dioxide as nanoparticles.

1.2 Polymers

The term polymer is derived from the Greek words –poly" (many) and –meros" (parts) (Gowariker *et al.,* 1986). The polymer can be defined as a macromolecule which containing a long chain of simple molecular structures, called ‗monomers' that are linked to each other by covalent bonds. Generally, the concept of a polymer is often associated with plastic materials which are having insulating properties, as they are vastly used in the production of packaging and of electrical and electronic devices or liquid crystal and rubber. The monomers react together chemically to give a variety of molecular architectures ranging from linear structures to three dimensional networks of polymer chains.

1.3 Conducting polymers

A sub-group of organic and also inorganic electrical conductors are conducting polymers which can be investigated as interdisciplinary technology and science. The field of conducting polymers, which show elegant electric and optical properties with potential importance in advanced technologies, has become one of the interesting fields multidisciplinary of materials science and technology. This field covers variety of capability and multidisciplinary knowledge. Their electronic properties and structures can be investigated by physicists and chemists while the design and fabrication of electronic and optoelectronic devices fall into engineering domain. Therefore,

conducting polymer studies are located in the intersection of all three disciplines, physics, chemistry and engineering. A unique combination of properties can be observed in conducting polymer materials. In these macromolecular materials, the electronic and optical properties of metals and semiconductors are combined with the processing advantages and mechanical properties of polymers (Hadziioannou & Malliaras, 2006).

In some texts, a physical blend of a non-conductive polymer with conducting materials which is similar to a metal, is so-called as ‗conducting polymer'. By adding metals, metal oxide, carbon black, graphite fibers and etc., this kind of composite can be prepared (Freund & Deore, 2007). In some references, conducting polymer composite also can be fabricated from an aqueous solution of monomer and insulating polymer in different methods such as chemical or electrochemical polymerization by using a suitable dopants and oxidant or supporting electrolyte (Iroh & Levine, 2002; Wang *et al.,* 1990).

Nevertheless, one of the potential advantages of conducting polymers such as polypyrrole is their easy and low cost synthesis, while most of them suffer from weakness of process ability. The well-known conducting polymer, Polypyrrole, has some problems such as low degree of possibility and the weakness in the mechanical properties like brittleness. Many studies have been done to improve their mechanical, electrical and magnetic properties (Iroh & Levine, 2002; Mahmud *et al.,* 2006).

Among the conducting polymers, polypyrrole, which is the most abundant among the conducting polymers, can be synthesized easily under chemical or electrochemical polymerization reactions in aqueous and non-aqueous environment in the presence of a broad range of dopants (Diaz & Lacroix, 1988; Skotheim, 1998). Historically, polypyrrole was prepared by oxidative polymerization of pyrrole in 1888 and by electrochemical polymerization in 1957. In 1963 researchers found out that polypyrrole

possess electrical and conductivity properties. Ppy also attracted special attention because of their high environmental and thermal stabilities and application in different fields of application such as in gas sensors, electrochromic devices and batteries.

1.4 Nanocomposite materials

Nanotechnology has great effect in developing new classes of materials with improved functionality and applications. Nanocomposites can be defined as multiphase materials, where one or more of the phases have at least one dimension less than 100 nm (Ajayan, *et al.,* 2006). Size limits for these effects have been proposed, <5 nm for catalytic activity, <20 nm for making a hard-magnetic material soft, <50 nm for refractive index changes, and <100 nm for achieving superparamagnetic, mechanical strengthening or restricting matrix dislocation movement (Advani, 2007). The phases can be inorganic, organic, or both, with amorphous, semi-crystalline or crystalline phases or combinations of these phases (Xiong *et al.,* 2005). Organic-inorganic composites with nanoscale dimensions are of great attention due to their unparalleled characterizations, and various applications in the improvement of the quality of conductivity (Coronado *et al.,* 2000; Croce *et al.,* 1998), catalytic activity (Sidorov *et al.*, 2001), chemical selectivity (Merkel *et al.,* 2002; Joly *et al.,* 1999) etc. In these materials, inorganic and organic components are mixed or hybridized at nanometer scale, virtually at any composition leading to the formation of nanocomposite materials (Hajji *et al.,* 1999).

The enormous kinds of nanocomposites with a plentiful variety of properties have been of all nanocomposites is a combination of two or more different substances (or phases) in order to prepare a single substance which acts as homogenous entity and has predictable and reproducible properties (Gerstle, 1988; Kelly, 1990). As non-enzymatic glucose sensors, inorganic metal oxides with nanostructures are often used. In this study, Fe_3O_4 and TiO_2 have been selected as a source of inorganic oxides nanomaterials.

1.5 Non-enzymatic glucose biosensor

In recent years, many researchers have concentrated on the development of glucose biosensors because of their extensive applications in clinical diagnosis (Song *et al.,* 2006; Huang *et al.,* 2011). The detection of glucose in the blood is the most feasible approach for the measurement of blood sugar concentration (Koschwanez & Reichert, 2007). Glucose sensors have already experienced the development of sensors based on enzymatic catalysts and non-enzymatic catalysts. In the past decades, three-generation enzymatic glucose sensors have been developed, but they suffer from the inherent instability of the enzyme due to its pH and temperature sensitivity as well as sensor performance variation due to oxygen concentration variability (Karyakin *et al.*,1999; Ramanavicius *et al.,* 2006). Additionally, the high cost of enzyme also limits the wide application of enzymatic glucose biosensors in developing countries. Due to the above-mentioned factors, considerable research efforts have been concentrated on the development of non-enzymatic glucose sensors which allow glucose to be oxidized directly on the electrode surface (Welch & Compton, 2006; Zhang *et al.,* 2008).

In order to develop sensitive non-enzymatic glucose sensors, a variety of metals and metal oxides, have been explored (Xiao *et al.,* 2014; Kiani *et al.,* 2014; Wooten *et al.,* 2010; Gorski & Kennedy, 1997). Composite or nanocomposite films are serve the purpose (Kaur *et al.,* 2015). Newer approaches focus on developing nanocomposite films. In the bulky polypyrrole (Ppy), electron transfer is relatively slow but coupling with nanostructured materials, the sensitivity is increased due to faster diffusion in the sensing area. The objective of these approaches is to enhance the sensing capabilities of biosensors, such as sensitivity, stability, biocompatibility, reproducibility, and selectivity (Esmaeili *et al.,* 2015). Amperometric electrochemical electrodes are receiving widespread attention due to their simplicity, fast response time, and sensitivity to a wide range of biomolecules (Masoomi *et al.,* 2014). These biosensors operate on

applying a base current between a working electrode and reference electrode, with the reduction or oxidation of a compound causing a shift in the current allowing for quantification of the specific molecules (Thévenot *et al.,* 2001) The nanomaterials in biosensors support the biocompatibility, lifetime, and have been found cost effective (Toghill & Compton, 2010; Chen & Chatterjee, 2013).

Iron oxide (Fe_3O_4) and titanium dioxide (TiO_2) nanoparticles in composite films have been used for glucose sensors to contribute the electron transfer and increase the surface area of the sensors and thus possess the good electrocatalytic activity (He *et al.,* 2011; Chen *et al.,* 2012). The combination of both metal oxide and the polymeric features throughout the nanocomposite structure lead to great potentials in glucose sensors (Chen, *et al.,* 2008; Chen *et al.,* 2014).

1.6 Research objectives

The main research objective is to prepare polypyrrole conducting polymer films with chitosan and some metal oxides such as Fe_3O_4 and TiO_2 by electrochemical technique for non-enzymatic glucose biosensors. The polypyrrole-chitosan composite films (Ppy-CS) , polypyrrole-chitosan-metal oxide nanocomposite films (Ppy-CS-Fe_3O_4 and Ppy-CS-TiO_2) were directly formed by one-step electrochemical deposition technique which has not been addressed before as non-enzymatic glucose sensors. Therefore, the present research has been encompassed with the following objectives:

1. To prepare conducting polymer composite and nanocomposite films of Ppy-CS, Ppy-CS-Fe_3O_4 and Ppy-CS-TiO_2 on the ITO glass electrode by cyclic voltammetry.
2. To characterize the prepared conducting polymer nanocomposites by various analytical techniques such as FTIR, FE-SEM, EDX, HR-TEM, XRD and XPS.
3. To test the performance of the conducting polymer-nanocomposite films as non-enzymatic glucose biosensors and to study the sensitivity, selectivity and stability towards glucose sensing.

1.7 Thesis structure

The thesis presents the fabrication of conducting polymer composite and nanocomposite films with and without metal oxide nanoparticles, then study their characterizations and applications for non-enzymatic glucose biosensors.

Chapter 1 describes the general introduction about conducting polymers, nanocomposite materials and their application based on non-enzymatic glucose biosensors, including the aims of the study.

Chapter 2 covers the literature review on conducting polymers in biosensors, biopolymer materials, electrochemical sensors, iron oxide and titanium dioxide nanoparticles, and the fabrication of nanocomposite films for non-enzymatic glucose biosensor.

Chapter 3 explains the materials and techniques that are used in characterization of nanocomposite films including the general technique for fabrication based on non-enzymatic glucose sensors.

Chapter 4 describes the preparation of the composite films and non-enzymatic glucose detection by the prepared polypyrrole conducting polymer and chitosan composite films on indium tin oxide electrode (Ppy-CS/ITO). The composite films were characterized by X-ray diffraction technique (XRD), Fourier transform infrared spectroscopy (FTIR), Field emission scanning electron microscopy (FESEM), High-resolution transmission electron microscopy (HR-TEM), X-ray photoelectron spectroscopy (XPS), Electrochemical impedance spectroscopy (EIS).

Chapter 5 presents the preparation of polypyrrole conducting polymer, chitosan and iron oxide nanoparticles on indium tin oxide glass electrode (Ppy-CS-Fe_3O_4/ITO) and the detection of glucose. The nanocomposite films were characterized by X-ray diffraction technique (XRD), Fourier transform infrared spectroscopy (FTIR), Field emission scanning electron microscopy (FESEM), Energy-dispersive X-ray spectroscopy (EDX),

High-resolution transmission electron microscopy (HR-TEM), X-ray photoelectron spectroscopy (XPS) and Electrochemical impedance spectroscopy (EIS).

Chapter 6 describes the preparation of polypyrrole conducting polymer, chitosan and titanium dioxide nanoparticles on indium tin oxide electrode (Ppy-CS-TiO_2/ITO) and the non-enzymatic detection of glucose. The nanocomposite films were characterized by X-ray diffraction technique (XRD), Fourier transform infrared spectroscopy (FTIR), Field emission scanning electron microscopy (FESEM), Energy-dispersive X-ray spectroscopy (EDX), High-resolution transmission electron microscopy (HR-TEM), X-ray photoelectron spectroscopy (XPS) and Electrochemical impedance spectroscopy (EIS).

Chapter 7 presents the main conclusions obtained from the present study and the suggestions and recommendations for future work.

CHAPTER 2: LITRETURE REVIEW

2.1 Overview

The chapter presents an overview of the framework developed to account of conducting Back ground on biopolymer, metal oxide and polymers composite in biosensors, literature review on electrochemical biosensors, and fabricated nanocomposite films based on non-enzymatic glucose biosensors have also been discussed briefly in this chapter.

2.2 Conducting polymer and polypyrrole

Conducting polymers are easy to be synthesized through chemical or electrochemical processes, and their molecular chain structure can be modified conveniently by copolymerization or structural derivations. The conducting polymers, such as polypyrrole (Ppy), polyaniline (PAni), polythiophene (PTh), etc all refer to intrinsic conducting polymers. Their main chains consist of alternative single and double bonds, which lead to broad π-electron conjugation. However, the conductivity of these pure conducting polymers are rather low ($<10^{-5}$ S cm^{-1}). In order to achieve much higher conductivity for these polymers, doping process is necessary.

The conductivity of a semiconductor is entirely low, due to narrow band gap, but the conductivity can be increased by introducing impurities as dopants. This process is known as "doping". The concept of doping is the central theme, which distinguishes conducting polymers from all other conventional polymers (MacDiarmid, 2001). The main conductivity mechanism of conducting polymers is according to the movement of charges carrier, defects or over the conjugated π-system or between soliton, polaron or bipolaron states, which is caused by doping. The reason of conductivity of this kind of polymers is due to polaron, bipolaron and soliton which are generated by doping process. The last one, bipolaron is the predominant charge in conjugated polymers in degenerate ground states such as polyacetylene while polarons and bipolarons are

significant stored charge the conjugated polymers in non-degenerate ground states such as polypyrrole (aromatic rings) (Freund & Deore, 2007). Moreover, solitons which are very important can be created in the couple forms by doping (Freund & Deore, 2007). The cations and radicals, which neutral and positive solution respectively, are created during the oxidation process. By joining two radicals, a spineless charge carrier as positive bisoliton is created.

The dopants can not only remove but add electrons to the substance such as iodine as well. The mobility of charge carriers over the chain of polyacetylene can be high. The counter ion (I^{3-}) is not highly movable compared to the positive charge, therefore; the high concentration of counter ions is needed to move in the area near counter ions (Roth & Carroll, 2015). The inter-soliton hopping between various polymer chains via charge-hopping, is the mechanism introduced by Roth and his co-worker for conductivity (Roth & Carroll, 2015). Soliton moving over the chain and an electron are exchanged with the nearest charged soliton (Figure 2.1).

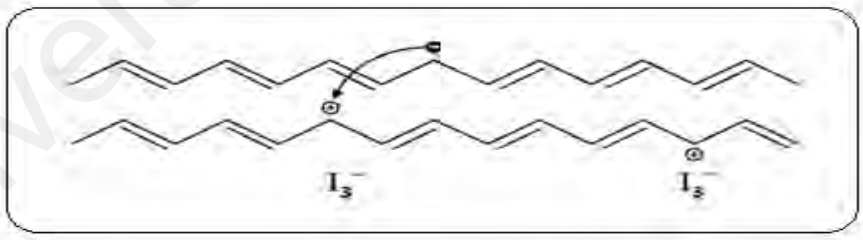

Figure 2.1: Intersoliton hopping in polyacetylene chains.

The doping process corresponds to the oxidation or reduction of the polymer, with the associated incorporation of a counter ion in order to preserve overall electrical neutrality. It is the charge introduced onto the polymer backbone, which imparts electrical conductivity. The change in the delocalized π system induced by doping not only increases the conductivity by many orders of magnitude (typically by a factor of

10^{10}) but also creates substantial alterations in the visible absorption spectrum of conducting polymers. These characteristics are responsible for the potential of conducting polymers in a number of applications. In the early years of 1977, the field of electronically conducting polymers has been discovered and overcame to such heights that it is far ahead of what could have been envisaged when the field was in its formative years. A variety of other conducting polymers and their derivatives were discovered in the subsequent years after the discovery of conductivity in polypyrrole (Epstein & MacDiarmid, 1991; Cui & Kertesz, 1989; Lee *et al.,* 1993; Groenendaal *et al*., 2000). Figure 2.2 shows the molecular structures of some of popular conducting polymers that have been synthesized during the last few decades and applied in different application areas.

Polypyrrole (Ppy) is one of the conducting polymer which is a π conjugated system via aromatic rings, charge carriers (conductivity reason) are polarons and bipolarons. The process of the oxidative doping of polypyrrole start by removing an electron from the π system of the backbone to create free radical and a spineless positive charge. The radical cation is formed by the coupling of them (radical and cation) through their local resonance of the charge and the radical. This combination of a charge site and a radical is called a polaron in (Figure 2.3). This could be either a radical cation or radical anion.

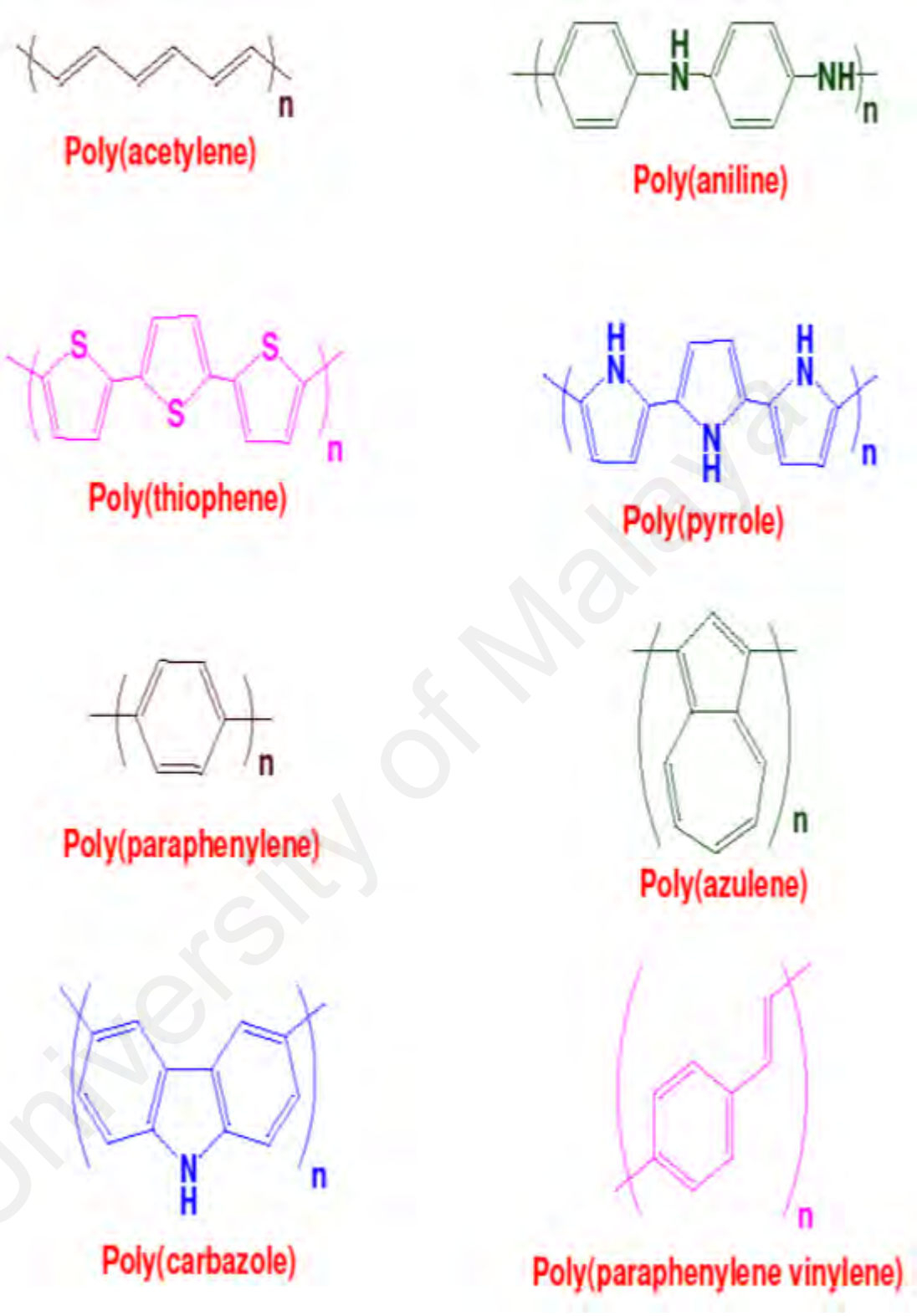

Figure 2.2: Structures of some conducting polymers.

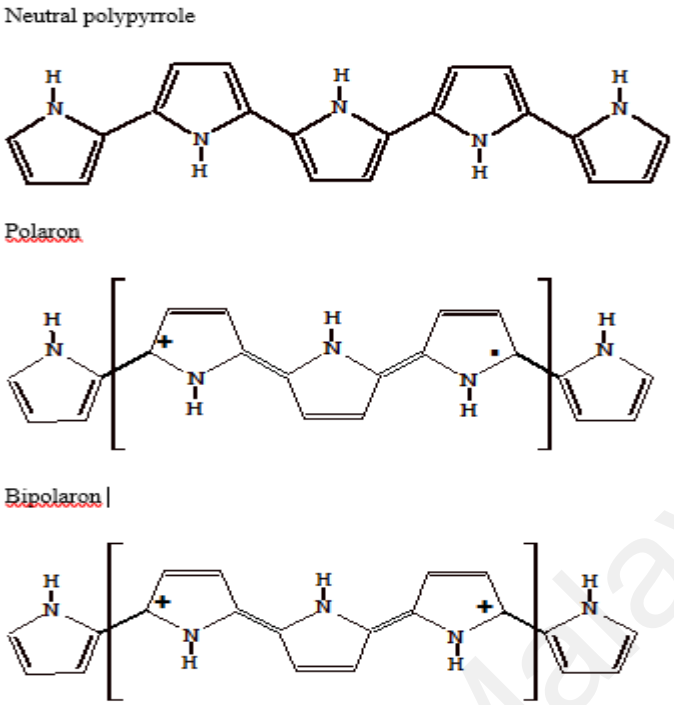

Figure 2.3: Structure of (a) neutral polypyrrole, (b) polaron and (c) bipolaron.

Upon further oxidation doping of Ppy, the free radical of the polaron is removed, a new spineless defect which called a bipolaron created. This is of lower energy than the creation of two distinct polarons. At higher levels of doping the polarons are replaced with bipolarons. It becomes possible that two polarons combine to form a bipolaron. Thus at higher doping levels. Bipolaron develop over four pyrrole rings as well.

2.3 Polymerization of pyrrole

Ppy can be prepared by a variety of synthetic procedures. However, polymerization of pyrrole is generally classified into two more popular categories, electrochemical polymerization and chemical polymerization conducting polymers can be prepared via different techniques. There are other alternative methods which are less popular, including photochemically initiated polymerization, enzyme/acid catalyzed polymerization (Ramanavičius *et al.*, 2006).

Electrochemical polymerization has been broadly investigated because the thickness and morphology of polymer thin film can be controlled easily and also this kind of polymerization is cleaner than chemical polymerization. In this technique, which is a well-known deposition method, Ppy is deposited on the surface of electrodes in the electrochemical cell as a thin film. Electrochemically synthesized Ppy has some advantages such as good conductivity and very high adherence to most substrates for biosensor design. (Ramanavičius *et al.,* 2006). In spite of advantage of electrochemical polymerization, there are some benefits for chemical polymerization such as mass production, short time of reaction and in addition to low cost, ease, simplicity and availability in any laboratories. A chemical method of polymerization can be used for a wide range of polymer productions because there is no need to use electrodes to prepare polymer.

Kassim and co-authors prepared a film of Ppy-polyethylen glycol conductive polymer composite via electrochemical polymerization on a glass electrode of indium tin oxide using p-toluene sulfonate (*P*-TS) as a dopant in aquatic environments (Kassim *et al.,* 2006). They have found that composite conductivity has been changed with the concentration of dopant. Oxidative polymerization of a monomer by oxidants can be done in different solvents, aqueous or non-aqueous (Ansari, 2006). There are various types of used oxidants as salts of transition metals like Fe^{3+}, Cu^{2+}, Cr^{6+}, Ce^{4+}, $Ru^{3+}$and Mn^{7+} and $(NH_4)_2S_2O_8$, $Na_2S_2O_8$, H_2O_2 (Wang *et al.*, 2000). Several parameters influence on the efficiency of polymerization and Ppy properties, first, the kind of oxidants play the most important role, dopants, and some environment factors such as reaction time and temperature. In the oxidant chemical polymerization sometime the oxidant also can be considered as a dopant. As an example, when pyrrole is polymerized chemically in a solution of an oxidant and a functional anion, this functional anion can be a part of oxidant such as $FeCl_3$ as oxidant while Cl^- is an anion which incorporates as

a dopant in a matrix of Ppy easily. However, the efficiency of the doping via the functional anion is not very high.

2.4 Mechanism of polymerization

In spite of broad investigation on the polymerization of polypyrrole regarding various topics such as boosting conductivity, there is no clear, known and pervasive mechanism for pyrrole polymerization, and still a questionable issue that need more study (Sadki *et al.,* 2000). In each mentioned mechanism in literature, there is a variety of proposed initiation stage models including electron transfer, proton transfer and direct formation of radical pyrrole. Solvent, temperature and pH are some parameters that have been considered in mechanism of Ppy preparation. Investigation of each step of mechanism is difficult due to the speed of the polymerization. In addition, the morphology of PPY (non-crystalline) and insolubility difficult to investigate (Diaz & Bargon, 1986). Anyhow both polymerization mechanism, chemical or electrochemical, are the presumably similar. The Diaz‘s mechanism, is the most acceptable mechanism till now, and has been also confirmed by Waltman and Bargon (Diaz & Bargon, 1986). The mechanism has been described by the following chain reactions step by step:

Step 1: Oxidation of pyrrole monomer

In the first stage, the radical cation is generated via oxidation of pyrrole (monomer). Based on the following figures, a structure of several resonances can be observed (Figure 2.4)

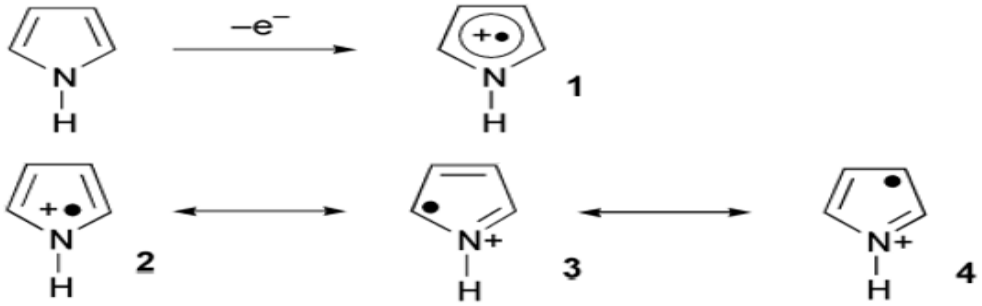

Figure 2.4: Oxidation of pyrrole monomer and resonance forms of radical cation.

Step 2: Formation of the dihydromer dication

The density of unpaired electron is more considerable in the α-position than others, therefore, two radicals are joining at α-positions, a dihydromer dication 5 indicates this formation. (Figure 2.5)

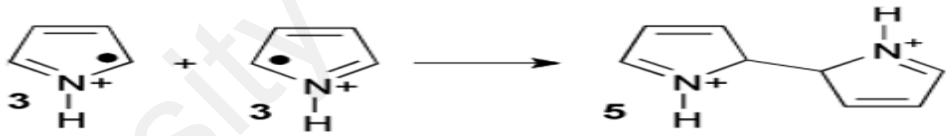

Figure 2.5: Formation of the dihydromer dication.

Step 3: Formation of the aromatic dimer

The formation of aromatic dimer which is resulted from losing two protons of dications in this step radical cation becomes stable state by forming dimers. (Figure 2.6)

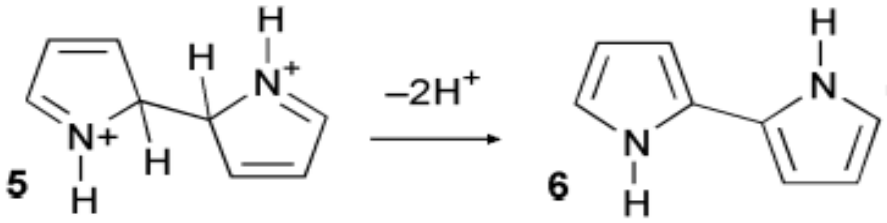

Figure 2.6: Formation of the aromatic dimer.

Step 4: Oxidation of the aromatic dimer

This step is including formation a cation radical (7) via oxidation of dimer (6). The oxidation potential of dimer 6 is less than the oxidation potential of the monomer is due to delocalized unpaired electron over the two rings. Moreover, the reactivity of dimer radical cation in compared with monomer is low and the most reactive zone is α –α' position. (Figure 2.7)

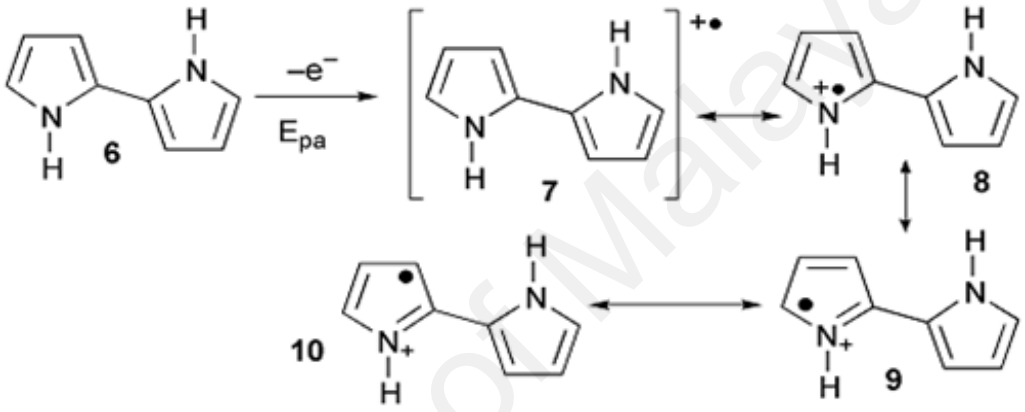

Figure 2.7: Oxidation of the aromatic dimer and resonance forms of radical cation.

Step 5: Propagation and Termination

Mainly the dimer radical in the position α reacts with a monomer radical to form a trimer dication, two protons of trimer dication are used to form trimer which is again oxidized to from the trimer radical cation after that the chain is growing in both, and β-position coupling of the trimer radical cation. Anyhow α-position coupling is superior to the β-position because of the effect of steric effect as seen in figure (2.8).

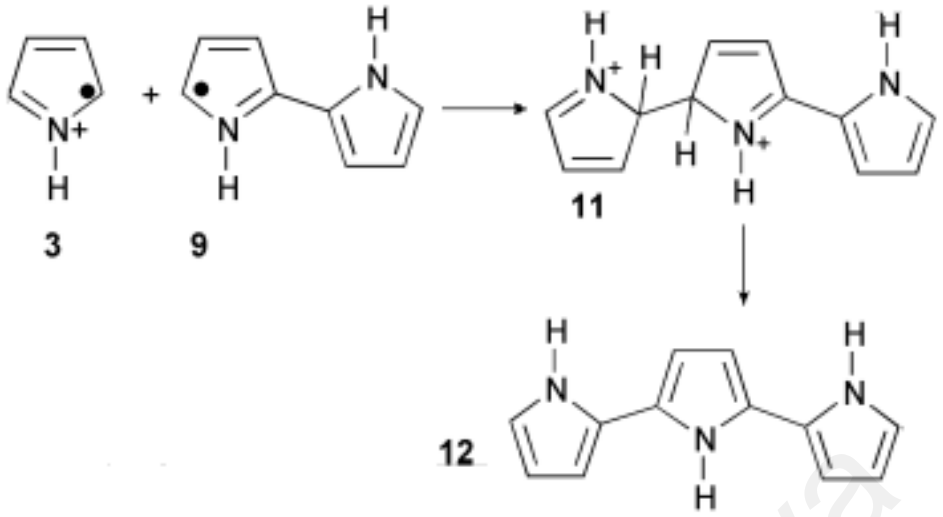

Figure 2.8: The reaction between the dimer radical and a monomer.

On the other hand, in the higher β-coupling, the chain length is longer due to elongation of the chain and the delocalizied unpaired electron. In low level of crystallinity and conductivity, the β-coupling is the cause. The deprotonation is happened after the coupling reaction to form Ppy.

Step 6: By oxidization of the neutral trimer, the radical cation is formed:

By increasing the number of rings (pyrrole), the delocalization increases continuously and the α-position in coupling may no longer is the only possible position. The β-position also can be under coupling reaction with the oligomers (in below). Despite of the domination of α-coupling, the number of this coupling (β-coubline) will be increase by increasing the length of chain; therefore, the Ppy crystallinity drop due to the β-position. The only improved crystallinity form of α-coupling is (ß, ß´-dimethylpyrrole) Figure (2.9).

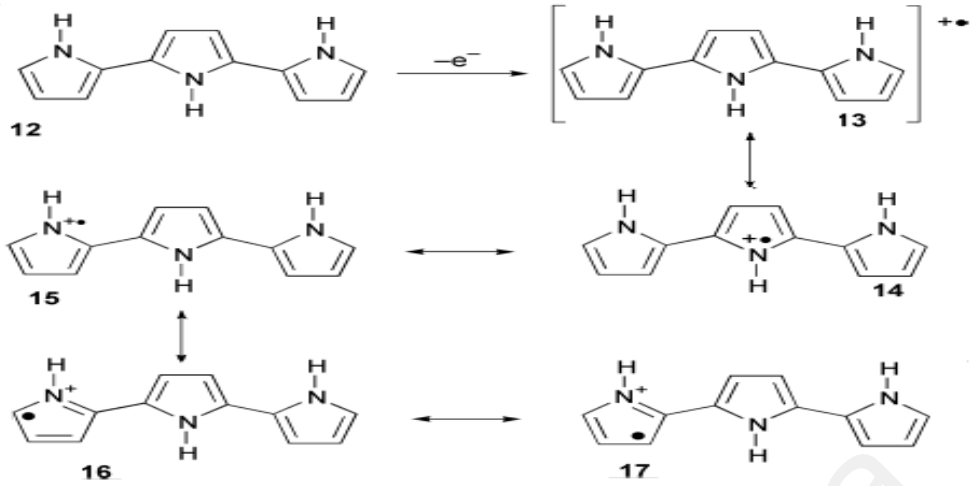

Figure 2.9: The formation of radical cation.

Step 7: Continue to the final polymer

The continuing of mentioned steps (Figure 2.9) include oxidative, coupling, deprotonation which lead to the final polymer.

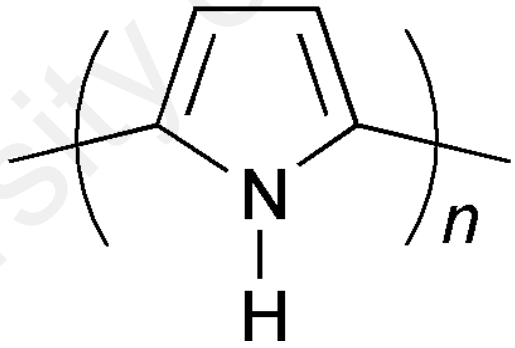

Figure 2.10: Doping step of polypyrrole.

The final product of step 7 (Figure 2.10) is neutral polyprrole, which lacks electrical conducting property, and needs to oxidize to transfer to a conducting polymer (doped form); therefore, as the Figure (2.10) in the final product, each 3 to 4 units of pyrrole are carrying positive charge balancing by an anion A^-, (dopant). It is determined that the number of donor electron by each molecule is about 2.25 to 2.33 (molar ratio of pyrrole molarity to dopant or oxidant molarity).

This mechanism which is possibly the best one to explain the reaction was also proved by Electron paramagnetic resonance (EPR) spectra studies via revealing the presence of π-type radical. Moreover, the reduction of the pH is also confirmed by the removing of measuring (H) bond strength using a Fourier Transform Infrared Spectrophotometer (FTIR) and Carbon (13) nuclear magnetic resonance (C-NMR) data on undoped polypyrrole illustrated that polymerization mainly proceeds via α-α position (Street *et al.*, 1983; Street *et al.*, 1982) and the conjugated structure of Ppy is a planar in all trans form. (Street *et al.*, 1985).

In recent years, distinct development has also been made in understanding of the structure-property relationships for many of the conducting polymers. This attractive progress rate has been encouraged by the field‘s fundamental synthetic novelty, importance to interdisciplinary research and to the emerging technological applications of these materials in different areas such as molecular electronics (Saxena & Malhotra, 2003), electrochromic displays (Mortimer et al., 2006), chemical sensors (McQuade *et al.,* 2000) electromagnetic shielding (Wang & Jing, 2005) and biosensors (Gerard &Malhotra, 2002; Xia & Wan,2010).

2.5 Biopolymers, chitosan and conducting polymers composite

As most of the polymers are synthetic materials, their biocompatibility and biodegradability are much more limited than those of natural polymers such as cellulose, chitin, chitosan and their derivatives. However, these naturally abundant materials also exhibit a limitation in their reactivity and process ability. In this respect, chitin and chitosan are recommended as suitable resource materials; because the natural polymers have excellent properties such as biocompatibility, biodegradability, non–toxicity, adsorption property and so on (Muzzarelli, 1977; Rinaudo, 2006).

Most commercial applications use the deacetylated derivative chitosan rather than chitin. Chitosan is a polysaccharide and a linear polymer formed primarily of repeating

unit of β– (1–4) 2–amino–2–deoxy–D–glucose (or (D–glusomanie)), as present Figure 2.11 (c). The first patent on producing chitosan was taken out in the 1920. Since then there have been taken out several hundred patents on production and even more application (Zakaria, *et al.,* 1995). Chitosan is insoluble in water and alkaline solutions but a small quantity of acid is needed to change the glucosamine into soluble R–NH3+ group. Acetic acid is recommended and widely used for this purpose, at acidic pH's, the free amino groups (–NH2) become protonated to form cationic amino groups (–NH3) and then the salt of chitosanium is formed. (Muzzarelli, 1983; Sandford, 1989; Krajewska, 2004). The present of free amine – groups in chitosan enhances the solubility of these polysaccharides in dilute acids as compared with chitin (Sandford & Hutchings, 1987).

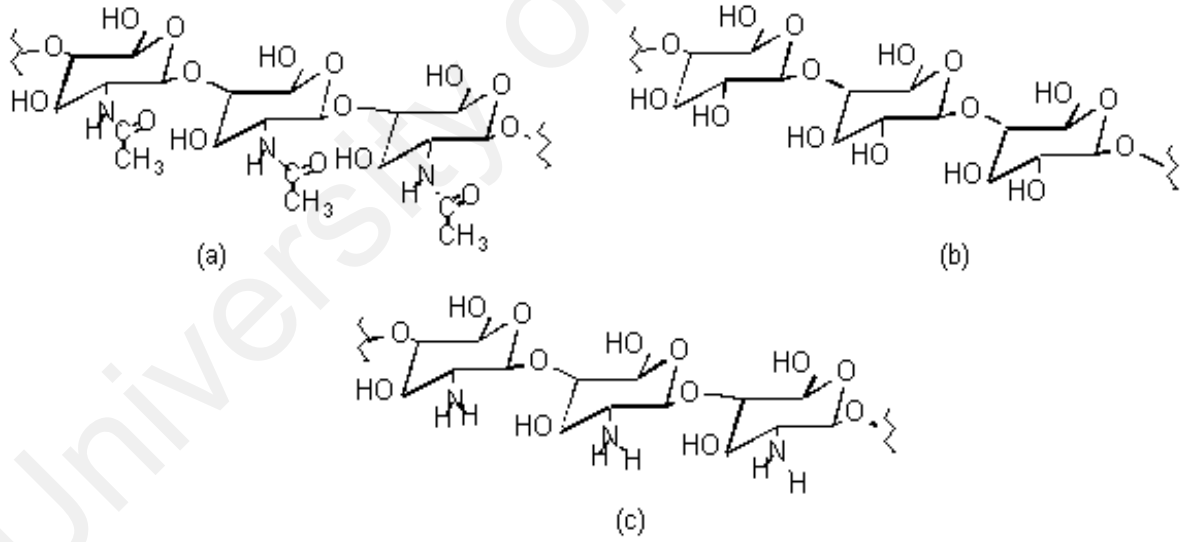

Figure 2.11: Structures of (a) Chitin, (b) Cellulose, and (c) Chitosan.

Chitosan (CS) is a biodegradable, biocompatible, non-toxic and reasonable biopolymer which displays a vast range of applications. Using of bio-polymers in electrical fields is very attractive due to its safety to environments and economic issue. By using bio-

polymers, the production cost is lower than using expensive engineering-polymers (Suh & Matthew, 2000).

The hybrid biomaterials are resulting from the reaction between conducting polymers and bio-polymers (e.g. Chitosan), maybe improvement some remaining properties that make them suitable for forthcoming applications specially when conductivity is favorite for example artificial nerves or blood vessels. The interaction between chitosan and some conducting polymers such as polyaniline and polypyrrole has been reported. The soluble chitosan-polyaniline copolymers were used for such appication (Yang *et al.,* 1989). Chitosan can also be used as a unique biocompatible steric stabilizer to functionalize the surface of conducting nanoparticle. The poly (methyl methacrylate), poly (butyl cyanoacrylate) (Yang *et al.,* 2000) and polystyrene (Marie *et al.,* 2002) are examples of polymer nanoparticles that have been successfully stabilized via chitosan.

Chitosan has been employed for the dispersion polymerization of aniline as a steric stabilizer. In the dispersion polymerization of aniline, there were two roles for chitosan. firstly, the role as a steric stabilizer for polyaniline (PANI) - chitosan. Secondly, based on the mechanism of the steric stabilization (JanČa *et al.,* 2001), PANI-CS nanoparticles were formed during the polymerization of aniline in the presence of chitosan where chitosan was coating the exterior surface of the nanoparticle. Therefore, the surface of PANI-CS has been functionalized via the amino groups on the chain. Poly (ethylene oxide) (Vincent &Waterson, 1990) polyacrylamide (Ghosh *et al.,* 1999) and poly (vinyl alcohol) were also used to stablized PANI dispersions as steric stabilizers, but there are only a few reports on using chitosan (Gangopadhyay *et al.,* 2001) in the aniline polymerization (Yang *et al.,* 1989). Therefore, the precipitation of polyaniline has been successfully hindered via PANI-CS nanoparticles.

Functionalizing the particle surface via hydrophilic groups, like carboxylic acids or amines, is strongly favorable for diagnostic testing methods. It has been informed that in

the presence of biological cations, nanoparticles which are charged positively, are more stable (Calvo *et al.,* 1997), so it's a desirable for drug molecules because there will be an attraction between negative charge of biological membranes and site-active of target inside the body of weight (Meisner *et al.,* 1989).

2.6 Metal oxides

Metal oxides shows a significant role in many areas of chemistry, physics and materials science (Nylander *et al.,* 1983; Rahman *et al,* 2010; Timmer *et al.,* 2005). The metal elements are able to form a large diversity of oxide compounds (Maksymiuk, 2006). These can adopt a huge number of structural geometries with an electronic structure that can show metallic, semiconductor or insulator properties. In the developing area of nanotechnology, a purpose is to make nanostructures or nano arrays with special properties with respect to those of bulk or single particle species (Ameer & Adeloju, 2005; Noguera, 1996; Kung, 1989). Metal Oxide nanoparticles can play unique physical and chemical properties due to their partial size and a high density of corner or advantage surface sites. Particle size is likely to influence three important groups of basic properties in any material. Bulk oxides are usually robust and stable systems with well-defined crystallographic structures. However, the growing importance of surface free energy and stress with decreasing particle size must be considered. Nanoparticle can play a good role to interactions with its surrounding environment and a high surface free energy. In order to display mechanical or structural stability, a nanoparticle must have allowed surface free energy. As a significance of this requirement, phases that have a low stability in bulk materials can be stable in nanostructures (Gleiter, 1993; Valden *et al.,* 1998; Rodriguez *et al.,* 2002). Among the metals oxides, zinc oxide (ZnO) (Zhang *et al.,* 2015), titanium oxide (TiO_2) Bao, *et al.,* 2008), iron oxide (Fe_3O_4) (Wei & Wang, 2008), cobalt oxide (Co_3O_4) (Hou *et al.,* 2012) are mostly generally known oxides and scientifically played a transition metal oxide since last four decades.

These oxides have become important both scientifically and industrially due to of their applications for sound and picture recording, data storage, humidity and gas sensors, conducting composite super capacitors, electrochromic display devices, etc. In the present study, the following metal oxides are used for electrochemical deposition in application of detect glucose.

1. Iron Oxide Nanoparticles
2. Titanium Dioxide Nanoparticles

2.6.1 Iron oxide (Fe_3O_4) nanoparticles

Iron oxides nanoparticle are a group of raw materials common in nature and readily synthesized in laboratory. There are three major types of iron oxide: Hematite (α-Fe_2O_3), Maghemite (γ-Fe_2O_3) and Magnetite (Fe_3O_4) in Figure (2.12). The γ-Fe_2O_3 occurs naturally in soils as a weathering product of Fe_3O_4, to which it is structurally related. Both γ- Fe_2O_3 and Fe_3O_4 exhibit a spinel crystal structure, wherein the oxygen atoms form a Fe closed packed orientation and the iron cations occupy the interstitial tetrahedral and octahedral. Bulk iron oxide consists of both Fe^{2+} and Fe^{3+} atoms and exhibits ferromagnetic behavior.

In the past year academics peoples are focusing on shape and size dependent magnetic properties of iron oxide nanoparticles for biomedical applications. Thus, of the dipolar interaction between the magnetic particles, they are intriguing building blocks for self-assembly into various nanostructures. Magnetic behavior is an important parameter in design and synthesizing of superparamagnetic iron oxide nanoparticles in order to maximally facilitate their imaging and therapeutic efficacies as these applications involve high magnetization values. Although this can be accomplished by applying a maximum magnetic field acceptable under the clinical settings, the reaction conditions

during the synthesis processes can be controlled to generate particle size with a large surface area, which in turn allows these particles to exhibit high magnetic.

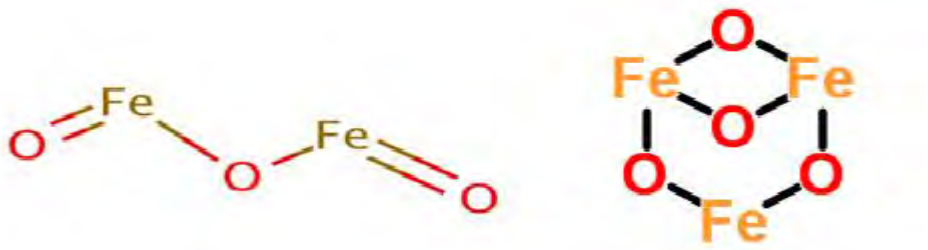

Figure 2.12: The structure type of Fe_2O_3 and Fe_3O_4.

2.6.2 Titanium Dioxide (TiO_2) nanoparticles

Titanium (IV) Dioxide is also known as titania. It is the logically occurring oxide of titanium of chemical formula TiO_2. It shows in three polymorphic forms viz. rutile, anatase and brookite Figure (2.13). Brookite is a very common pigment utilized in various industries. Rutile and anatase are produced commercially in large quantities for the usage as pigments, catalysts and in the production of ceramic and electronic materials. Due to its high refractive index, durability, dispersion and tinting strength, chemical inertness and non-toxicity, TiO_2 is widely used in welding-rod coatings, specific paints, inks, acid-resistant vitreous enamels and sensors.

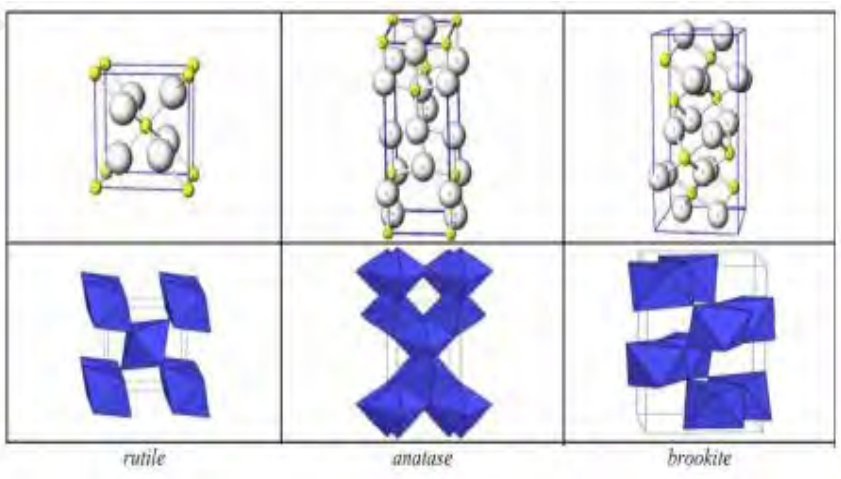

Figure 2.13: The structure of the type of TiO_2.

2.7 Conducting polymer, composites and nanocomposite in biosensors

Conducting polymer composites are usually prepared by the addition of conducting fillers in the insulating polymer matrix. Generally, several materials such as conductive carbon black, graphite flakes, fibers, metal powders, or nano powders etc. are used as conductive fillers. These fillers are loaded in the common insulating polymers, which have been used as major matrix, like Polypyrrole (Ppy), Poly Aniline (PANI), Poly vinyl alcohol (PVC), Nylon etc., to get conducting polymer composites or conducting polymer nanocomposites. Various polymer materials including both amorphous polymers can be made electrically conducting. The electrical conductivity of the polymer is obvious by the volume fraction of the filler. A transition from insulating to non-insulating behavior is commonly observed when volume fraction of conductive filler in the mixture reaches a threshold of about 25%. Conducting polymers, such as polypyrrole (Ppy), polyaniline (PANI), polythiophene (PTh) and their derivatives, have been used as the active layers of sensors since early 1980s (Huang *et.al.,* 1986). In comparison with most of the commercially sensors on metal oxides and operated at high temperatures, the suggested conducting polymers made of the sensors improved.

The main standards are in development of simple and efficient methods for the synthesis of conducting polymer based nanostructured materials and the influence of size on the physical properties must be properly investigated. Some sophisticated characterization techniques have to be used or even developed in certain special cases for detailed analysis of the molecular structure and physico-chemical properties of the conducting polymer nanostructures in order to bring out their difference with the bulk and the mechanism underlying their formation. This can help in tailoring the properties of these nanomaterials for specific applications. Tremendous amount of development is also required in the fabrication technology to improve the application of these materials

as efficient nano devices and for future commercial applications. Conducting polymer based nanostructured materials may be broadly classified into two categories:

1. Conducting polymer nanostructures such as nanofibers, nanoparticles, nanowires, nanotubes of pure conducting polymers.
2. Conducting polymer nanocomposites, which are mixtures of metal / metal oxide / ceramic nanoparticles with conducting polymer at nanoscale or nanoscale mixture of conducting polymer nanostructures with another polymer.

Composite materials are naturally occurring or engineered materials made from two or more component materials with significantly different physical or chemical properties as compared to their individual components which remain separate and distinct at the macroscopic or microscopic scale. However, in the microscopic world, due to the reduced particle size of the components the interface interactions play a pivotal role in composite mixtures and this is especially important for a new class of recently developed materials named, the nanocomposites.

Nanocomposites can be defined as multiphase solid materials having unique physical properties and wide application potential with at least one of the phases constrained by some means to grow more than 100 nm in either one, two or three dimensions that are obtained from molecular level mixing of two or more nano sized objects using an appropriate technique (Gurrappa & Binder, 2008). Depending upon the macroscopic physical structures nanocomposite materials can be classified into three broad categories: (a) Fiberous (b) Laminar and (c) Particulate nanocomposites (Xie *et.al.*, 2014).

The first generation of nanocomposites was the nanocomposite plastics which were homogeneous dispersions of small sized inorganic particles throughout a polymer matrix. These nanocomposites were prepared in the 1970‘s employing sol-gel

technique, however, the inorganic phase in these nanocomposites were in some cases not attached chemically to the organic phase. Nanocomposite plastics found tremendous applications in surface coating technology. The second generation of nanocomposite materials emerged in the 1980‘s when fine particles, minerals and clay fillers were used as a secondary phase in plastics. Nanocomposites of intrinsically conducting polymers are materials that utilize conjugated polymers and at least one secondary component that can be inorganic or organic materials or biologically active species (Hatchett & Josowicz, 2008). One can derive exciting novel properties from nanocomposites by successfully combining the characteristics of its parent constituents into a single material. Generally, in polymer nanocomposites the polymeric component is utilized to provide mechanical strength and possibility to the resulting nanocomposite material. However, in case of nanocomposites of intrinsically conducting polymers the secondary components such as inorganic, biological or organic active species are generally used to enhance the possibility and mechanical strength whereas the functionalities of intrinsic conducting polymers are used for different applications (Hatchett & Josowicz, 2008). The properties of the secondary components are also utilized in some applications.

2.8 Electrochemical biosensor based on enzymatic glucose sensors

Researchers have been explored in the area of biosensors since 1962 with the development of enzyme electrodes by (Clark & Lyons, 1962). Later then, scientists starting in the areas of physics, chemistry, biochemistry, molecular biology and material science have reported to this various application (Tian *et al.,* 2007; Rodriguez *et al.,* 2006).

According to The International Union of Pure and Applied Chemistry (IUPAC) (Thévenot *et al.,* 2001), an electrochemical biosensor is a self-contained integrated device, capable of giving the detailed of quantitative or semi-quantitative analytical information using a biological recognition element (biochemical receptor) which is

retained in direct spatial contact with an electrochemical transduction element. The biochemical signals can be used to generate a current/charge or may change conductivity between two electrodes. A design representation of an electrochemical sensor is given in Figure 2.14.

Figure 2.14: Design of an electrochemical sensor.

One of the main objectives of the present work is the development of glucose biosensor; hence a brief history of the glucose biosensor is given. The history of glucose enzyme electrodes dates back to 1962 when the first device was developed by Clark and Lyons of the Cincinnati Children's Hospital (Clark & Lyons, 1962). The researchers relied on a thin layer of glucose oxidase (GOx) entrapped over an oxygen electrode via a semipermeable dialysis membrane. Measurements were made based on the monitoring of the oxygen consumed by the enzyme catalyzed reaction Eq. (1.1).

$$\text{Glucose} + GO_2 \longrightarrow \text{gluconic acid} + H_2O_2 \qquad 1.1$$

A negative potential was applied to the platinum cathode for a reductive detection of the oxygen consumption Eq. (1.2).

$$O_2 + 4H+ + 4\,e^- \longrightarrow 2H_2O \qquad 1.2$$

(Guilbault & Lubrano, 1973) designated an enzyme electrode for the measurement of blood glucose based on amperometric monitoring of the hydrogen peroxide product (eq. 1.3).

$$H_2O_2 \longrightarrow O_2 + 2H + 2e^- \qquad 1.3$$

The resulting biosensor offered good accuracy and precision in connection with 100 μL blood samples. A wide range of amperometric enzyme electrodes, differing in electrode design or material, immobilization approach, or membrane composition, has since been described. In the 1990s, widespread studies were showed toward the formation of electrical communication between the redox center of GOx and the electrode surface (Degani & Heller, (1987). Specific note was the work of researchers, that presented the use of flexible polymer with osmium redox sites (Ohara, et al., 1994). During this period, the world also observed the development of slightly invasive subcutaneously implantable devices (Csoregi *et al.,* 1995; Henry, 1998; Schmidtke *et al.,* 1998).

Though the enzymatic glucose sensors are widely considered and applied, the most common and serious problem with these sensors is insufficient long-term stability, which originates from the intrinsic nature of the enzymes. Additionally, a difficult process, including adsorption, cross-linking, entrapment, and electropolymerization, is required for the immobilization of the enzyme on the solid electrode (Wilson, 1992; Yang *et al.,* 2006; Yang *et al.,* 2006), and this possibly will reduce the activity of the GOx. Because the sensitivity of these glucose sensors essentially depends on the activity of the immobilized enzymes reproducibility is still a serious problem in quality control (Park *et al.,* 2006).

On the other hand, there are many advantages in using non-enzymatic sensors in the electrochemical methods for the detection of glucose including stability, simplicity, reproducibility, low cost, and no oxygen limitation (Park *et al.,* 2006). Considering

these aspects, the enzymeless glucose sensor is an attractive alternative technique. Many efforts in this direction have been reported for the amperometric measurements of glucose using a bare electrode of platinum (Vassilyev, 1985) and copper (Nagy *et al.,* 2001).

2.9 Electrochemical biosensor based on non- enzymatic glucose sensors

The use of non-enzymatic electrodes as glucose sensors potentially promises a fourth generation to analytical glucose oxidation. Instead of facilitating the needs of a fragile and relatively difficult enzyme however, non-enzymatic electrodes strive to *directly* oxidise glucose in the sample. This is an ideal system that was first investigated a century ago by (Walther Loeb,1909) who electrochemically oxidised glucose in sulphuric acid at a lead anode. This occurred long before to the fabrication of the Clark oxygen electrode (Clark & Lyons, 1962), though extensive research into the non-enzymatic approach actually coincided with enzymatic development (Wroblowa *et al.*; Bockris *et al.,* 1964). Despite decades of research into non-enzymatic systems however, the problems associated with this approach have prevented the practical application of the sensors. This is mostly due to a lack of selectivity at the electrode, but also the slow kinetics of glucose oxidation at many ‗bare' electrodes, fouling of the electrode by real sample constituents, and the limited number of systems that are applicable to physiological pH. In spite of periods of study into non-enzymatic systems however, the difficulties associated with this approach have prohibited the practical application of the sensors. This is mostly due to a lack of selectivity at the electrode, but also the slow kinetics of glucose oxidation at many ‗bare' electrodes, fouling of the electrode by real sample constituents, and the partial number of systems that are applicable to functional pH. The following lists table (Table 2.1) shows the non-enzymatic glucose sensors that use fixed potential amperometric analysis, as would be used in physiological

applications. Limits of detection are generally within the realm of blood glucose concentration (i.e. 2-10 mM), sensitivity varies with respect to surface structure and the catalyst used, with the development of nano-dimensioned materials in the last decade coinciding with a sudden surge in non-enzymatic systems.

Table 1: Non-enzymatic glucose sensors that have only used fixed potential, amperometry methods for electrochemical determination.

Electrode composition	Sensitivity (mA mM^{-1} cm^{-2})	Linear Range (mM)	LOD (μM)	References
Au Nps ITO	0.1835	$4x10^{-3}$ - 0.5	5.0	Ma, et.al., 2009
CuS_2-Nanocrystal-CNT	0.035	$1x10^{-3}$ - 12	0.0	Myung, et al,2009
PtPb Nps/MWCNT	0.0178	up to 11	1.8	Cui, et.al., 2007
Ni/GC-Pt Nps	0.00144	Up to 8	15.0	Scavetta, et.al., 2008
Au-chitosan Nps	not given	0.4 - 10.7	0.370	Feng, et al., 2009

Carbon nanotubes (CNT) , Nanoparticles (Nps) , multi-walled carbon nanotubes (MWNT)

Direct non-enzymatic electrooxidation of glucose significantly depend on the electrode material used. Electrocatalytic methods are significant to glucose oxidation, as it is or else a kinetically very slow method that would produce no obvious Faradaic current at most commercial electrodes. This describes are showing that direct glucose oxidation regularly does not observe to scan rate dependent voltammetry, representing a non-diffusion controlled process.

A number of metal oxides have been used in conjunction with conducting polymers to produce electrocatalytic glucose sensors. MnO_2 was coupled with carbon nanotubes (Chen *et al.,* 2008) a novel non-enzymatic glucose sensor, which displayed a wide linear range to 28 mM and a reasonable sensitivity of 33.19 μA mM^{-1} cm^{-2}. The alternative

metal oxide showed a high tolerance to electrode fouling too, displaying no interference from chloride ions or common electroactive interference species. Most remarkably the MnO_2 caused an extensive negative shift of the anodic peak potential to +0.1 and +0.4 V vs. Ag/AgCl, a shift of over 200 mV relative to the unmodified multi-walled carbon nanotubes MWCNTs. SnO_2 were deposited on double wall carbon nanotubes, however the latter gave a relatively poor response to glucose and H_2O_2. Moreover, SnO_2 was speculated to be most active due to the presence of more active sites, yet this was clearly not the case (Myung *et al*., 2009).

2.10 Glucose and naturally occurring interferences

Glucose, a monosaccharide, known as grape sugar, blood sugar, or corn sugar, serves as a source of energy for a living cell and a metabolic intermediate. It is one of the main products of photosynthesis and is responsible for cellular respiration in both prokaryotes and eukaryotes. Only D-glucose (dextrose) is biologically active while L-glucose cannot be metabolized by cells in the biochemical process. Structures of some biologically important molecules are given in figure 2.15.

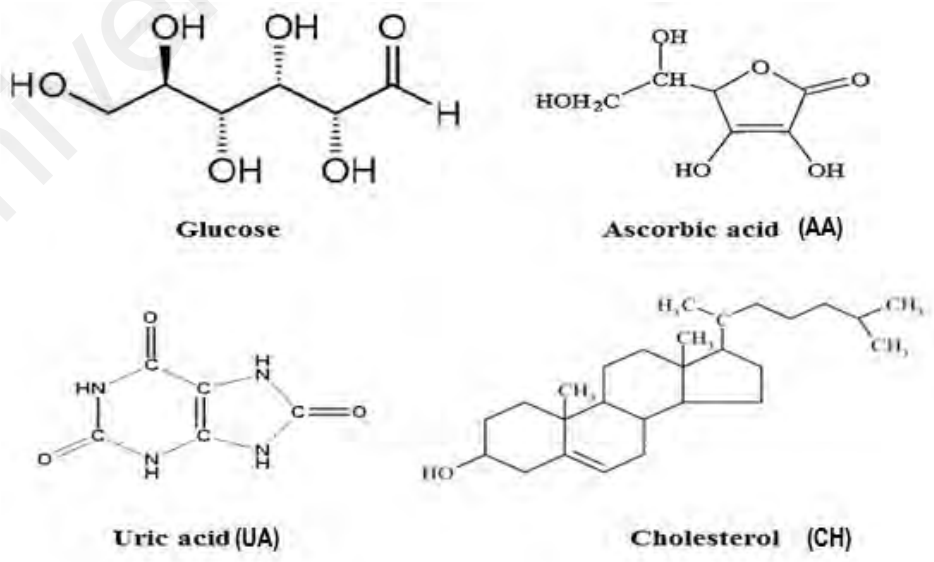

Figure 2.15: Structures of some biomolecules.

Most dietary carbohydrates contain glucose as in starch and glycogen, or together with another monosaccharide, as in sucrose and lactose. Ferraris presented a detailed mechanism of the metabolism of glucose (Ferraris, 2001). It is partly utilized as an energy source by brain cells, intestinal cells and red blood cells, while the rest reaches the liver, adipose tissue and muscle cells, gets absorbed and stored as glycogen. Liver cell glycogen gets converted to glucose and returns to the blood when insulin is low or absent; muscle cell glycogen does not return due to lack of enzymes. In fat cells, glucose is used to power reactions that synthesize some types of fat. Glycogen is the body's _glucose energy storage' mechanism because it is much more _space efficient' and less reactive than glucose itself.

The wide use of glucose in organisms is mainly due to its lower tendency to non-specifically react with the amino groups of proteins, since the non-specific action is detrimental to the function of many enzymes. The carbohydrates, a key source of human energy, provide through aerobic respiration approximately 3.75 kcal (16 kJ) per gram of food material (Maclean *et.al,* 2003). Glucose being a primary source of energy for the brain, influences psychological processes; when it is low, mental efforts like self-control, decision-making etc., are impaired (Gailliot*et.al,* 2007; Gailliot & Baumeister, 2007).

Ascorbic acid (AA) and uric acid (UA), and cholesterol (CH) (Figures 2.15) are three electroactive species naturally occurring in blood that cause the most electrochemical interference during glucose sensing. The biochemical structures of various were known electroactive interferences species. Like glucose they are strong reducing agents, therefore readily oxidized at moderate electrode potentials. AA is commonly known as vitamin C, and although concentrations in blood vary on dietary intake. The important biological function of AA is quenching of free radicals, such as hydroxyl (Fessenden & Verma, 1978), singlet oxygen (Bodannes & Chan, 1979) and the superoxide

(Peterkofsky & Prather, 1977) which are resulting from oxygen. Its anti-inflammatory activity defends cell against oxidative damage and its reductive capacity has a definite role in iron metabolism for the incorporation of iron into ferritin and for the reduction of ferric iron.

Uric Acid (UA) is an end product of purine metabolism and is related to the purine bases of the nucleic acids in human. UA is present as the final metabolite of purine, and is present in the blood as an antioxidant at concentrations of ca. 0.18 to 0.42 mM. Ever present, most recent papers of the past period of years‘ effort on these three main electroactive interference compounds when testing the practical application of the sensor, be it enzymatic or non-enzymatic. Cholesterol is an important lipid for human body. The desired total plasma cholesterol for an individual is less than 5.2 mM (200 mg/dL) and it poses a potential health threat when the level is greater than 6.2 mM (240 mg/dL). CH has been named as an electroactive interference with respect to glucose sensing by a number of researchers (Heller & Feldman, 2008) and is present in the blood at very low concentrations of 3 to 15 μM.

CHAPTER 3: MATERAILS AND METHODOLOGY

3.1 Overview

The common experimental procedures, chemicals and instruments used in this work are presented in this chapter. The performance characteristics of fabricated biosensor are controlled by achieving an understanding and control over the properties and behaviour of the materials used. To accomplish the same physical and chemical characterization of materials used in addition to response characteristics of biosensor after each modification step becomes pertinent. Morphological characterization of these nanocomposite films is of paramount importance since their properties vary drastically with their size and shape. Microscopic techniques like Field emission scanning electron microscopy (FESEM), High-resolution transmission electron microscopy (HR-TEM), are exploited for morphological analysis. Moreover, chemical and electrochemical characterization of the nanocomposite and biosensors, in the present work, is done through spectroscopic techniques, Fourier transform infrared spectroscopy (FTIR), Energy-dispersive X-ray spectroscopy (EDX), X-ray diffraction technique (XRD), X-ray photoelectron spectroscopy (XPS), the potential analysis of ameprometry study, cyclic voltammetry (CV) and Electrochemical impedance spectroscopy (EIS). Present chapter gives a brief description of these characterization techniques.

3.2 Chemicals and reagent materials

Chemicals and reagents were used the stock solution was prepared using deionized water. Chitosan $(C_6H_{11}O_4N)_n$, (molecular weight: 100,000-300,000) was purchased from (ACROS Organics), New Jersey, USA. D (+) glucose, iron oxide (Fe_3O_4) nanoparticles size >50 nm, and titanium dioxide (TiO_2) nanoparticles size >20 nm were purchased from (Sigma-Aldrich). Freshly distilled pyrrole 99% was used as the monomer from (Merck Organic), and sodium para toluene sulfonate (*P*-TS) from (Sigma-Aldrich) was used as an oxidant. Uric acid ($C_5H_4N_4O_3$), ascorbic acid ($C_6H_8O_6$),

and cholesterol ($C_{27}H_{46}O$) from (Sigma-Aldrich) were used for the interference studies. Acetic acid (CH_3COOH) 99.8%, sodium hydroxide (NaOH) and potassium chloride (KCl) were provided by (Merck). All the other reagents used in this experiment were of analytical grade and used as received without further purification. Indium tin oxide (ITO) glass electrode was purchased from (Fluka, Japan). Before using pyrrole, it was distilled at 131˚C under atmospheric pressure; after that it was stored at 4˚C in a refrigerator under protection from light.

A stock solution of D (+) glucose was prepared (1M) and left the solution overnight to study the performance sensing of the composite and nanocomposite films. A stock solution of sodium hydroxide (0.1 M) was prepared using distilled water. A stock solution was prepared containing potassium ferricyanide ($1x10^{-3}$) M $K_3[Fe(CN)_6]$ in potassium chloride (0.1) M KCl. A stock solution uric acid, ascorbic acid, and cholesterol were prepared (0.1 mM). Phosphate buffer solution (PBS), (0.1 M) was prepared from Na_2HPO_4 and KH_2PO_4 (Sigma-Aldrich).

3.3 Electrochemical deposition

The polymer electrodeposition method involves the polymerization of the monomer on the working electrode from the solution of the monomer and a dopant in an electrochemical cell at the oxidation potential of the monomer. In this study, cyclic voltammetry was used for the electrochemical deposition of conducting polymer nanocomposite films on ITO glass electrode where all the components like the monomer, the dopant, chitosan, and the nanomaterial were dissolved in the solvent in the electrochemical cell.

3.4 Electrochemical deposition and nanocomposite films preparation

The electrochemical deposition was performed using a computerized potentiostat PGSTAT 302N/Auto lab. A conventional three-electrode system comprising of an ITO

glass as the working electrode (WE), graphite rode as the counter electrode (CE), and Ag/AgCl with (3M KCl) as a reference electrode (RE) was employed for the electrochemical deposition, Figure 3.1. The working surface area of the ITO glass rod electrode was ($1cm^2$ X $1cm^2$). All the experiments were performed at room temperature in 25 mL solution of all the reactants by cyclic voltammetry using the potential ranging from (-1 to 1.2) V vs Ag/AgCl with the scan rate of 50 mV/s.

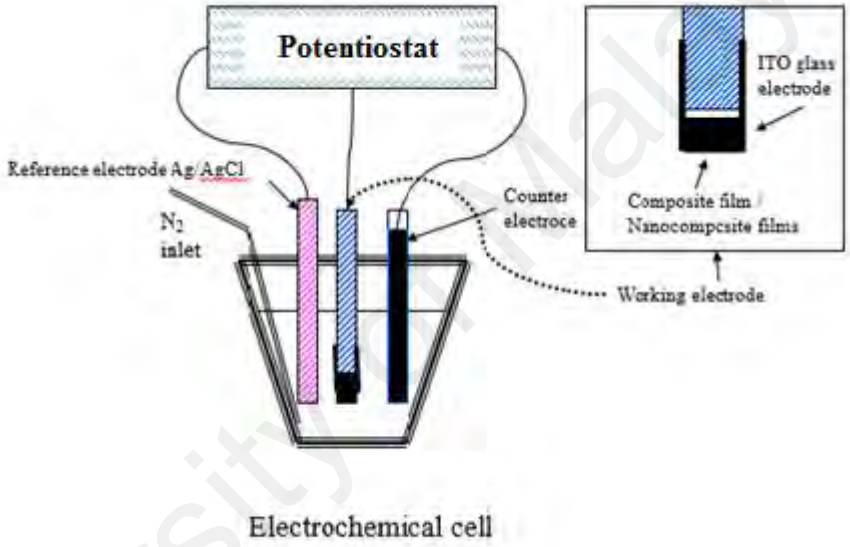

Figure 3.1: Equipment for electrochemical film deposition.

3.5 Preparation of Ppy-CS / ITO composite films

50 mg/mL of chitosan was dissolved in 25 mL deionized water and soaked in acetic acid 1% under continuous stirring at room temperature for 2 hours. Later the solution of pyrrole (0.1M) and *p*-TS (0.3M) was added to the solution of CS for 5 min. The prepared solution of Ppy-CS was taken in a glass cell for electrochemical deposition of the film on ITO glass electrode by cyclic voltammetry scanning from -1V (vs. Ag/AgCl) to +1.2 V (vs. Ag/AgCl) with the scan rate of 50 mV/s using the three-

electrode system. The composite films were then washed repeatedly with distilled water to remove any unbound particles and later dried at room temperature. The composite Ppy-CS films were characterized by X-ray diffraction technique (XRD), Fourier transform infrared spectroscopy (FTIR), Field Emission scanning electron microscopy (FE-SEM), High-resolution transmission electron microscopy (HR-TEM), and X-ray photoelectron spectroscopy (XPS).

3.6 Preparation of Ppy-CS-Fe_3O_4 NP/ ITO nanocomposite films

Fe_3O_4 nanoparticles were dispersed into 25 mL of CS (50 mg/mL) solution under continuous stirring at room temperature and sonicated for about 2 h to obtain a viscous solution of CS with uniformly dispersed Fe_3O_4 nanoparticles. Later the solution of pyrrole and (*p*-TS) (10 mL) was added to the solution of CS and iron oxide and was stirred for 5 min. The prepared solution of (Ppy-CS- Fe_3O_4) was taken in a glass cell for electrochemical deposition of the film on ITO glass electrode by cyclic voltammetry scanning from -1V (vs. Ag/AgCl) to +1.2 V (vs. Ag/AgCl) with the scan rate of 50 mV/s using the three-electrode system. The nanocomposite films (Ppy-CS-Fe_3O_4) were then washed repeatedly with distilled water to remove any unbound particles and later dried at room temperature then used it for characterization and its application in glucose sensors. The nanocomposite films of Ppy-CS-Fe_3O_4 NP/ITO were characterized by X-ray diffraction technique (XRD), Fourier transform infrared spectroscopy (FTIR), Field emission scanning electron microscopy (FE-SEM), Energy-dispersive X-ray spectroscopy (EDX), High-resolution transmission electron microscopy (HR-TEM) and X-ray photoelectron spectroscopy (XPS). Appendix-A shows the process of electrochemical deposition of Ppy-CS-Fe_3O_4 nanocomposite films.

3.7 Preparation of Ppy-CS -TiO_2 NP/ ITO nanocomposite films

TiO_2 nanoparticles were dispersed into 25 mL of CS (50 mg/mL) solution under continuous stirring at room temperature which was sonicated for about 2 h to obtain a viscous solution of CS with uniformly dispersed TiO_2 nanoparticles. Later the solution of pyrrole and (*p*-TS) (10 mL) was added to the solution of CS and titanium oxide and was stirred for 5 min. The prepared solution of Ppy-CS-TiO_2 was taken in a glass cell for electrochemical deposition of the film on ITO glass electrode by cyclic voltammetry scanning from -1V (vs. Ag/AgCl) to +1.2 V (vs. Ag/AgCl) with the scan rate of 50 mV/s using the three-electrode system. The nanocomposite Ppy-CS-TiO_2 films were then washed repeatedly with distilled water to remove any unbound particles and later dried at room temperature then used this film for characterization and its application in glucose sensors. The nanocomposite films of Ppy-CS-TiO_2 / ITO were characterized by X-ray diffraction technique (XRD), Fourier transform infrared spectroscopy (FTIR), Field emission scanning electron microscopy (FESEM), Energy-dispersive X-ray spectroscopy (EDX), High-resolution transmission electron microscopy (HR-TEM) and X-ray photoelectron spectroscopy (XPS) Appendix B shows the process of electrochemical deposition of Ppy-CS-TiO_2 nanocomposite films.

3.8 Fourier transmission infrared spectroscopy (FT-IR)

The composite films and nanocomposite films were investigated by using Fourier transmission infrared spectroscopy (FT-IR). Fourier Transform Infrared Spectroscopy (FT-IR) is an analytical technique used to identify organic (and in some cases inorganic) materials (Griffiths & De Haseth, 2007). This technique measures the absorption of various infrared light wavelengths by the material of interest. These infrared absorption bands identify specific molecular components and structures. The regions of the electromagnetic spectrum which is between microwaves and visible regions are called the infrared radiation. When the level of energy is changed through the molecular

transmission between various energy levels, rotational or vibration state relating to each other for various types of molecules, a spectrum of transmission or absorption will be obtained. The functional groups of molecules have been characterized by their vibration frequencies. FT-IR spectroscopy is an important and powerful tool to investigate the structure of molecular like a fingerprint. The presence of a functional group and bonds of organic materials are detected by characteristic frequency absorption in FT-IR spectroscopy. Fourier transform infrared (FT-IR) spectra of the powdered samples were recorded using a Perkin Elmer RX1 FT-IR ATR spectrometer in the range of 400–4000 cm^{-1} in spectral-grade KBr pellets. Therefore, IR spectroscopy can result in a positive identification (qualitative analysis) of every different kind of material. Figure (3.2 shows the FT-IR spectroscopic instrument.

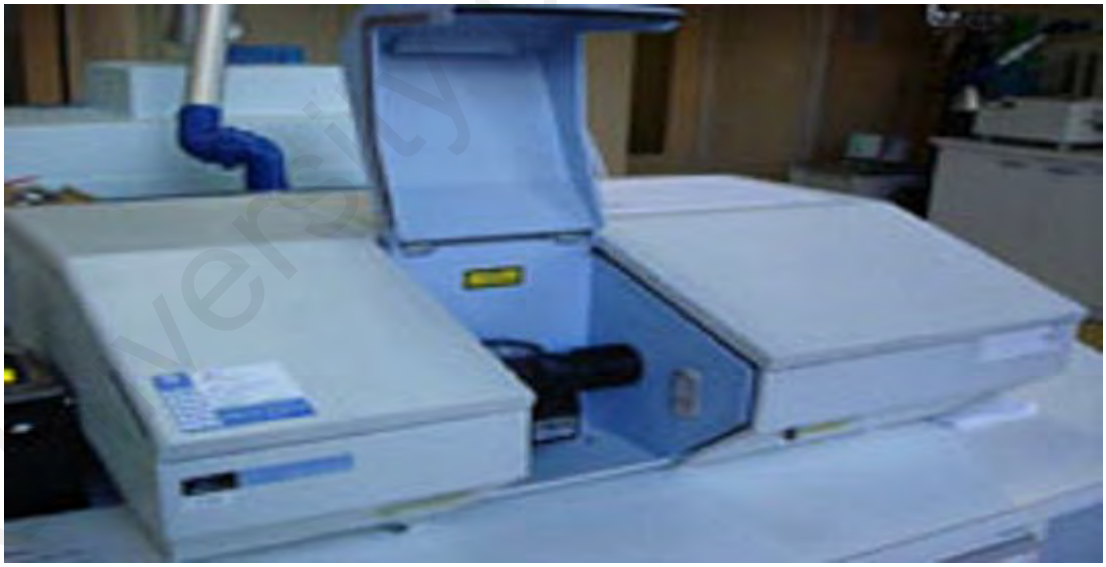

Figure 3.2: Schematic diagram of Fourier transform infrared spectroscopy.

3.9 Field emission scanning electron FE-SEM microscopy and EDX

The surface morphology of composite and nanocomposite films were observed via field emission scanning electron microscopy (FESEM, Hitachi Brand, Model SU 8220, equipped with EDX) (Tokyo, Japan). The slides were characterized at slow scan speeds

less than 2 kV and at 50,000× magnification. The testing area was 2.1 mm at an accelerating voltage of 2 kV. FESEM is a technique for analyzing microstructure and investigating properties, processing and behaviors of microstructure materials such as the topography, morphology, distributed phase, composition, the orientation of crystal, and also the presence and location of electrical defects. The result is the ultimate SEM electron source offering the highest gun brightness, high stability and incredible resolution performance at all accelerating voltages due to its smallest energy width. The enhanced stability and probe current provides opportunities for enhanced low voltage elemental microanalysis. Figure 3.3 shows the FESEM microscopy instrument.

Figure 3.3: Schematic diagram of Emission scanning electron microscopy (FESEM).

3.10 High-resolution transmission electron (HR-TEM) microscopy

The fundamental principle operation of High-resolution transmission electron microscopy (HR-TEM) is similar to the light microscope; while in this HR-TEM technique, the role of light is played by the electron. In a light microscope, it is limited by the light wavelength, while in TEM, the source of light is electron with lower wavelength, therefore, the resolution can be improved till thousands of times rather than a light microscope. In this research, a (Tecnai model G2-F20)-Twin manufacture (FEI,

USA). HR-TEM machine at accelerating voltage of 120 kV was used. The samples were prepared for HR-TEM experiments into some steps:

1. Pell off the thin film from ITO substrate.
2. Put the film into the small bottle, and then added deionized water.
3. Sonicate in Ultrasonic, for 20 min.
4. Dip the carbon coated copper grid into the solution and let it dry in room temperature.
5. Inspect into HR-TEM for characterization.

By using this technique, the tiny objects in the size of a few angstroms (10 m) can be observed. It is the best technique to study small details such as nanoparticles and nanocomposites. Due to high magnifications, it is a very valuable tool in medical, biological and materials research. From this characterization method (HR-TEM), the inner morphology, distribution of particle (nanoparticle) and also the shape and the size of nanoparticle of Ppy-CS -Fe_3O_4 and Ppy-CS-TiO_2 nanocomposite can be determined. Figure 3.4 shows the HR-TEM microscopy instrument.

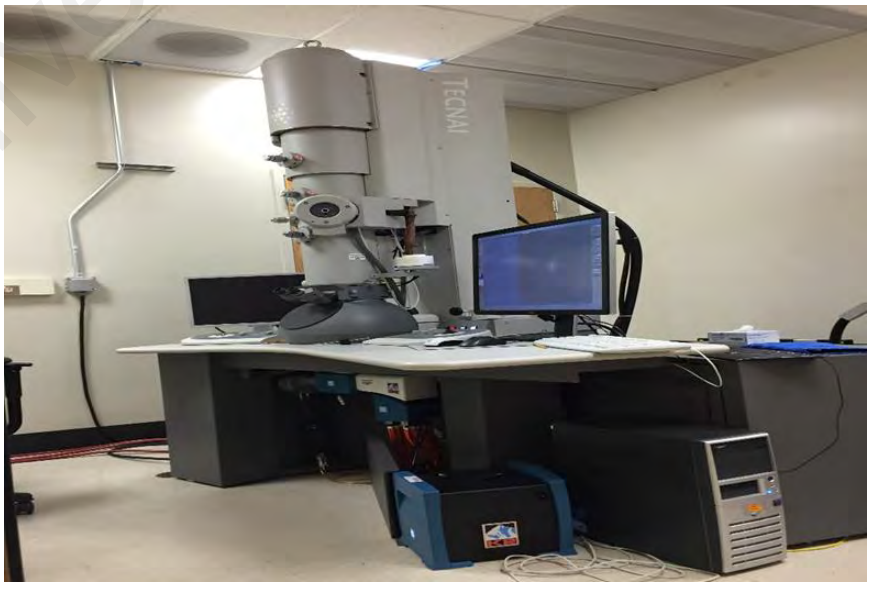

Figure 3.4: Schematic diagram of High-resolution transmission electron microscopy (HR-TEM).

3.11 X-ray Diffraction (XRD)

To examine and determine the physical properties of different solids like polymer materials and metals, one of the powerful methods is XRD (X-ray diffraction). X-ray diffraction (XRD) is extremely valuable to determine the crystallity of the samples, confirm its phase, and measure the average crystallite size.

Modern computer controlled diffractometer systems use automatic routines to measure record and interpret the unique of diffract to gram produced by individual constituents in even highly complex mixtures. Figure 3.6 shows the D8 Advance X-Ray Diffractometer. It has the ability to perform very rapid phase identifications of powdered specimens in a fully automated mode. The XRD analysis was performed using a Bruker X-ray diffraction model D-8 (made in Germany) equipped with EVA diffraction software for data acquisition and analysis. Data were acquired using CuKα monochromatized radiation using source operated at 40 kV and 40 mA at ambient temperature.

X-ray diffraction characterization was carried out on the Ppy-CS-Fe_3O_4, Ppy-CS-TiO_2 nanoparticle and Ppy-CS composites films by using CuKα radiation source (λ= 1.5418 Å). For all composite samples, a vast range of 2θ was scanned from 4º to 80º with a scanning step of 0.03 s^{-1}. The foundation of diffraction is Bragg's law (Cullity & Graham, 2008):

$$n\lambda = 2\mathrm{d}\sin\theta \qquad (3\text{-}1)$$

Where λ is the wavelength of the X-ray beam, d is the lattice spacing and θ is the angle of the beam with respect to the plane of the lattice, and n is the order of the lattice plane. When a wavelength of the x-ray with a specific angle enters, and collides with a crystal, a coherent diffraction of ray segment will be created by the lattice planes and the

dispersed rays jointly strengthening each other to create a signal peak. This is shown schematically in Figure 3.5. The instrument of XRD is shown in Figure 3.6.

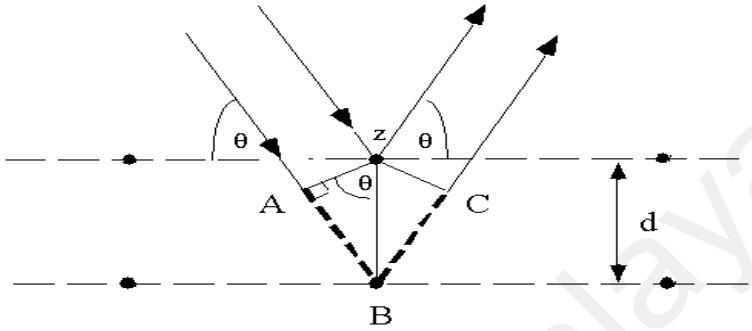

Figure 3.5: The X-ray beam striking the surface.

Figure 3.6: Schematic diagram of X-ray diffraction.

3.12 X-ray photoelectron spectroscopy (XPS)

Wide scan spectra and core level spectra were obtained for Ppy-CS-Fe_3O_4, Ppy-CS-TiO_2 nanoparticle and Ppy-CS composites films surfaces using X-ray photoelectron spectroscopy (XPS). X-ray photoelectron spectroscopy (XPS) brand (ULVAC-PHI Quantera II (Ulvac-PHI, INC. with a hemispherical analyser, a multichannel detector

and a monochromatic Al-Kα source; 1486.6 eV). Spectra were accumulated at a take-off angle of 90° with a 0.9 mm 2 spot size at a pressure of less than 1×10^{-8} mbar. Survey scans (0−1000 eV) were carried out at a 1.0 eV step size, 100 ms dwell time, and 100 eV analyser pass energy. High-resolution scans (S2p, C1s, and N1s) were performed using a 0.1 eV step size, and 20 eV pass energy. Binding energies of elements were adjusted with reference to the C1s peak of graphitic carbon (284.4 eV). Operated at 25.6 W (beam diameter of 100 μm). Wide scan analysis was performed using a pass energy of 280 eV with 1 eV per step.

Narrow scan (chemical states analysis) was performed using a pass energy of 112 eV with 0.1 eV per step. Prior to de-convolution, charge correction was performed at C 1s by setting binding energies of C-C and C-H to 284.8 eV. The instrument of XPS is shown in Figure 3.7.

Figure 3.7: Schematic diagram of X-ray diffraction.

3.13 Electrochemical set-up for glucose sensing

All electrochemical measurements were performed using a computerized potentiostat Instrument (Model: DY2300), made by Digi-ivy, Inc.(USA) with software version DY2312X050A0149IR in amperometry mode. A conventional three-electrode system comprised of an ITO glass electrode as the working electrode (WE), graphite rode as a

counter electrode (CE) and Ag/AgCl as a reference electrode (RE), was used. They are immersed in a solution containing an analyte and a background electrolyte. The electrochemical information about the analyte in this study was extracted from the current flowing through the WE at a potential. During the data collection, the potential (E) of the WE is monitored with respect to constant potential of RE. The RE contains a chemical system of constant composition and known potential. Typically, the Ag|AgCl|KCl 3M system is selected as the RE because it is used for its reproducibility, reliability and convenience. In an electrochemical workstation, the voltage changes ensure that almost no current flows through the RE. To study the glucose biosensor and electrochemical behavior of fabricated composite and nanocomposite films, the cyclic voltammetric response of analyte is investigated by successively adding various concentrations of analyte into the background electrolyte. Amperometric biosensors' role is determined by the output of a current when a potential is applied between two electrodes. They usually have response times, dynamic ranges and sensitivities. Amperometric system includes a remotely located data receiving device, a sensor for producing signal indicative of a characteristic of a user and a source device as shown in Figure (3.8). The sensitivity of electrochemical sensors was obtained by linear dynamic range (LDR) and limit of detection (LOD). The stability of the developed sensor was investigated by measuring its current response for glucose over ten days. The selectivity of the nanocomposite for the detection of glucose was examined by injecting three different interfering biomolecules, namely, uric acid (UA), ascorbic acid (AA) and cholesterol in the evenly stirred 0.1 M NaOH solution.

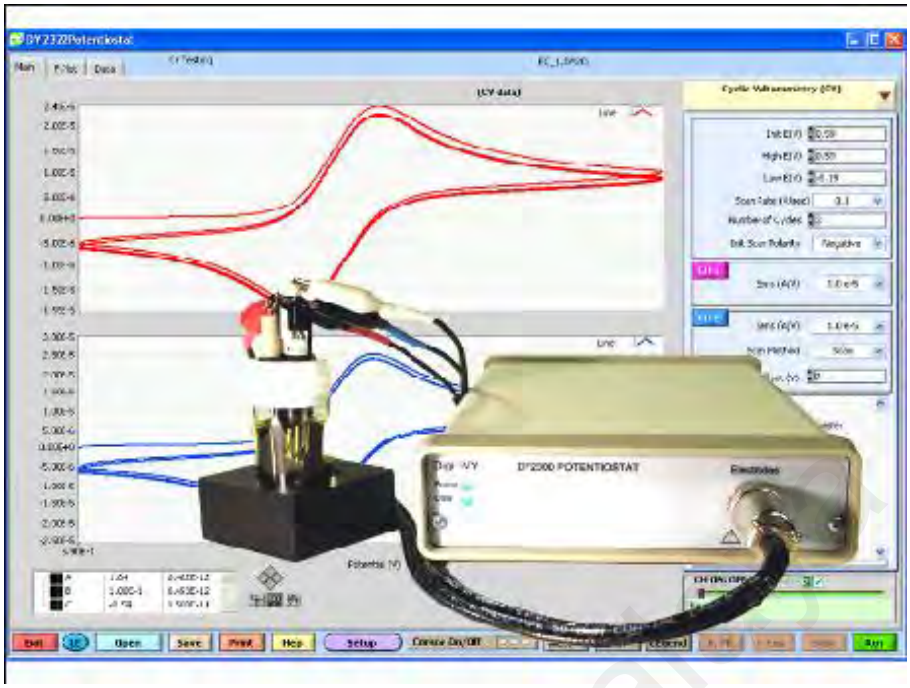

Figure 3.8: The instrument of electrochemical Setup.

3.14 Determination of detection limit

The detection limit of an individual analytical procedure is the lowest amount of analyte in a sample which can be detected but not necessarily quantitated as an exact value. The detection limit is determined by the analysis of samples with known concentrations of analyte and by establishing the minimum level at which the analyte can be reliably detected. Based on Signal-to-Noise (S/N), the determination of the signal-to-noise ratio is performed by comparing measured signals from samples with known low concentrations of analyte with those of blank samples and by establishing the minimum concentration at which the analyte can be reliably detected. The detection limit of an electrochemical method for determining the concentration of an analyte was calculated based on the reported method.

Based on the Standard Deviation of the Response and the Slope: The detection limit (DOL) may be expressed as following equation

LOD=3.0*Sb/m (3.2)

Where Sb = the standard deviation of the response

m = the slope of the calibration curve

The slope (m) may be estimated from the calibration curve of the analyte. The estimate of Sb may be carried out based on the calibration curve. A specific calibration curve should be studied using samples containing an analyte in the range of DOL. The residual standard deviation of a regression line or the standard deviation of y-intercepts of regression lines may be used as the standard deviation.

3.15 Determination of Quantification Limit (LOQ)

The quantification limit of an individual analytical procedure is the lowest amount of analyte in a sample which can be quantitatively determined with suitable precision and accuracy. The quantification limit is a parameter of quantitative assays for low levels of compounds in sample matrices, and is used particularly for the determination of impurities and/ or degradation products. Based on visual evaluation: The detection limit is determined by the analysis of samples with known concentrations of analyte and by establishing the minimum level at which the analyte can be quantified with acceptable accuracy and precision. Based on Signal-to-Noise the determination of the signal-to-noise ratio is performed by comparing measured signals from samples with known low concentrations of analyte with those of blank samples and by establishing the minimum concentration at which the analyte can be reliably quantified.

Based on the standard deviation of the response and the slope: The quantitation limit (LOQ) may be expressed as:

LOQ=10*3.0*Sb/m (3.3)

Where Sb = the standard deviation of the response

m = the slope of the calibration curve

The slope (m) may be estimated from the calibration curve of the analyte. The estimate of Sb may be carried out based on the calibration curve. A specific calibration curve should be studied using samples containing an analyte in the range of DOL. The residual standard deviation of a regression line or the standard deviation of y-intercepts of regression lines may be used as the standard deviation.

3.16 Electrochemical Impedance Spectroscopy (EIS)

The Electrochemical Impedance Spectroscopy (EIS) is a more general concept of resistance. In direct current (DC) circuits, only resistors oppose the flow of electrons. In alternating current (AC) circuits, the capacitors (impedance) influence the flow of electrons in addition to resistors. Electrochemical impedance spectroscopy is usually measured by applying an AC potential with small amplitude (5 to 10 mV) to an electrochemical cell and measuring the current flowing through the working electrode. The advantage of EIS is that the electrochemical cell can be modeled by using a purely electronic model. An electrode - electrolyte interface undergoing an electrochemical reaction is treated as an electronic circuit consisting of a combination of resistors and capacitors. EIS measurements provide information about the charge transfer dynamics and differences in the photoelectrochemical performance of the fabricated composite and nanocomposite films. To obtain the randles circuit parameters, the experimental data are fitted to the model circuit using the non-linear least-squares procedures which are available in the modern EIS software. Typically, the result of such fitting is presented in the form of the Nyquist plot. Such plot displays the kinetic control in the region of high frequencies and a mass transfer (Warburg diffusion) control at low frequencies. The charge transfer resistance of electrodes (Rct) is determined by measuring the diameter of a semicircle, which is proportional to the Rct.

CHAPTER 4: POLYPYRROLE-CHITOSAN COMPOSITE FILMS

4.1 Introduction

The electronically conducting polymers like polypyrrole, polyaniline, polythiophene etc. have established and consideration with many scientific research because of their interesting physical and electro conductive properties (Jin, *et al.,* 2002; González *et al.*, 2008). Among them, polypyrrole (Ppy) is the right electroactive polymer for medical applications. It is biocompatible and has antioxidant activity (George *et al.,* 2005). However, Ppy process ability problems because of its poor mechanical properties and high chemical sensitivity (Sangawar, & Moharil, 2012). Chitosan is a biopolymer that is biodegradable, biocompatible, nontoxic in nature (Portes *et al.,* 2009). However, this material possesses combination of properties required for biomedical applications. It shows antibacterial properties and has good membrane forming ability (Crini, 2005). The present chapter is focused on the synthesis and characterization of polypyrrole/chitosan (Ppy/CS) to design a product with good biocompatibility and enhanced properties for glucose sensors.

A method of conducting polymer composite film synthesis is reported here. First, chitosan was dissolved in slightly in acidic solution of acetic acid (1 %). During this process the polymer chains open up and the $–NH_2$ groups present in the chitosan chain become protonated ($-NH^{3+}$), changing to a poly cationic electrolyte. The prepared solution of Py-CS was taken in a glass cell for electrochemical deposition to produce polymer film composite on ITO glass electrode by cyclic voltammetry at the potential range of -1 to 1.2 V (vs Ag/AgCl) with the scan rate of 50 mV/s, the reactant composition was added with *p*-toluene sulphonate (*p*-TS) as a dopant to carry out for of polymerization process. The composite films were then washed repeatedly with distilled water to remove any unbound particles and later dried at room temperature then used

this film for characterization and application. The schematic of the Ppy-CS/ITO composite film is shown in figure (4.1).

For comparison purposes, the film formed from chitosan and Ppy, and the film without chitosan were prepared. The composite films were then washed repeatedly with distilled water to remove any unbound particles and later dried at room temperature then used this film for characterization and application. The composite films of Ppy-CS/ITO were characterized by Fourier transform infrared spectroscopy (FTIR), X-ray diffraction technique (XRD), Field emission scanning electron microscopy (FESEM), High-resolution transmission electron microscopy (HR-TEM) and X-ray photoelectron spectroscopy (XPS). The composite films of Ppy-CS/ITO were studied for the electrochemical sensor based on non-enzymatic glucose.

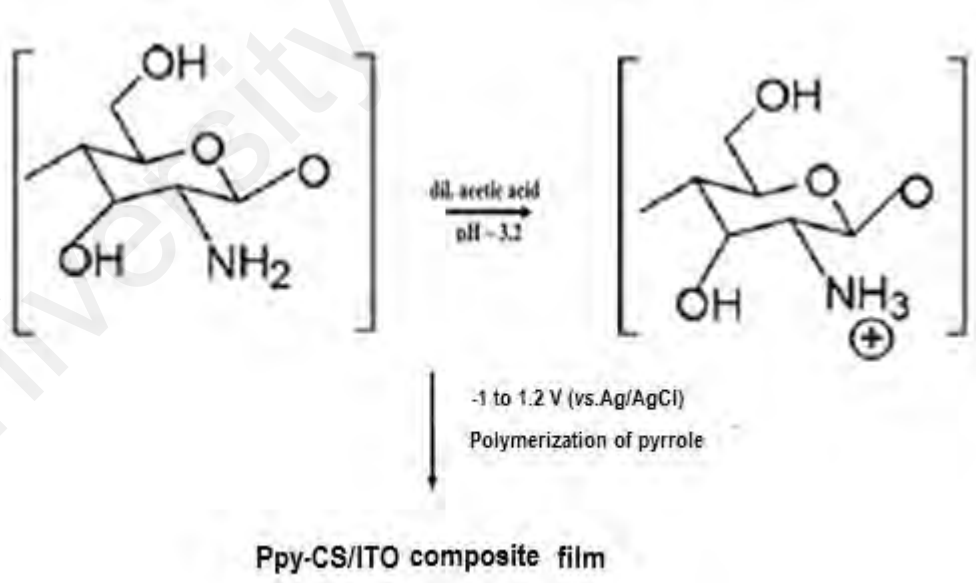

Figure 4.1: Schematic presentation of the Ppy-CS/ITO composite film.

4.2 Results and discussion

4.2.1 FTIR characterization of Ppy-CS composite film

Figure 4.2 shows the FTIR spectra of chitosan and Ppy-CS composite film. The FTIR spectrum of chitosan shows a broad band at 3150-3700 cm^{-1} due to axial stretching of O-H and N-H bonds. A peak at 1630 cm^{-1} is presented to amide group and peaks at 1446 cm^{-1} and 1378 cm^{-1} is the result of coupling of C-N axial stretching and N-H angular deformation. The stretching vibration of C-O-C linkage in the glucosamine rings peaks appear at 1055 cm^{-1}, 1030 cm^{-1} and 980 cm^{-1} The FTIR spectrum of PPy-CS composite exhibits a broad band at 3571 cm^{-1} due to the N-H stretching of pyrrole and O-H stretching of chitosan. The typical peaks of polypyrrole at 1580 cm^{-1} (C=C benzoic form), 1420 cm^{-1} (C-N stretching) was confirmed (Li *et al.,* 2006; Yoon & Jang, 2009). The peak at 1320 cm^{-1}, which is assigned to the –C–O stretching mode of $–CH_2–OH$ groups in CS, has shifted to lower wave numbers in Ppy-CS composite film. A peak around 1006 cm^{-1} is related to the C–O stretching of CS, which has overlapped with Ppy. The peaks at 1160 cm^{-1} (S-O stretching) and 1035 cm^{-1} (S-C stretching) confirm the formation of chitosan/polypyrrole composite doped with p-TS. (Abdi *et al.,* 2009; Guan *et al.,* 2009; Wang X, *et al.,* 2004). The additional peaks at 902, 768 and 670 cm^{-1} are due to the C-H out of plane deformation vibration of the ring. Some of the important FTIR spectra data shown in Table 2.

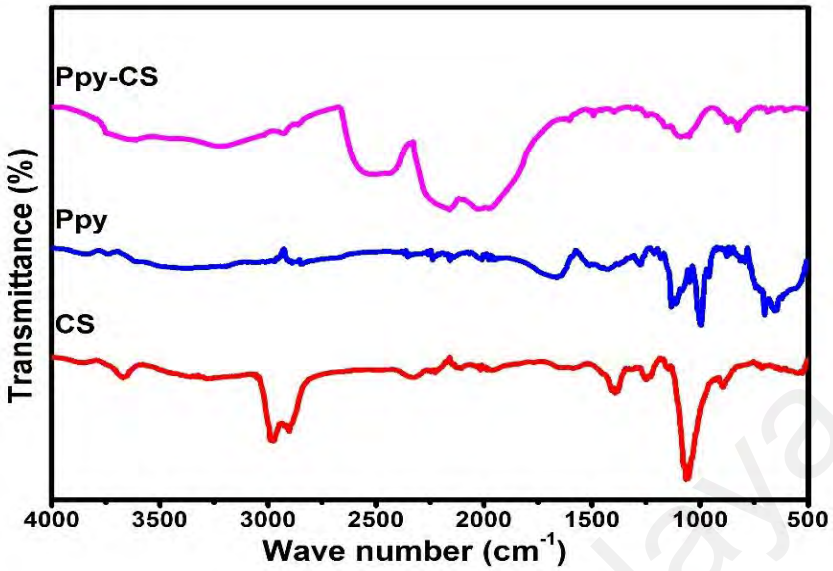

Figure 4.2: FTIR spectra of CS, Ppy and (Ppy -CS) composite film.

Table 2: FTIR spectra data Ppy-CS composite films.

Band Assignment	**Peak position (cm^{-1})**
–N–H stretching vibration	3571
–C–H stretching vibration	2340
–C–C stretching mode in pyrrole ring	1420
–C–N stretching mode in pyrrole ring	1478
–C–O stretching deformation	1006
–C–H in-plane deformation	1160
–C–H in-plane deformation	1035
–C–H out of plane deformation	902
–C–H waging vibration	768
-C-H vibration of the ring	670

4.2.2 XRD characterization of Ppy-CS composite film.

The XRD pattern (Figure. 4.3) of Ppy-CS composite showed a broad scattering peak at ~ 22° which shows the highly amorphous structure for Ppy/CS expanding from the Ppy chains close to the interplanar van der Waals distance for aromatic groups (Mitchell & Geri, 1987; Kassim *et al.,* 1992). The sharp crystalline peaks of chitosan are evident in Ppy-CS peaks with the shift in 2θ° to lower degree. This shift in 2 θ° value indicates the *d*-spacing increase in the Ppy-CS composite films.

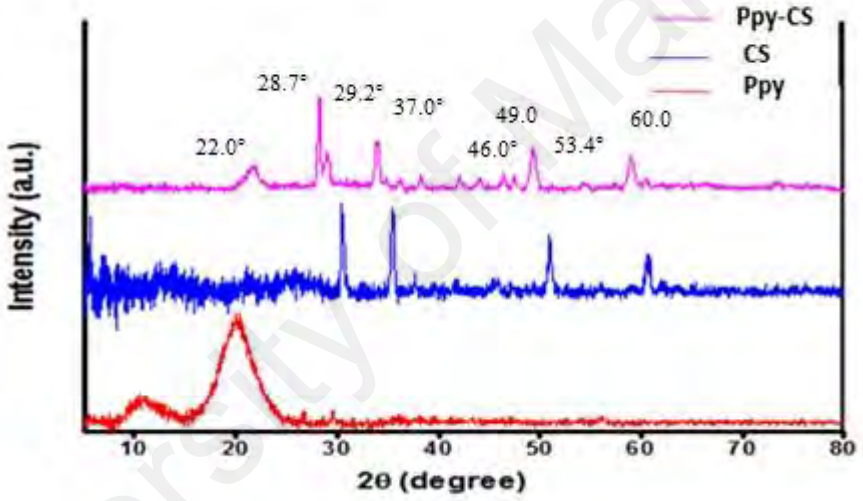

Figure 4.3: X-ray diffraction patterns of Ppy/CS composite, Ppy and CS

4.2.3 Morphology studies

The FE-SEM and HR-TEM images of Ppy/CS composite film are shown in Figure 4.4 (a) and (b) respectively. The FE-SEM image in Figure 4.4 (a) shows that the Ppy/CS film has small globular morphology with a large number spherical ball shapes of Ppy particles that were successfully covered with a thin layer of chitosan. with an average particle size of about 150 nm. Figure 4.4 (b) shows the TEM image of the Ppy-CS composites. It could be observed that the Ppy particles (in black) were well-dispersed in reticular CS polymer.

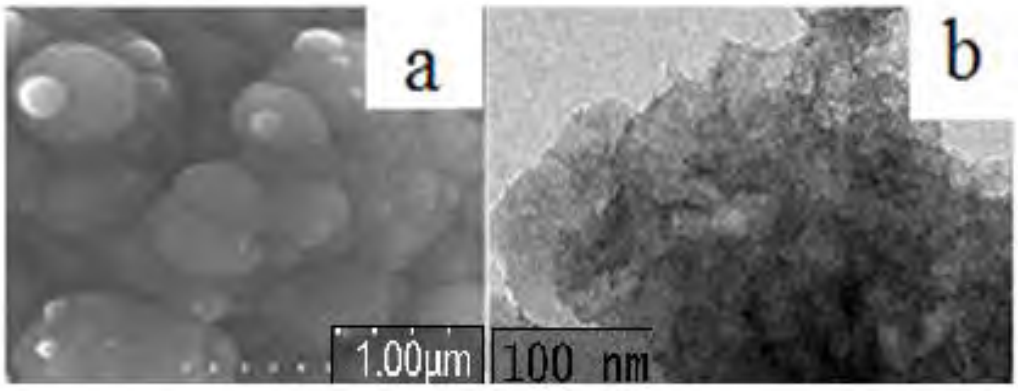

Figure 4.4: (a) FESEM and (b) HR-TEM images of (Ppy-CS) composite film.

4.2.4 XPS characterization

The XPS survey scan and narrow scan of Ppy–CS composite films was employed to identify and analyse the chemical components of the films as depicted in Figure. 4.5. The major peaks such as C 1s, O 1s, and N 1s were present in the curves for Ppy–CS composite films on the Ppy–CS composition. The background deduction was achieved with the shirley algorithm and the carbon C–C peak (C 1s, binding energy equal to 284.8 eV) was performed for a final calibration of each spectrum. The XPS wide-scan spectra is presented in (Figure. 4.5 a) and the XPS quantitative elemental analysis of narrows scan is presented in (Figure. 4.5 (b), (c) and (d) respectively. The results clearly show no contamination of the obtained structure with elements that could be extracted from the inner or outer electrode during the reaction process. It can be seen that characteristic peaks of carbon (C 1s), nitrogen (N 1s), and oxygen (O 1s) originate is from chitosan and polypyrrole compound in the samples. The main carbon peaks at 286.2 eV and at 286.3 eV in CS correspond to carbon bonded with both the hydroxyl group and nitrogen. In the carbon-related spectrum, two other significant peaks were appearing, which can be assigned to carbon to carbon single bonds (284.8) eV and carbonyl groups (approx. 287.8 eV), both are present in chitosan structure. Moreover, the minor peak in the position of approximately (289.0) eV is noticeable. This peak can be observed as unreacted acidic acid hydroxyl groups (-COO) bond (Lawrie *et al.,*

2007) The narrow scan and resolution (survey) spectrum of composites consists of observed Ppy has 3 peaks: C ls around (285) eV, N ls around (400) eV, O ls around (531) eV. The high-resolution spectrum, however, exposes at least two chemically different nitrogen‘s. The stronger peak at (399.8) eV can be assigned to neutral -N- whereas the higher binding energy peak at (401.0) eV is assigned to the oxidized -N^{+}- moieties. These values are considered for the conducting of Ppy associated well with the value obtained electrochemically (Kang *et.al.,* 1993).

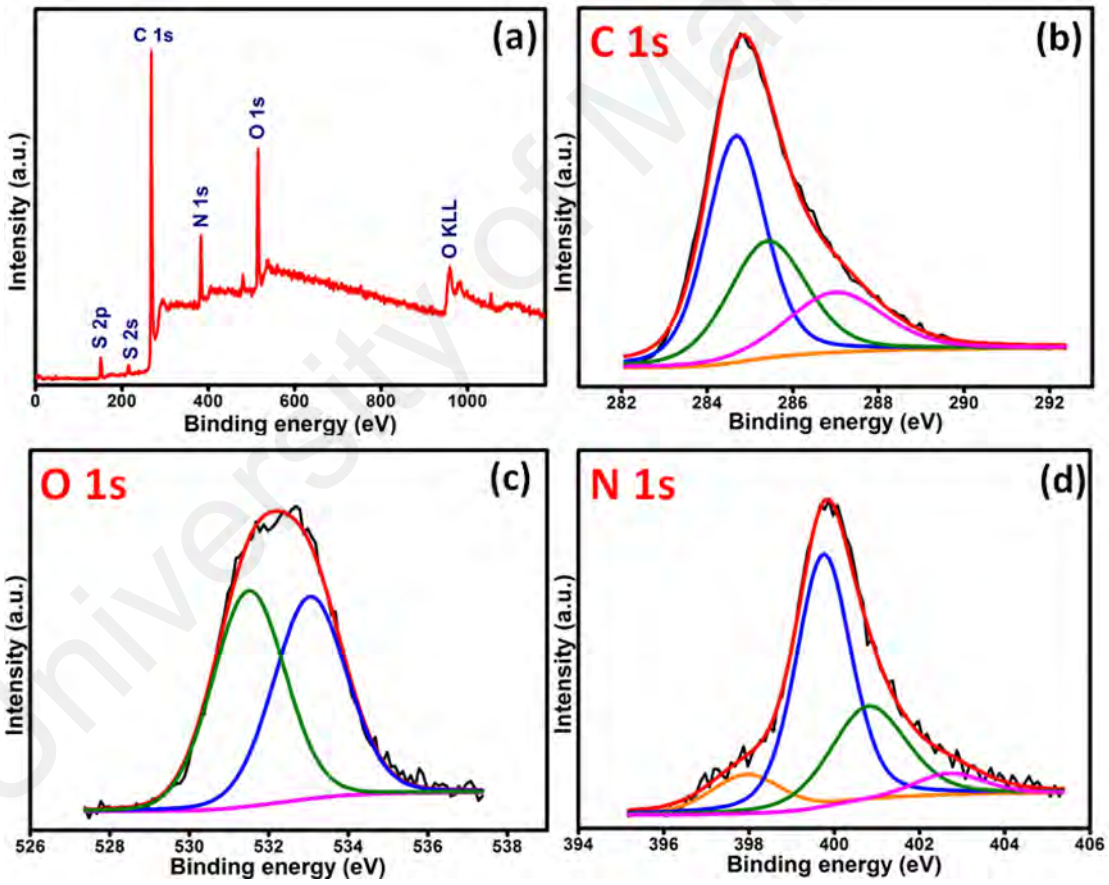

Figure 4.5: The XPS survey scan (a) and narrow scan (b, c, and d) of Ppy–CS composite films.

4.3 Glucose sensing performance of Ppy–CS composite film

4.3.1 The role of pH

The initial study shows that the non-enzymatic sensor has synergistic electrocatalytic activity to the oxidation of glucose. To enhance the electrocatalytic activity of PPy-CS composite for glucose sensing, an alkaline medium was required. When the concentration of 0.1 M NaOH (pH 13) was used, the current response was higher but, when a buffer of pH 10 was used, the current response for glucose oxidation was found low as can be observed in Figure 4.6. It is clearly shown that in alkaline media (Fig. 4.6 a), glucose is oxidized at a relatively low potential with enhanced current response. However, when pH is lowered, a positive shift in the oxidation potential was observed (Fig. 4.6 b). Hence, 0.10 M NaOH solution was selected as supporting electrolyte for the electrocatalytic oxidation of glucose.

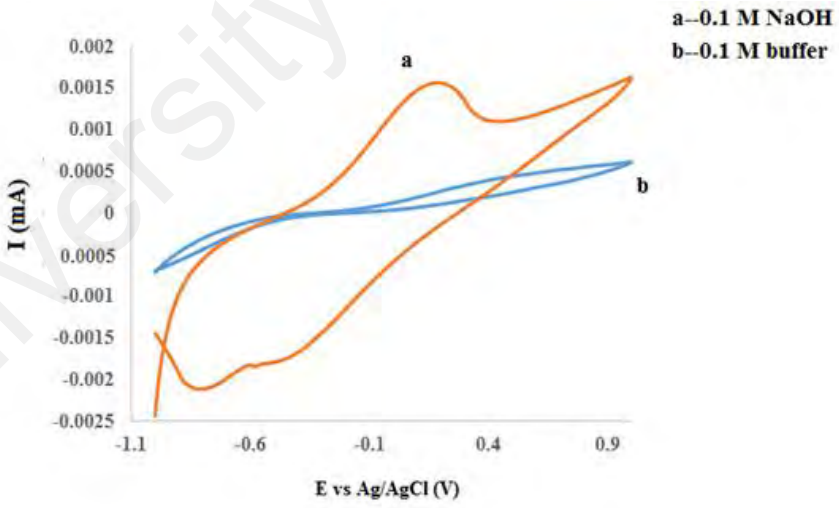

Figure 4.6: CV responses of composite film of Ppy–CS/ITO with 1mM glucose in 0.1M NaOH electrolyte (a) and in buffer electrolyte (b) at the scan rate of 50 mVs^{-1}.

4.3.2 Film deposition from various cycles

The composite films were electrochemically deposited on the ITO electrodes under multicyclic voltammetry (5, 10, 15 and 20). The potential window was scanned from -1.0 to 1.2 V (vs. Ag/AgCl) at a scan rate of 50 mV/s. The composite film of Ppy-CS formed from using 10 cycles of deposition shows higher current in 0.1mM glucose sensing than the composite films formed from 5,15, and 20 cycles as shown in Figure 4.7. The lower current response associated with films formed from 5 cycles maybe attributed to the lower content of polymer composite (Ppy-CS) for glucose oxidation. On the other hand, the films formed from 15 and 20 cycles are associated with high content of polymer composites with rough surface which hinder the oxidation of glucose exhibiting lower current response in 0.1M glucose sensing (Figure 4.7). Therefore, 10 cycles were chosen for the deposition of Ppy-CS films.

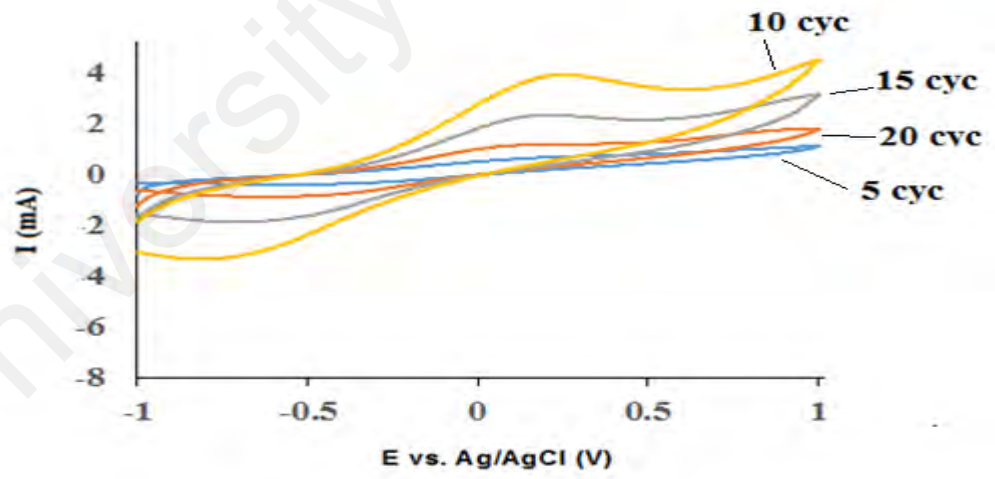

Figure 4.7: CV responses of composite films of Ppy–CS/ITO under multicyclic voltammetry deposition (5, 10, 15 and 20) with 1mM glucose in 0.1M NaOH at the scan rate of 50 mVs^{-1}.

4.3.3 Ppy-CS composite film for glucose sensing

The glucose sensing performances of Ppy-CS composite /ITO was carefully examined by cyclic voltammetry (CV) in Figure 4.8 with and without glucose in alkaline medium (0.1M NaOH) at the scan rate of 50 mVs^{-1}. The peak currents for Ppy-CS composite /ITO associated with the addition of 1 mM glucose indicate a good glucose sensing.

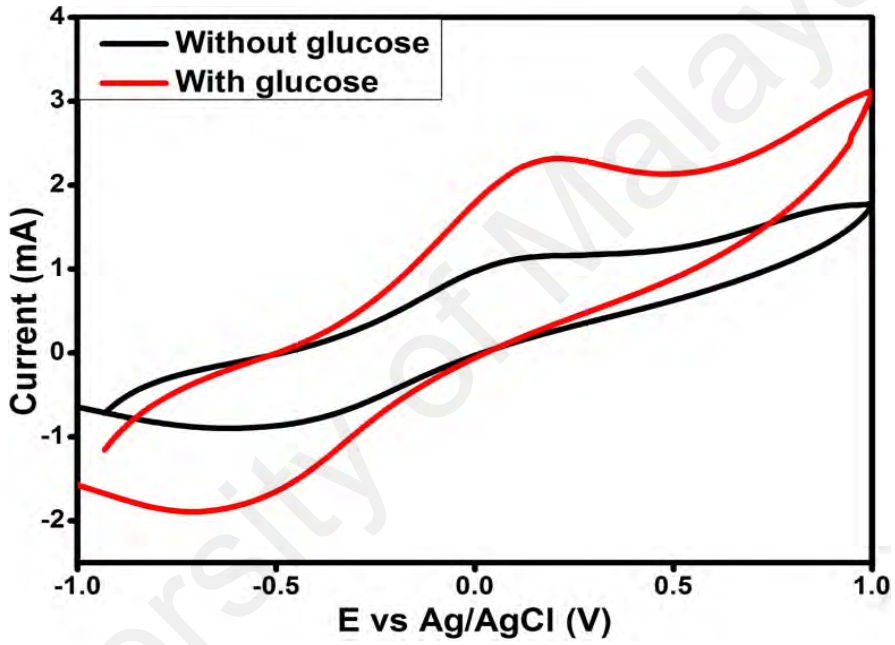

Figure 4.8: CV responses of Ppy-CS/ITO in 0.1M NaOH electrolyte with 1mM glucose and without glucose at the scan rate of 50 mVs^{-1}.

Figure 4.9 shows typical steady-state amperometric responses of Ppy-CS /ITO on successively increasing glucose concentrations at an applied potential of 0.18V (vs. Ag/AgCl). Ppy–CS composite /ITO shows linearly increased responses to the change of glucose concentrations while the current responses of Ppy–CS/ITO were observed and show increasing with the addition of glucose into the cell. The results are consistent with those obtained from cyclic voltammograms. The calibration curve for Ppy-CS

composite/ITO is presented in the inset of 4.9. The glucose sensors show linear dependence in the glucose on concentration of dynamic range of 1–16 mM with a correlation coefficient of 0.957, a sensitivity of 0.0084 mA cm^{-2} mM^{-1}, a detection limit (LOD) of 945 µM at single of noise (S/N=3), and determination of quantification limit (LOQ) value was 3156 µM. This novel Ppy–CS composite /ITO glucose sensor exhibits high sensitivity, low detection limit and fast response time at 3 second.

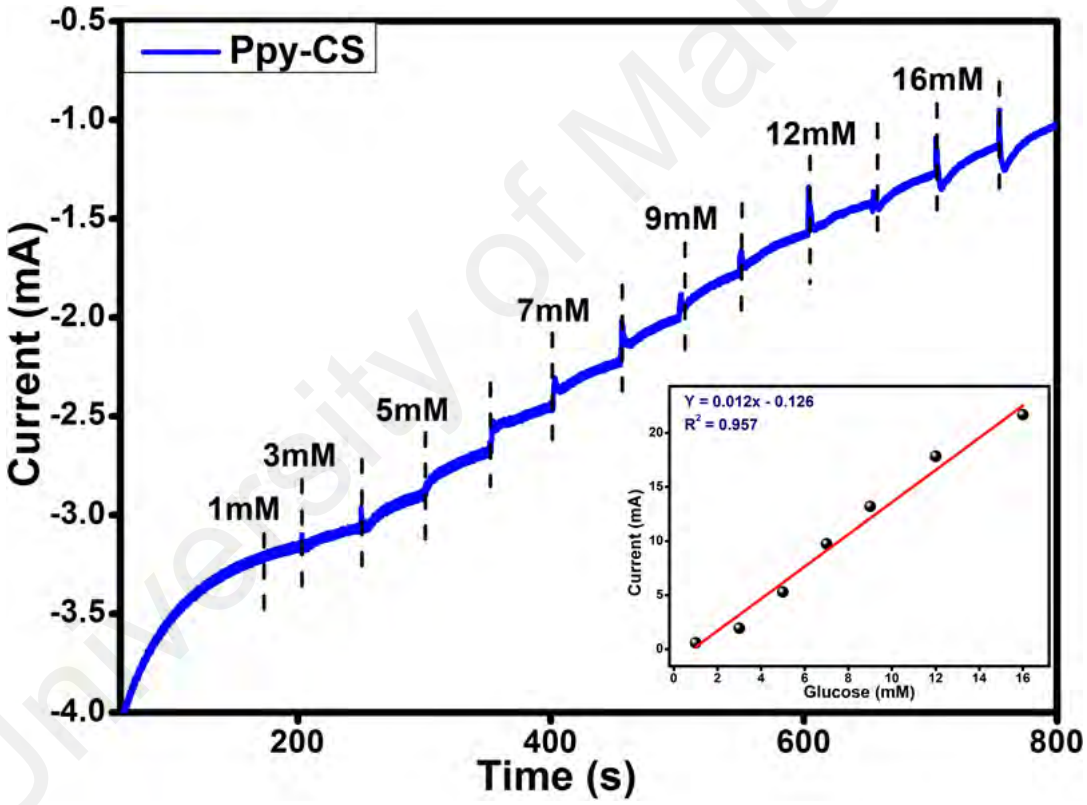

Figure 4.9: Amperometric responses to successive addition of glucose concentration in 0.1M NaOH solution at 0.18V (vs. Ag /AgCl). The inset shows the steady-state calibration curve for the of Ppy–CS composite /ITO electrode.

4.3.4 Electrochemistry of the redox marker $[Fe(CN)_6]^{3-/4-}$ and electrochemical impedance spectroscopy analysis

The study of the kinetic barrier of the electrode-solution interface, the redox behavior of the $[Fe(CN)_6]^{3-/4-}$ couple was used since the electron-transfer between the electroactive species in the solution and the electrode surface occurs by tunneling of electrons using the barrier, the defects or pinholes present in the barrier (Rubio *et al,* 2006). Fig. 4.10 shows the comparison of cyclic voltammetric responses obtained at the bare ITO, and Ppy-CS composite for 1 mM $K_3[Fe(CN)_6]$ in 0.1 M KCl at a scan rate of 50 mV s^{-1}. The bare ITO electrode shows a reversible voltammetric characteristic for the one electron redox process of the $[Fe\ (CN)_6]^{3-/4-}$ couple with the peak-to peak separation of 80 mV at a scan rate of 50 mV s^{-1}. The redox peak currents a peak to peak of Ppy-CS composite electrode shows separator enhance of 124 mV specially when compared to bare ITO. The high conductivity of Ppy made the electron transfer which was more facilitated at composite electrode and thus showed a higher peak current of oxidation and reduction peaks values (480 μA and -500 μA) respectively. It was clearly found that the composite electrode performs as has a new electrode surface, due to the effect of Ppy that increased electrocatalytic activity and therefore showed a good electrical communication with the original electrode surface.

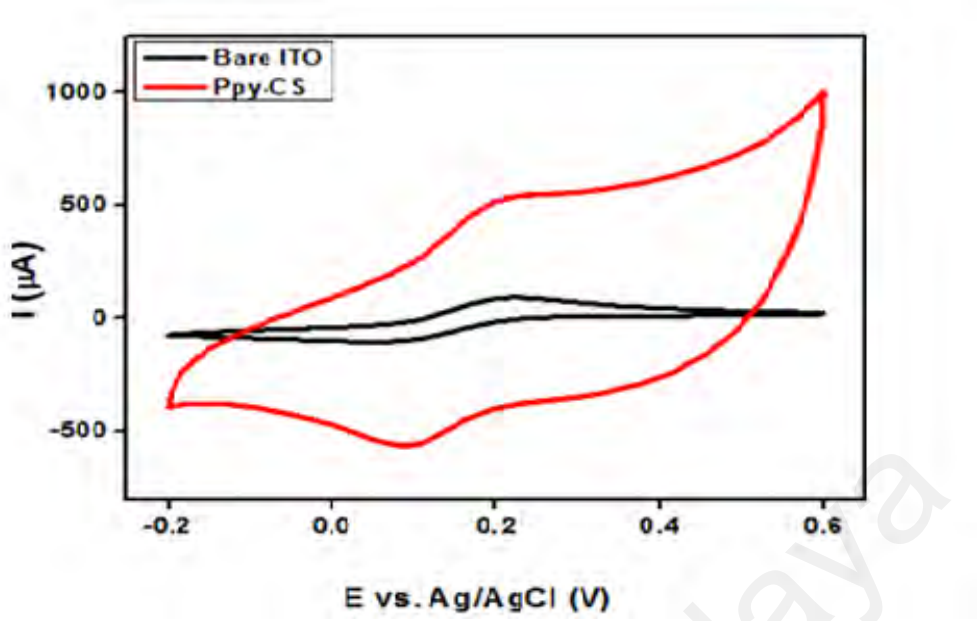

Figure 4.10: Cyclic voltammograms obtained for bare ITO, Ppy-CS composite for 1 mM K_3 [Fe (CN) $_6$] in 0.1 MKCl at a scan rate of 50 mV s^{-1}.

The interfacial properties of composites electrode were studied by electrochemical impedance spectroscopy (EIS) and determined for 1 mM $[Fe(CN)_6]^{3-/4-}$ in 0.1 M KCl at all electrodes in Figure. 4.11 (Choi *et al.,* 2012). The Nyquist graph of the complex impedance shows the imaginary versus the real part of the impedance, it observed the semicircle at higher frequencies corresponding to the electron transfer limited process and the linear portion at lower frequencies corresponding to the diffusion-limited process. The bare ITO electrode showed a semicircle-like shape Nyquist plot with a large diameter which suggests the hindrance to the electron-transfer kinetics at the electrode surface.

In case of Ppy-CS composite electrode there is no semi-circle was observed which shows the higher electron transfer kinetic. Additionally, it showed only the linear portion at lower frequencies indicating the diffusion-limited process at the electrode-solution interface. The diffusion-limited process was much more facilitated at the composite electrode due to the conducting performance of Ppy. A perfect linear portion was observed at lower frequencies for the composite electrode when compared to ITO

electrode. These results indicate that the Ppy-CS composite was positively formed and it facilitated a diffusion-limited process at the electrode-solution interface.

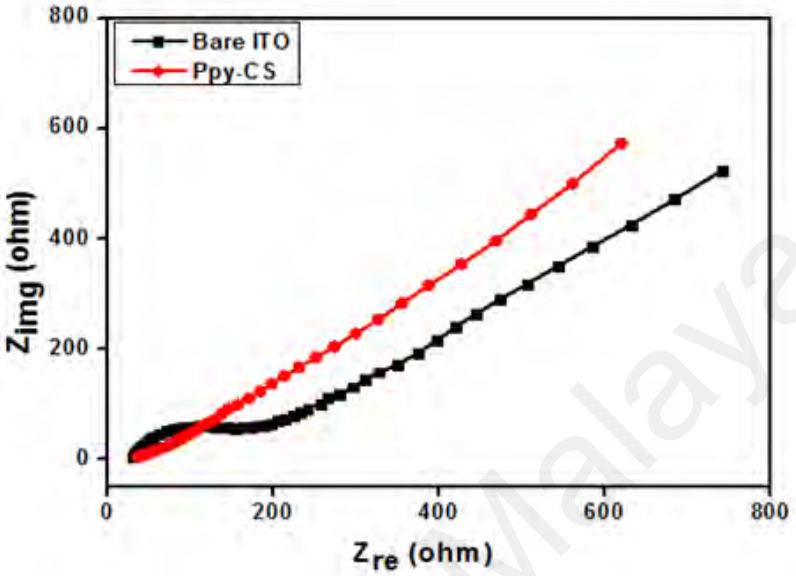

Figure 4.11: Nyquist plots obtained for bare ITO, Ppy-CS composite electrodes for 1mM $K_3[Fe(CN)_6]$ in 0.1 M KCl.

Bode-phase plots of the composite electrodes were studied in the frequency range of 0.01–10000 Hz (Fig.4.12). The phase peaks appeared at a frequency range of 100-10000 Hz corresponded the charge-transfer resistance of the composite electrodes. The shifting of peaks toward the low frequency region of 1-0.01 Hz for composite electrodes attribute to the fast electron-transfer performance of composites. The conductivity of Ppy present in the composite electrode facilitates the peak shifting in the Bode plot. Fig.4.13 shows the Bode impedance plot of the composite electrode and presented a lesser log Z value in a low frequency range of 1-100 Hz when compared to bare ITO electrode

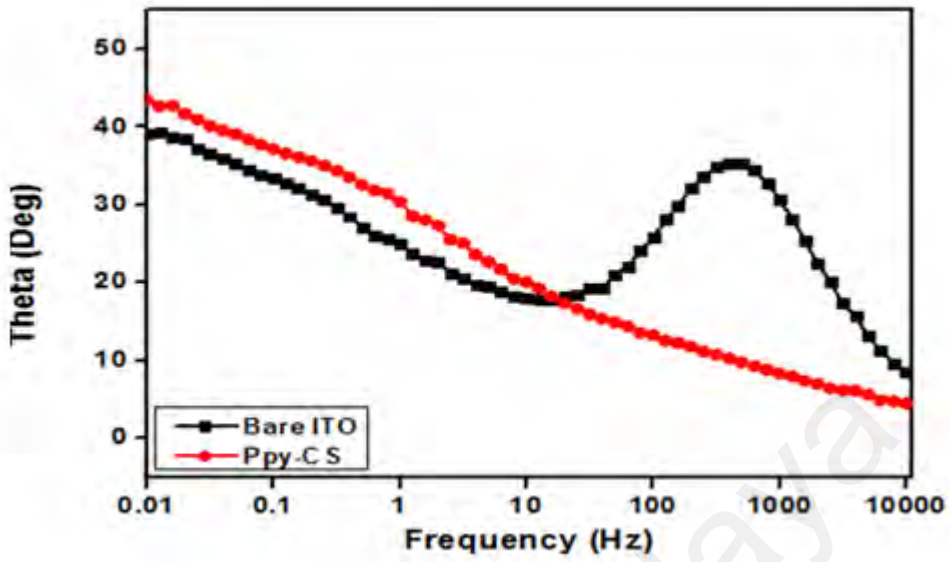

Figure 4.12: Bode phase plots obtained for bare ITO, Ppy-CS composite for 1x 10^{-3} M $K_3[Fe(CN)_6]$ in 0.1 M KCl.

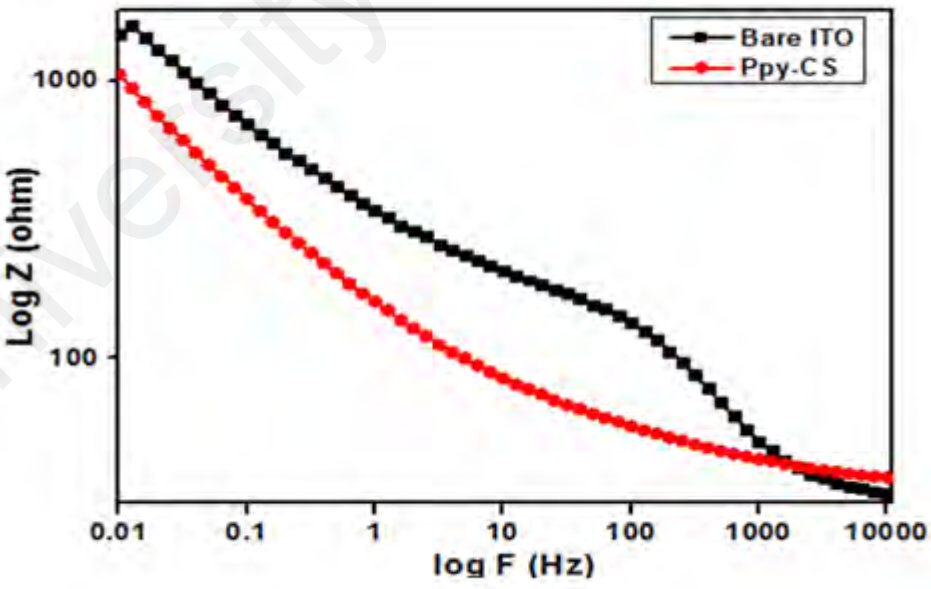

Figure 4.13: Bode impedance plots obtained log Z for bare ITO, Ppy-CS composite for 1 x 10^{-3} M K_3 [Fe (CN) $_6$] in 0.1 M KCl.

4.4 Conclusion

The preparation of Ppy-CS composite films as a non-enzymatic glucose sensor by one-step electrochemical technique is described in this chapter. The characterization of composite films by SEM and TEM images showed the small globular morphology with spherical ball and the particles well-dispersed in the polymer composite. The FTIR, XRD and XPS characterizations showed the evidence of confirmation of the formation of the composite films. The interfacial properties of the composite electrodes were considered by (EIS) that it was not semi-circle which shows the higher electron transfer kinetic. The electrocatalytic activity of composite film electrode was evaluated using amperometry by injecting glucose solution into the test solution. The response of the sensor towards glucose solution was good. The sensor has shown good sensitivity, linearity, wide detection range, and fast detection.

CHAPTER 5: POLYPYRROLE-CHITOSAN-IRON OXIDE NANOCOMPOSITE FILMS

5.1 Introduction

Organic–inorganic nanocomposite materials concerned extensive attention because of the possibility of combining the properties of organic and inorganic components. (Sanchez *et al.,* 2001; Mitzi, 2001). Conductive polymers and metal oxide nanocomposites have carried out more fields of application, such as biosensors, conductive paints, drug delivery, and so on (Tsai *et al.,* 2006; Butterworth *et al.,* 1995). Among the metal oxide nanoparticles (NPs), iron oxide (Fe_3O_4) NPs has been exploited as a potential material for numerous application of biosensor because of their unusual properties, including high surface area, high catalytic efficiency, nontoxicity, and chemical stability. Therefore, the bio nanocomposites designed by combining conducting polymers, and Iron oxide Fe_3O_4 NPs have all of the good properties of all constituents (Karaca *et al.,* 2015; Šafařík & Šafaříková, 2002). Among the different preparation methods, an important attention has been generated in the application of electrodeposition for the fabrication of nanocomposite films containing metal oxide NPs in a polymer matrix.

In the recent years, material scientists all over the world have used different preparative techniques like electrodeposition, sol-gel, vapor–liquid–solid, pulsed layer deposition, layer-by-layer method and thermal decomposition for the preparation of Fe_3O_4 nanoparticles. Compared with other procedures such as layer-by-layer self-assembly, electrodeposition recommend the advantages of higher deposition rate, shorter processing time, and the possibility of the deposition of thick films at room temperature. Moreover, uniform films of controlled composition with complex shapes can be found on the selected areas of the substrates. The fabrication of composite films can be

accomplished by electrochemical co deposition of organic and inorganic components (Zhitomirsky, 2006).

Metal oxides such as nickel oxide, copper oxide, iron oxide, zinc oxide and so on catalyze the oxidation of glucose in their native form or in modified forms were reported. Out of all these materials, iron oxide particles can be used for direct electrocatalytic oxidation of glucose. The advantage is its low cost, strong superparamagnetic property, easy preparation and use as several types of sensors (Willner &Willner, 2002). This chapter describes the development, characterization and application of nanocomposite film from polypyrrole-chitosan- iron oxide nanoparticles on electrode for the detection of glucose sensor. The developed electrode was characterized for its morphology, surface composition and tested for its potential to use as an amperometric glucose sensor. Its application was extended to test the glucose concentration for non-enzymatic glucose sensor.

A method of conducting polymer nanocomposite film synthesis and preparation are reported here. According the of earlier research (Karaca *et al.,* 2015) Fe_3O_4 nanoparticles were dispersed into 25 mL of CS (50 mg/mL) solution in acetic acid under continuous stirring at room temperature after which it was sonicated for about 2 h to obtain a viscous solution of CS with uniformly dispersed Fe_3O_4 nanoparticles. Later the solution of pyrrole (0.1M) and *p*-TS (0.3M) was added to the slurry of CS and iron oxide and was stirred for 5 minutes. The prepared solution of Ppy-CS- Fe_3O_4 nanocomposites was taken in a glass cell for electrochemical deposition of the film on ITO glass electrode by cyclic voltammetry using three electrode systems. The nanocomposite films were then washed repeatedly with distilled water to remove any unbound particles and later dried at room temperature then used this film for characterization and application.

5.2 Mechanism for the formation of Ppy-CS-Fe_3O_4

Figure 5.1 shows the mechanism of electrochemical polymerization of pyrrole (Matyjaszewski, 2002). First, the oxidation of pyrrole monomer occurs to form a radical cation followed by the coupling between two radical cations to form the dication. The loss of two protons then forms the aromatic dimer. The polymerization reaction follows the oxidation of dimer into the cation radical. This way, the propagation continues following the same sequence: oxidation, coupling and rearomatization until the final polymer, long chain polypyrrole forms.

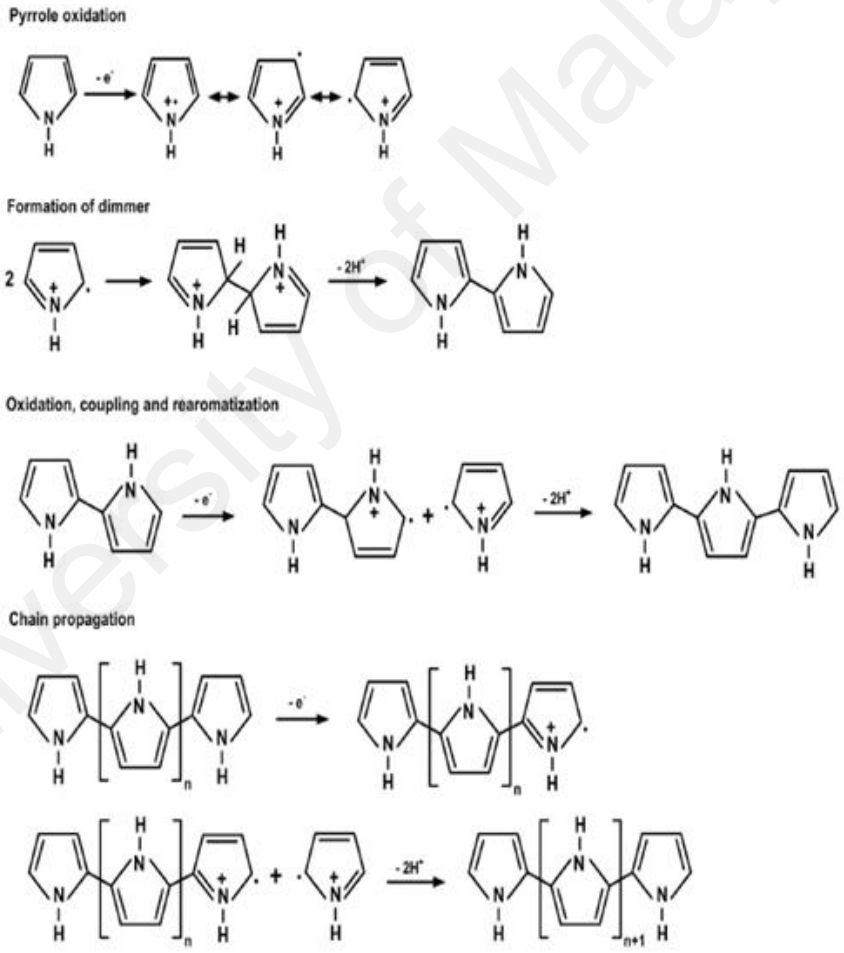

Figure 5.1: Electrodeposition mechanism of polypyrrole.

During the electrochemical formation of Ppy-CS–Fe_3O_4 nanocomposite films, polypyrrole is linked with CS-Fe_3O_4 through hydrogen bonding and iron-nitrogen ligand formation as shown in (Figure 5.2). The CS-Fe_3O_4 are linked with hydrogen bonding during ultra-sonication in the preparatory stage.

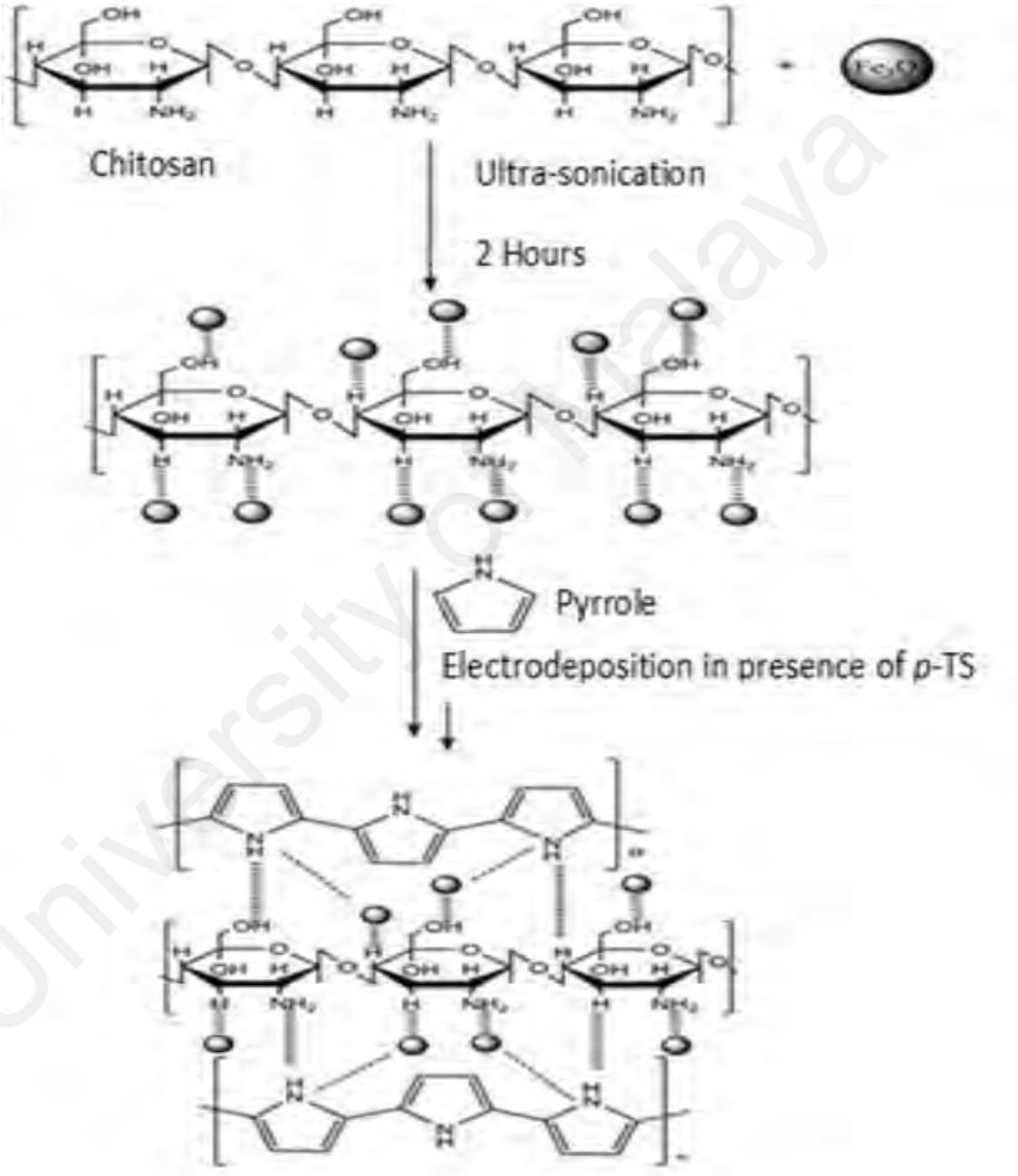

Figure 5.2: The formation of Ppy-CS-Fe_3O_4 nanocomposite films.

5.3 Results and discussion

5.3.1 FTIR characterization of Ppy-CS-Fe_3O_4 nanocomposites

Figure 5.3 shows the FTIR spectra of Ppy-CS-Fe_3O_4 nanocomposite, Ppy-CS composite film and Fe_3O_4 nanoparticles. The FTIR spectrum of Ppy-CS-Fe_3O_4 nanocomposite shows a broad band at 3700 cm^{-1} due to axial stretching of O-H and N-H bonds. A peak at 1630 cm^{-1} is presented to amide group and peaks at 1446 cm^{-1} and 1378 cm^{-1} is the result of coupling of C-N axial stretching and N-H angular deformation. The FTIR spectrum of PPy-CS composite exhibits a broad band at 3571 cm^{-1} due to the N-H stretching of pyrrole and O-H stretching of chitosan. The typical peaks of polypyrrole at 1580 cm^{-1} (C=C benzoic form), 1420 cm^{-1} (C-N stretching) was confirmed (Li *et al.,* 2006; Yoon & Jang, 2009). The peak at 1320 cm^{-1}, which is assigned to the –C–O stretching mode of $–CH_2–OH$ groups in CS, has shifted to lower wave numbers in Ppy-CS-Fe_3O_4 composite film. A peak around 1006 cm^{-1} is related to the C–O stretching of CS, which has overlapped with Ppy. The peak at 2700 cm^{-1} for Ppy-CS-Fe_3O_4 nanocomposite shows high intensity peak which is related with Fe_3O_4 nanoparticles. The peaks at 1160 cm^{-1} (S-O stretching) and 1035 cm^{-1} (S-C stretching) confirm the formation of Ppy-CS-Fe_3O_4 nanocomposite doped with *p*-TS. The additional peaks at 902, 768 and 670 cm^{-1} are due to the C-H out of plane deformation vibration of the ring. Some of the important FTIR spectra data shown in Table 3.

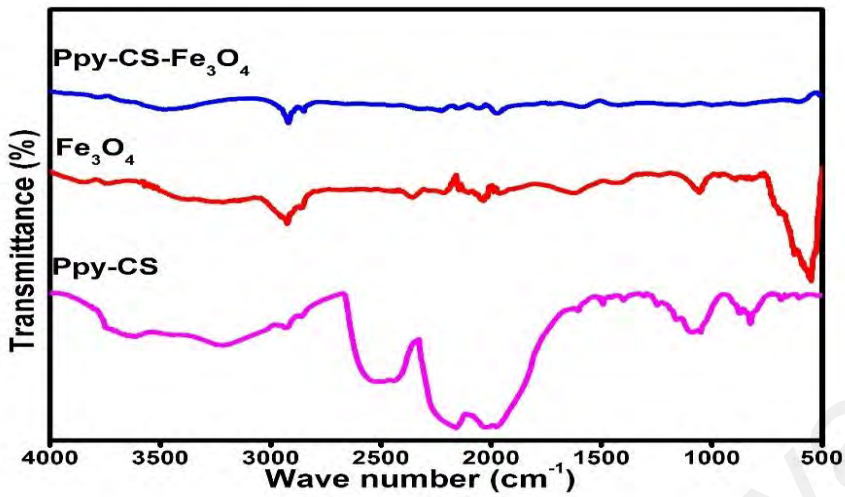

Figure 5.3: FTIR spectra of CS, Fe_30_4 and (PPy-CS-Fe_3O_4 nanocomposite.

Table 3: FTIR spectra data Ppy-CS-Fe_3O_4 nanocomposite film.

Band Assignment	**Peak position (cm^{-1})**
–N–H and -O-H stretching vibration	3700
–C–H stretching vibration	3000
–C–N stretching mode in pyrrole ring	1420
–C–OH stretching angular deformation	1320
–C–N stretching mode in pyrrole ring	1580
–C–O stretching deformation	1006
–C–H in-plane deformation	1160
–C–H in-plane deformation	1035
–C–H out of plane deformation	902
–C–H waging vibration	768
-C–H vibration of the ring	670

5.3.2 XRD characterization of Ppy-CS-Fe_3O_4 nanocomposites

The XRD pattern of Ppy-CS-Fe_3O_4 nanocomposite film shows abroad peak at ~ 22° indicating the amorphous form of Ppy-CS-Fe_3O_4 nanocomposite film The XRD pattern (Figure. 5.4) of Ppy-CS-Fe_3O_4 nanocomposite showed a broad scattering peak, which indicates a highly amorphous structure for Ppy-CS-Fe_3O_4 nanocomposite expanding from the Ppy chains close to the interplanar van der Waals distance for aromatic groups (Mitchell & Geri, 1987; Kassim *et al.,* 1992). Additionally, a broad peak at ~ 25° indicating the amorphous form of Ppy-CS-Fe_3O_4 due to crystalline of nanoparticle of Fe_3O_4. The sharp crystalline peak of Fe_3O_4 at 2 θ° value of 37° has shifted to 28° in Ppy-CS-Fe_3O_4 nanocomposite film. This lower shift of 2θ° values from 37 to 28 indicates the increased *d*-spacing due to the incorporation Fe_3O_4 in the nanocomposites.

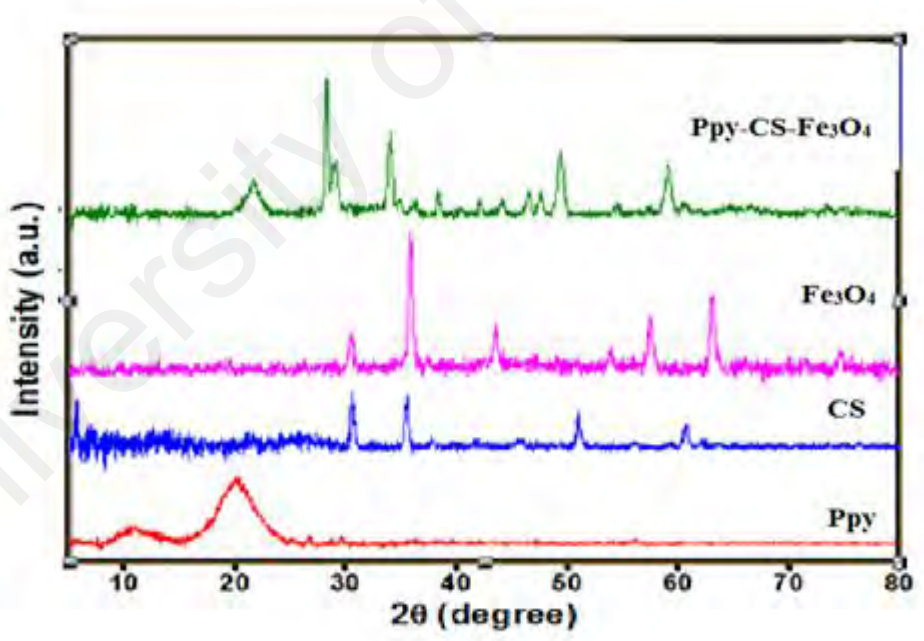

Figure 5.4:X-ray diffraction patterns of Ppy-CS-Fe_3O_4 nanocomposite, Ppy, CS, and Fe_3O_4.

5.3.3 Morphology studies

The FE-SEM micrographs of Ppy-CS and Ppy- CS-Fe_3O_4 nanocomposite are shown in (Fig. 5.5 a) and (Fig. 5.5 b), respectively. The changes in globular surface morphology reflects the successful incorporation of Fe_3O_4 nanoparticles into Ppy-CS films due to the electrostatic interactions between cationic CS and the surface charge of Fe_3O_4 nanoparticles producing Ppy- CS- Fe_3O_4 nanocomposite films. The EDX analysis of Ppy-CS- Fe_3O_4 nanocomposite shown in (Figure 5.5 c) clearly indicates the presence of (N, C, O, and Fe) components in the film. Based on the element analysis, it suggests that the Fe_3O_4 nanoparticles are incorporated in Ppy-CS composite.

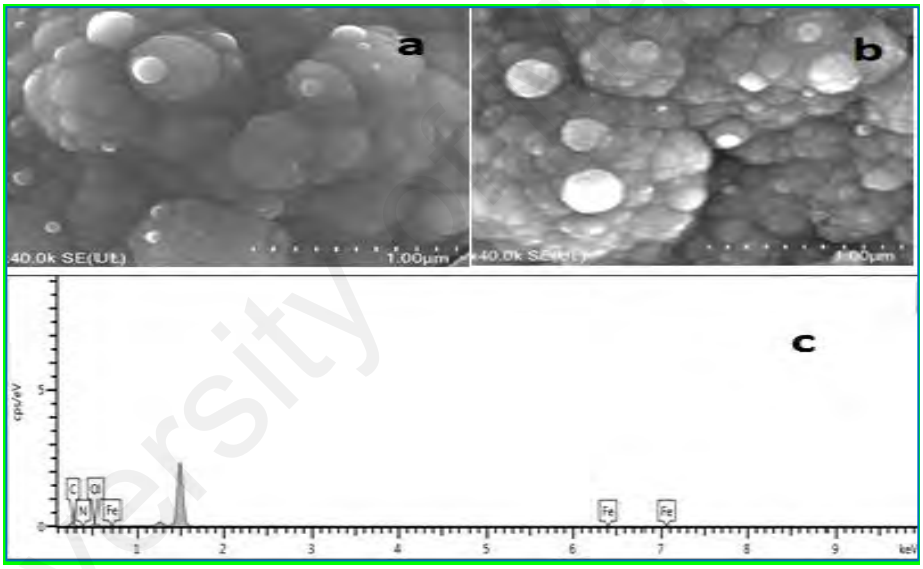

Figure 5.5: FE-SEM micrograph of (a) Ppy-CS, (b) Ppy-CS-Fe_3O_4, (c)The EDX analysis of Ppy-CS-Fe_3O_4 nanocomposite /ITO.

The size and dispersion of Fe_3O_4 nanoparticles and Py-CS-Fe_3O_4 nanocomposites were measured by HR-TEM in Figure 5.6 (a and b) respectively. Approximately spherical agglomerated particles were observed for Ppy-CS-Fe_3O_4 nanocomposites with the size ranging from 7 nm to 32 nm. The Fe_3O_4 nanoparticles were found to be spherical in shape in (Fig.5.6a) and the particle size distribution of Fe_3O_4 nanoparticles was narrow. The Py-CS-Fe_3O_4 nanocomposites were found to have typical core shell structure (Fig. 5.6 b). The darker Fe_3O_4 nanoparticle was seen as the core, whereas the gray colour

layer around it was the polymer. The mean size of Py-CS-Fe_3O_4 nanocomposites was bigger than the Fe_3O_4 nanoparticles, which clearly indicates the agglomeration of nanoparticles in the composites.

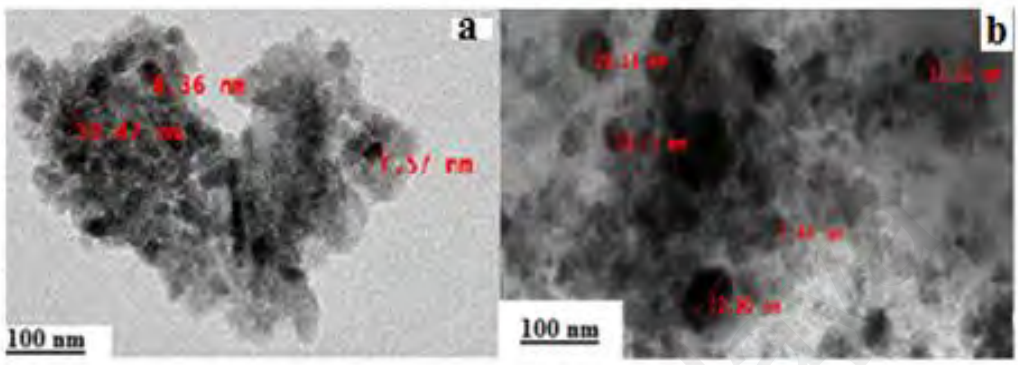

Figure 5.6: HR-TEM of Fe_3O_4 (a) and Ppy-CS-Fe_3O_4 nanocomposite films.

5.3.4 XPS characterization

The presence of Fe_3O_4 nanoparticles in the nanocomposite films was further confirmed by X-ray photoelectron spectroscopy (XPS). The XPS survey scan of Ppy-CS-Fe_3O_4 nanocomposite films was employed to identify and analyze the chemical components of the films as depicted in (Fig.5.7 a). As the peaks of Ppy-CS composite films in the previous chapter, the similar and major peaks such as C 1S, O 1S, N 1S were present in the curves for Ppy-CS Fe_3O_4 nanocomposite films (Fig.5.7 b, c, d, and e). New peaks located at the binding energies of 710 eV and 715 eV are assigned to Fe2p and Fe3p, respectively. In (Fig.5.7 a), the iron in Ppy-CS- Fe_3O_4 nanocomposite films clearly shows the linkage of Fe_3O_4 nanoparticles. These peaks of Fe2p and Fe3p are for Fe_3O_4 nanoparticles (Yamashita & Hayes, 2008; Cheng *et al.*, 2005).

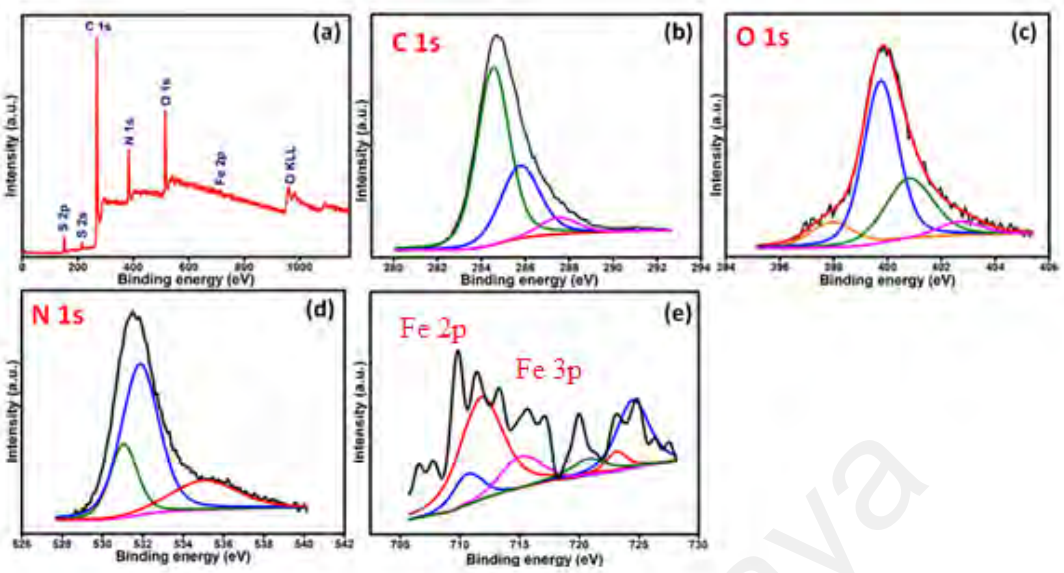

Figure 5.7: The XPS survey scan (a) and narrow scan (b, c, d, and e) of Ppy–CS Fe_3O_4 nanocomposite films.

5.4 Glucose sensing performance of Ppy–CS-Fe_3O_4 nanocomposite films

The glucose sensing performances of Ppy-CS-Fe_3O_4 nanocomposite deposition on ITO was examined by cyclic voltammetry (CV) with and without glucose in alkaline media (0.1M NaOH) at the scan rate of 50 mVs^{-1} as shown in figure 5.8. In presence of glucose the peak currents for Ppy-CS-Fe_3O_4 nanocomposite/ITO electrode were observed much higher than without glucose. Thus, Ppy-CS-Fe_3O_4 nanocomposite /ITO is acting as a good glucose sensor due to the glucose oxidation ability of Ppy-CS-Fe_3O_4 nanocomposite.

On the basis of the reported for glucose oxidation and our finding in this study, a possible catalytic of chemical equation for glucose oxidation at Ppy-CS-Fe_3O_4 nanocomposite is proposed as follows:

$$2Fe_3O_4 + C_6H_{12}O_6 \rightarrow 2Fe_3OOOOH + C_6H_{10}O_6 \quad (1)$$

glucose gluconolactone

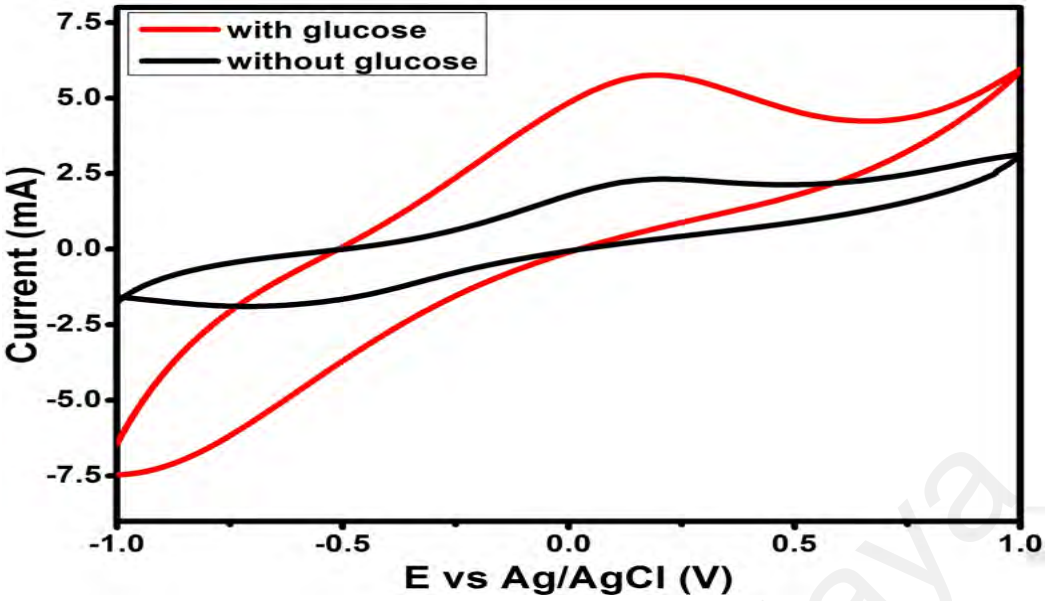

Figure 5.8: CV responses of Ppy-CS-Fe_3O_4 deposition on ITO in 0.1M NaOH electrolyte with 1mM glucose and without glucose at the scan rate of 50 mVs^{-1}.

5.4.1 Effect of Fe_3O_4 content in Ppy-CS-Fe_3O_4 nanocomposites film

The Ppy-CS-Fe_3O_4 nanocomposite films were electrochemically deposited on the ITO electrode using different ratios of Fe_3O_4 NP (0.5 %, 1%, 2%, and 3%) by cyclic voltammetry. The nanocomposite films were prepared at a scan rate of 50 mV s^{-1} using the potential window from -1.0 to 1.2 V (vs Ag/AgCl/3MKCl).

Figure 5.9 shows the linearly amperometric increased current response of the Ppy-CS-Fe_3O_4 electrode examined with several additions of (1,3,5,7,9,12,14,16) mM glucose (once every 50 s) spiked into 0.1 M NaOH solution into the cell. The response curve turns downward with increasing concentration because an increasing amount of intermediate species is adsorbed onto the electrode surface, prolonging the reaction time. The current observed for the electrode of Ppy-CS-Fe_3O_4 nanocomposite consisting of 1% Fe_3O_4 was found higher than the current for all other electrodes of Ppy-CS-Fe_3O_4 nanocomposite having different amounts of Fe_3O_4 contents (0.5 %, 2%, and 3%) for the current response of glucose Figure 5.9 (b). The current response of the performance of

glucose by the nanocomposite film containing the minimum amount of Fe_3O_4 (0.5%) appears to be less due to the low content of Fe_3O_4 NP. Increasing the amount of nanoparticles (2% and 3%) in the polymer composite make the polymer film surface heterogeneous and rough. This rough surface with high content of nanoparticles appears to be less effective in oxidation of glucose. The lower current response associated with the polymer nanocomposite electrodes containing 2% and 3 % Fe_3O_4 for the oxidation of glucose can be seen in Figure (5.9 c and d). It can be noticed that the current response for the electrode containing 0.5% Fe_3O_4 in the polymer composite is higher than the current response for the electrode containing of 2% and 3% Fe_3O_4 in the polymer composite for the oxidation of glucose (Fig.5.9).

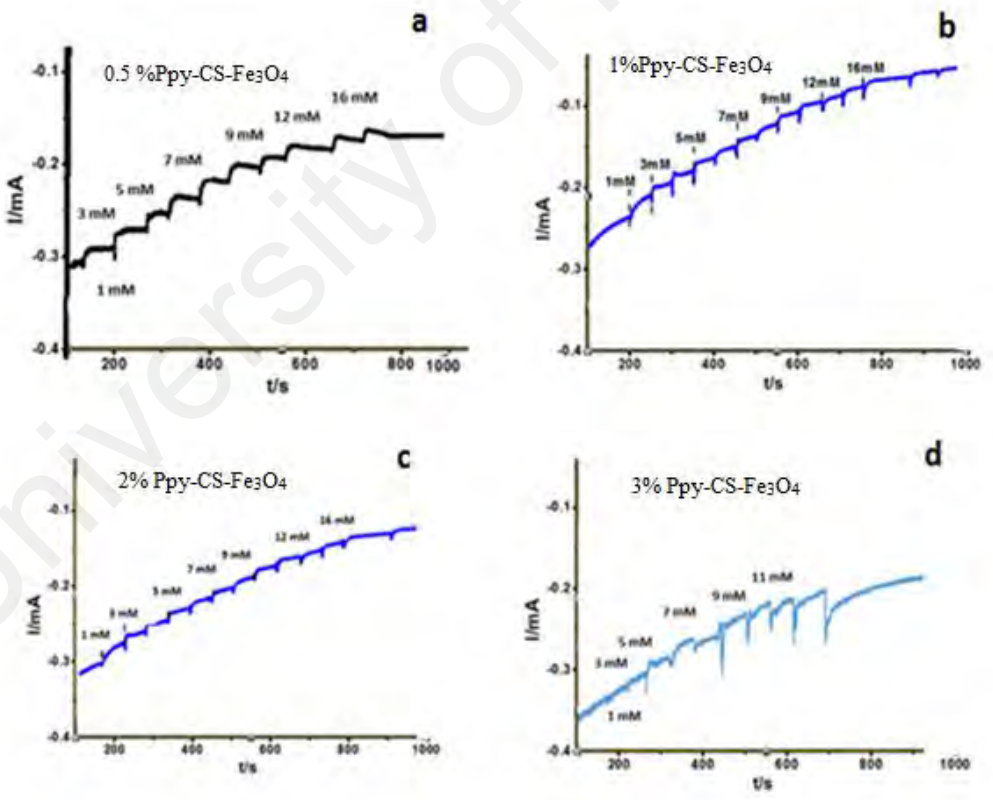

Figure 5.9: Amperometric response of examined of the Fe_3O_4 NP, (a) 0.5 %, (b) 1%, (c) 2%, and (d) 3 % of Ppy-CS-Fe_3O_4 electrode in 0.1 M NaOH with sequential additions of glucose concentration (1–16 mM) at scan rate of 50 mVs^{-1}.

Fig.5.10 shows typical steady-state amperometric responses of Ppy-CS-Fe_3O_4 nanocomposite /ITO (10 cycles) and Ppy-CS /ITO (10 cycles) on successively increasing glucose concentrations at an applied potential of + 0.18 V (vs. Ag/AgCl). Ppy-CS- Fe_3O_4 nanocomposite /ITO shows linearly increased responses to the change of glucose concentrations while the current responses of Ppy-CS/ITO were much lower and only show slight increase with the addition of glucose into the cell. The results are consistent with those obtained from cyclic voltammograms. The calibration curve for Ppy-CS- Fe_3O_4 nanocomposite /ITO is presented in the inset of Fig. 5.10. The glucose sensors show linear dependence in the glucose concentration of dynamic range of 1 to 16 mM with a correlation coefficient of 0.967, a sensitivity of 12 μAcm^{-2} mM^{-1}, and a detection limit (LOD) of 234 µM at signal of noise (S/N=3), and the determination of quantification limit (LOQ) value was 782.5 µM. This novel Ppy-CS-Fe_3O_4 nanocomposite /ITO glucose sensor exhibits high sensitivity, low detection limit and fast response time in less than 3 second.

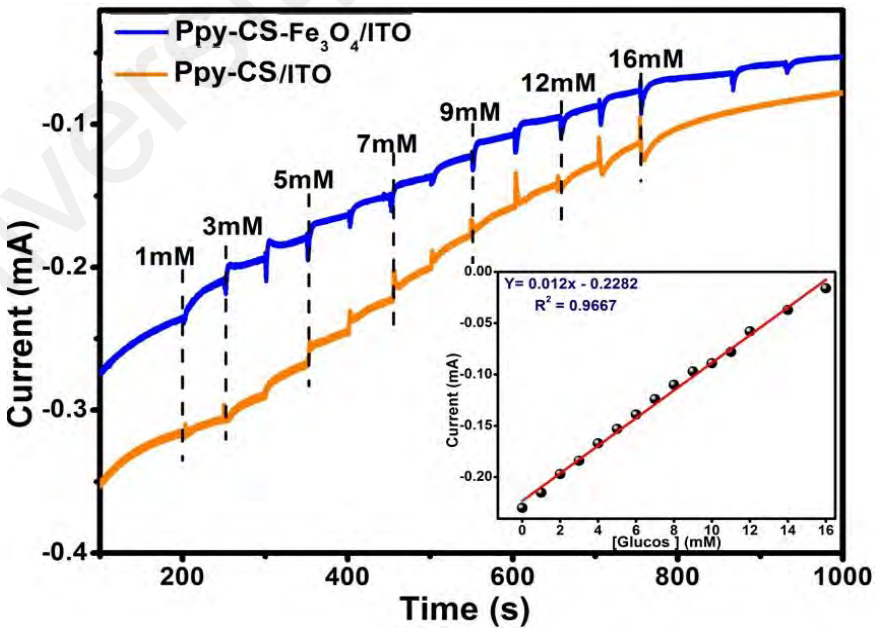

Figure 5.10: Amperometric responses to successive addition of glucose concentration in 0.1M NaOH solution at 0.18 V (vs. Ag/AgCl). The inset shows the steady-state calibration curve for the of Ppy-CS-Fe_3O_4 nanocomposite /ITO electrode.

The Ppy-CS-Fe_3O_4 nanocomposite films exhibited significant electrochemical performance towards glucose sensing. The limit of detection (LOD) of the developed sensor is comparable to the existing reports in the literature, which are summarized in Table 4.

Table 4: Comparison of LOD of the developed sensor with the existing reports in the literature

Electrode Material	Technique methods	Electrolyte	Linear range (mM)	Detection limit (µM)	References
Au/Nafion	Amperometry	0.1M NaOH	5.0–60	1200	Surareungchai *et al.*, (2001).
Layer-by-layerAu NPs/Au E	Nil	0.1M NaOH	Up to 8	500	Kurniawan *et al.*, (2006)
AuNPs/chitosan/GCE	Nil	PBS	0.4–10.7	370	Feng *et al.*, (2009).
AuRu NPs	Amperometry	0.1M NaOH	0–15	269	Yi *et al.*, (2010)
Ppy-CS-Fe_3O_4NP/ITO	Amperometry	0.1M NaOH	1–16	234	This work AL-Mokaram, A. *et.al.*,2016

NP: Nanoparticles; E: Electrode; GCE: Glassy carbon electrode

5.4.2 Glucose sensing by the electrode prepared from various cycles

Figure 5.11 shows the linearly increased current responses with several additions of (1, 3, 5, 7, 9, 12, 14, and 16) mM glucose (once every 50 s) spiked into 0.1 M NaOH solution into the cell. The current observed in Figure 5.10 for the electrode of Ppy-CS-Fe_3O_4 nanocomposite prepared by 10 cycles was found higher than the current for all other electrodes of Ppy-CS-Fe_3O_4 nanocomposite prepared by multicycles (5, 15, and 20 cycles) for the oxidation response glucose Figure 5.11. (Figure 5.11 a) The current response for the oxidation of glucose by the nanocomposite film prepared from 5 cycles appears to be lower due to the low content of thin deposition of the film. Increasing the multicycles (15 and 20 cycles) to produce the polymer composite, the film becomes

thicker with little rough surface making it less effective for glucose oxidation. The lower current response associated with the polymer nanocomposite electrodes prepared by 5, 15 and 20 cycles for the oxidation of glucose can be seen in Figure (5.11 a, b and c).

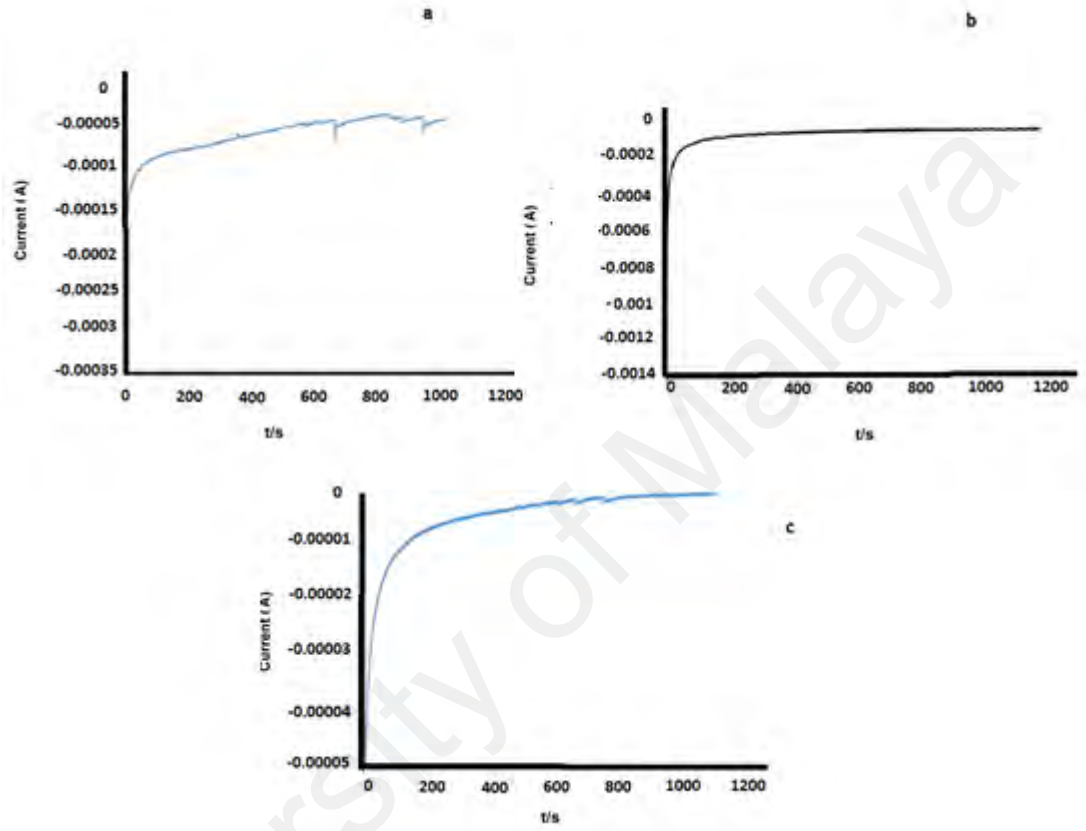

Figure 5.11: Amperometric response of examined of the Fe_3O_4 NP, (a).5 cycles, (b) 15 cycles (c) and 20 cycles of Ppy-CS-Fe_3O_4 electrode in 0.1 M NaOH with sequential additions of glucose concentration (1–16 mM) at scan rate of 50 mVs^{-1}

5.4.3 The stability study

The stability of the developed sensor was investigated by measuring its current response for glucose over ten days. The prepared Ppy-CS-Fe_3O_4 nanocomposite film on ITO was used to record the amparometric response for 1mM glucose on frequency of 2 days. Here, I_0 is the current response of fresh sensor and I is the current response after storage as shown in (Figure 5.12). During the first 6 days, the current response did not change

in a noticeable way, however at last day; the current response still remained above 90 % of its initial response, revealing the excellent stability of the sensor.

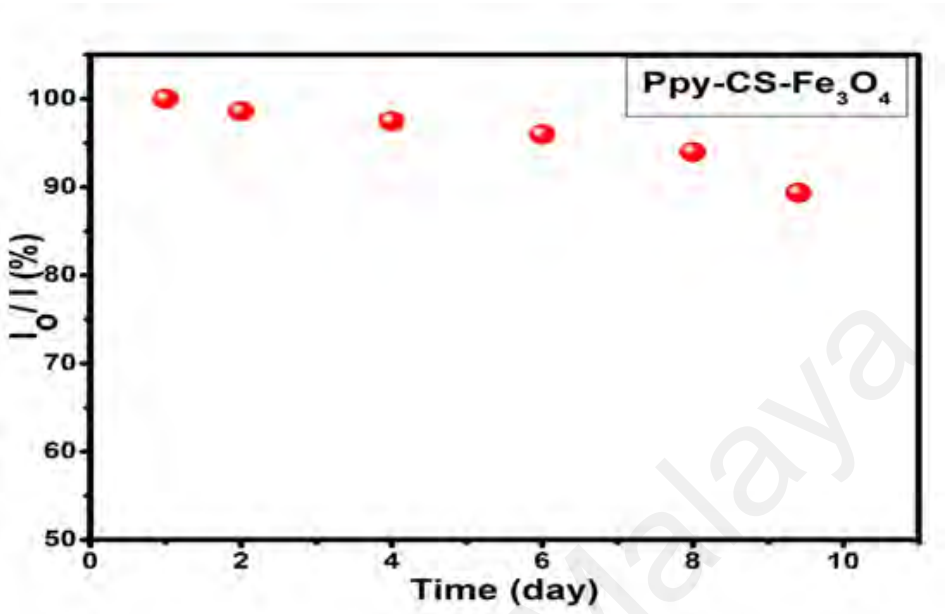

Figure 5.12: Stability of the sensor stored at ambient conditions over 10 days in 0.1 M NaOH glucose at potential of 0.18 V (vs. Ag/AgCl).

5.4.4 The interference study

The selectivity of the Ppy-CS-Fe_3O_4 nanocomposite /ITO for the detection of glucose was examined by injecting three different interfering biomolecules, namely, uric acid (UA), ascorbic acid (AA) and cholesterol (Ch) in the evenly stirred 0.1 M NaOH solution containing glucose. The current response was observed in Figure 5.13. It depicts the recorded amperometric response for the consecutive additions of glucose and interfering biomolecules. First, the consecutive injections of glucose (each of 1 mM) were used to record the current response. Then consecutive injections (each of 0.1 mM) of UA, AA and cholesterol followed by three injections (each of 1 mM) of glucose were used (sample time of 50 s) to study the interference. It was found that, the addition of interfering biomolecules did not contribute significant current response contrary to glucose which responded for each injection. These results revealed that the present

sensor possesses a good selectivity and sensitivity towards the detection of glucose even in the presence of common physiological interfering biomolecules.

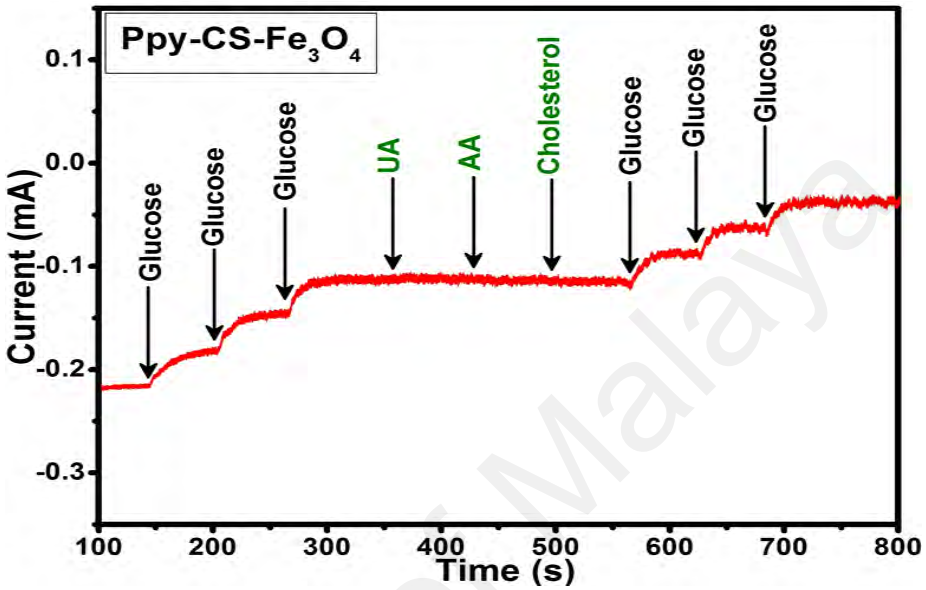

Figure 5.13: Amperometric responses obtained at successive addition of glucose and each of uric acid, ascorbic acid and cholesterol in 0.1 M NaOH solution at +0.18 V (vs. Ag/AgCl) with regular interval of 50 s.

5.4.5 Electrochemistry of the redox marker $[Fe(CN)_6]^{3-/4-}$ and electrochemical impedance spectroscopy analysis

The study of the kinetic barrier of the electrode-solution interface, the redox behavior of the $[Fe(CN)_6]^{3-/4-}$ couple was used since the electron-transfer between the electroactive species in the solution and the electrode surface occurs by tunneling of electrons using the barrier, the defects or pinholes present in the barrier (Rubio *et al*, 2006).Fig. 5.14 explains the comparison of cyclic voltammetric responses obtained at the bare ITO, Ppy-CS composite and Ppy-CS-Fe_3O_4 nanocomposites for 1 mM $K_3[Fe(CN)_6]$ in 0.1 M KCl at a scan rate of 50 mV s^{-1}. The bare ITO electrode shows a reversible voltammetric characteristic for the one electron redox process of the $[Fe(CN)_6]^{3-/4-}$ couple with the peak-to peak separation of 80 mV at a scan rate of 50 mV s^{-1}. The Ppy-CS composite and Ppy-CS-Fe_3O_4 nanocomposites electrode shows enhanced redox peak

currents a peak to peak separator of 124 mV and 145 mV respectively when compared to bare ITO. The high conductivity of Ppy made the electron transfer was more facilitated and presented a higher peak current of oxidation and reduction peaks values (480 μA and -500 μA) respectively for the Ppy-CS composite electrode likewise (600 μA and -600 μA) for the Ppy-CS-Fe_3O_4 nanocomposites respectively. It was noticeably found that the nanocomposite electrode performs as a new electrode surface, this is due to the effect of Ppy that increased electrocatalytic activity and had a good electrical communication with the original electrode surface.

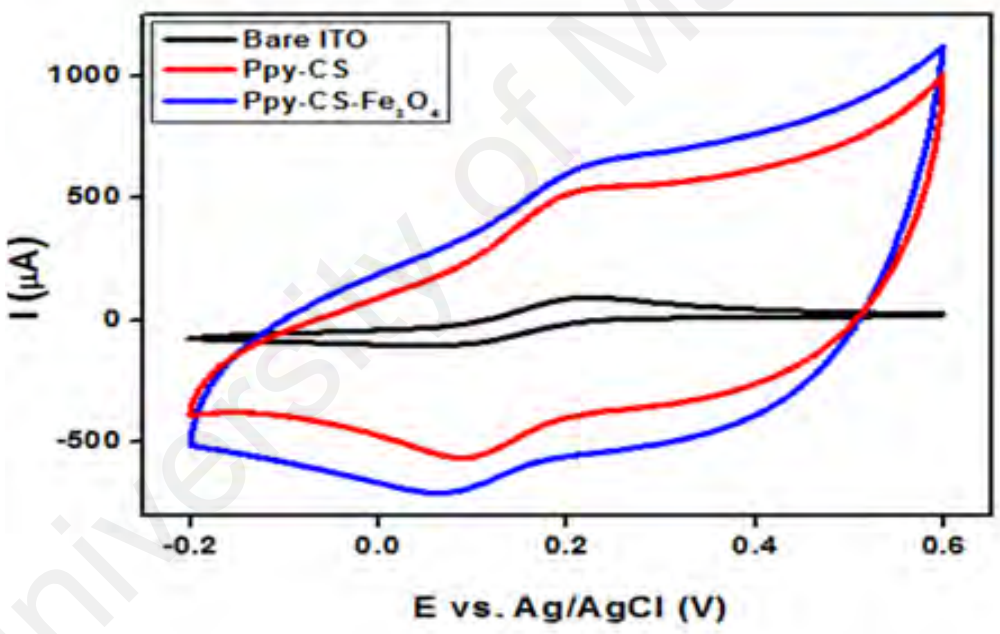

Figure 5.14: Cyclic voltammograms obtained for bare ITO, Ppy-CS composite and Ppy-CS-Fe_3O_4 nanocomposites for 1 mM $K_3[Fe(CN)_6]$ in 0.1 MKCl at a scan rate of 50 mV s^{-1}.

The interfacial properties of nanocomposites electrodes were considered by electrochemical impedance spectroscopy (EIS) and determined for 1 mM $[Fe(CN)_6]^{3-/4-}$ in 0.1 M KCl and study the conducting behavior of the Ppy-CS-Fe_3O_4 nanocomposite electrode in Figure. 5.15. The Nyquist diagram of the complex impedance shows the imaginary versus the real part of the impedance, and it observed the semicircle at higher

frequencies corresponding to the electron transfer limited process and the linear portion at lower frequencies corresponding to the diffusion-limited process. The bare ITO electrode showed a semicircle-like shape Nyquist plot with a large diameter which recommends the hindrance to the electron-transfer kinetics at the electrode surface. The Ppy-CS-Fe_3O_4 nanocomposite was observed that it was no semi-circle observed which shows the higher electron transfer kinetic.

Additionally, the composite and nanocomposite electrode presented only the linear portion at lower frequencies indicating the diffusion-limited process at the electrode-solution interface. The diffusion-limited process was much more facilitated at the nanocomposite electrode due to the conducting performance of Ppy and the nanoparticles of Fe_3O_4 present in the Ppy-CS-Fe_3O_4 nanocomposites. A perfect linear portion was observed at lower frequencies for the nanocomposite electrode when compared to bare ITO electrode. These results indicate that the Ppy-CS-Fe_3O_4 nanocomposite was positively formed and it enabled a diffusion-limited process at the electrode-solution interface.

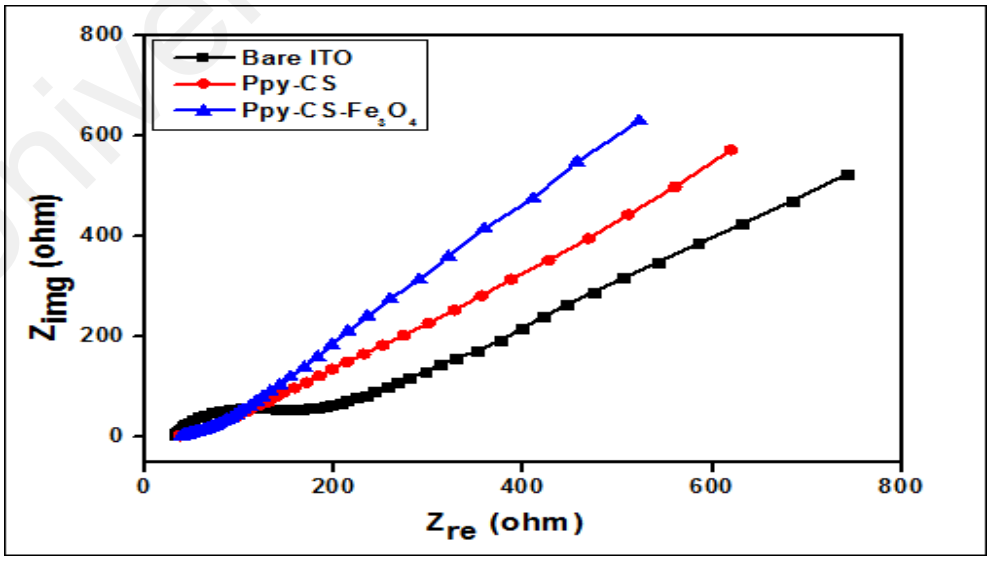

Figure 5.15: Nyquist plots obtained for bare ITO, Ppy-CS composite and Ppy-CS-Fe_3O_4 nanocomposite electrodes for 1 Mm $K_3[Fe(CN)_6]$ in 0.1 M KCl.

Bode-phase plots of the nanocomposite electrodes were considered in the frequency range of 0.01–10 000 Hz (Fig.5.16). The phase peaks appeared at a frequency range of 100–10000 Hz that correspond to the charge-transfer resistance of the nanocomposite electrodes. The shifting of peaks toward the low frequency region of 1– 0.01 Hz for the nanocomposite electrodes attribute to the fast electron-transfer behavior of the nanocomposites. The conductivity of Ppy present in the composite and nanocomposite electrode facilitates the peak shifting in the Bode plot. The Bode impedance plot of the nanocomposite electrode showed a lesser log Z value in a low frequency range of 1–100 Hz when compared to the other composite electrodes and bare ITO (Fig.5.17).

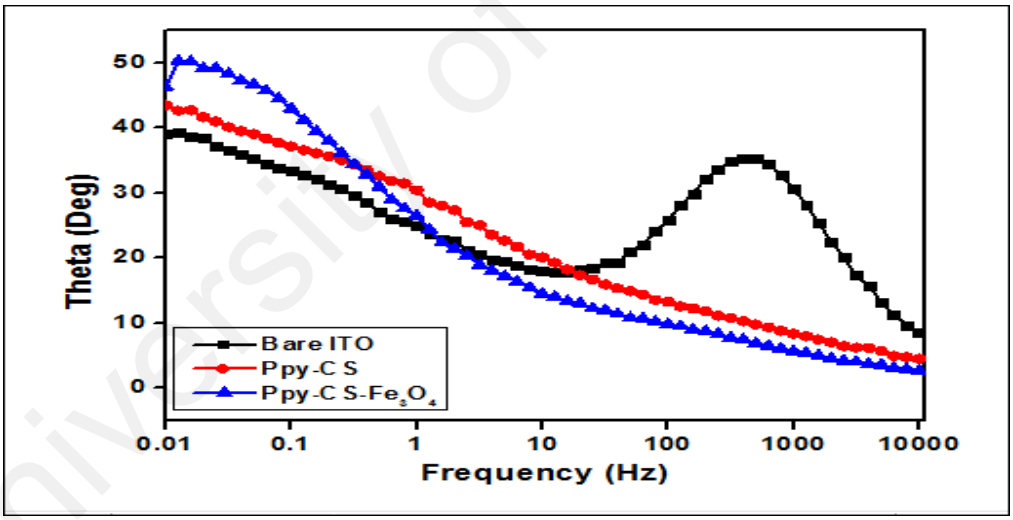

Figure 5.16: Bode phase plots obtained for bare ITO, Ppy-CS composite and Ppy-CS-Fe_3O_4 nanocomposite for 1 x 10^{-3} M $K_3[Fe(CN)_6]$ in 0.1 M KCl.

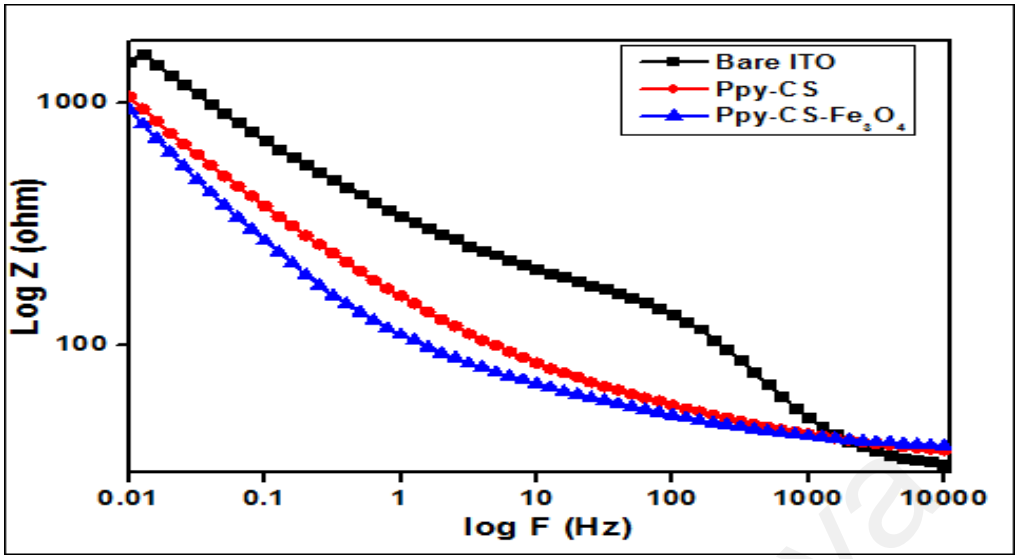

Figure 5.17: Bode impedance plots of log Z obtained for bare ITO, Ppy-CS composite and Ppy-CS-Fe_3O_4 nanocomposite for 1 x 10^{-3} M $K_3[Fe(CN)_6]$ in 0.1 M KCl.

5.5 Conclusion

In summary, one-step electrochemical synthesis procedure has been followed to prepare Ppy-CS-Fe_3O_4 nanocomposite films on ITO glass electrode successfully from an aqueous solution containing the monomer, dopant ions, nanoparticles and bio-polymers for glucose sensing. A high glucose sensing performance has been demonstrated by this fabricated sensor with high sensitivity, selectivity, fast response time and low detection limit due to the homogeneous film formation with Fe_3O_4 nanomaterial by this one-step electrochemical process. The role of Fe_3O_4 as a nanomaterial in glucose oxidation has been well realized by the polymer nanocomposite. The advantages of low-cost precursor and the simple preparation technique will make the material a promising economical candidate in glucose sensing.

CHAPTER 6: POLYPYRROLE-CHITOSAN-TITANIUM DIOXIDE NANOCOMPOSITE FILMS

6.1 Introduction

Titanium dioxide (TiO_2) has proven to be a promising n-type semiconductor material because of its wide band gap (3.2 eV) under UV light (Zaleska, 2008). In addition to this, it has a high physical and chemical stability and also a high refractive index. This makes the material widely used by material scientists (Abbas *et al.,* 2011; Xie, Qian, Zhong, Guo, & Hu, 2012). Several semiconductor oxides such as ZnO, TiO_2, NiO, CuO, Al_2O_3, Fe_2O_3, SnO_2, ZrO_2, and WO_3 have received considerable attention over the last few years due to their distinctive optical and electronic properties, but TiO_2 can also be used in several other domains such as photocatalysts, solar cells, sensors and bactericidal action (Chaturvedi, Dave, & Shah, 2012; Gómez *et al.,* 2003; Grieshaber, MacKenzie, Voeroes, & Reimhult, 2008). Recently, there is a considerable interest in using TiO_2 nanoparticles as a modifier since they have a high surface area, good biocompatibility and relatively good conductivity (Chaturvedi *et al.,* 2012; Z. Liu *et al.,* 2012).

There are several methods for synthesizing the TiO_2 nanoparticles. Some researchers have recommended using the microemulsion method due to its short processing time (Ki Do Kim, Lee, & Kim, 2003). On the other hand, by using physical vapor deposition (PVD), materials are condensed after evaporation to solid form (Prakash *et al.,* 2012). Other methods like hydrolysis (Manjari Lal, 1998) and hydrothermal (Campbell, Na, & Ko, 1992) have been frequently used. In the sol-gel method, materials undergo hydrolysis and polycondensation to form a sol; a gel forms after aging and eventually becomes solid after drying. It can be a simple method as it requires low temperature and controllable final product properties (Rao, Robin, & Komarneni, 1996; Tabata & Ikada, 1998; Vieira & Pawlicka, 2010).

6.2 Mechanism for the formation of Ppy-CS-TiO_2

The mechanism of electrochemical polymerization of pyrrole has been mentioned in chapter 5 (Matyjaszewski, 2002). During the electrochemical formation of Ppy-CS-TiO_2 nanocomposite films, polypyrrole is linked with Ppy-CS- TiO_2 through hydrogen bonding and titanium-nitrogen ligand formation as shown in Figure 6.1. The Ppy-CS-TiO_2 are linked with hydrogen bonding during ultra-sonication in the preparatory stage.

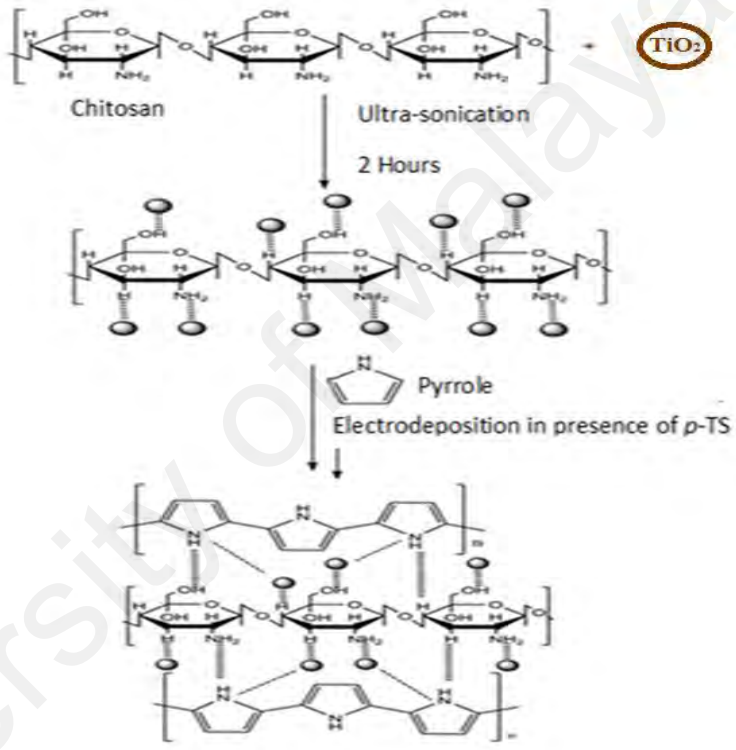

Figure 6.1: The formation of Ppy-CS-TiO_2 nanocomposite films.

6.3 Results and discussion

6.3.1 FTIR of Ppy-CS-TiO_2 nanocomposite film

Figure 6.2 shows the FTIR spectra of Ppy-CS- TiO_2 nanocomposite, Ppy-CS composite film and TiO_2 nanoparticles. The FTIR spectrum of Ppy-CS- TiO_2 nanocomposite shows a broad band at 3500 cm^{-1} due to axial stretching of O-H and N-H bonds. A peak at 1630 cm^{-1} is presented to amide group and peaks at 1446 cm^{-1} and 1378 cm^{-1} is the result of coupling of C-N axial stretching and N-H angular deformation. The FTIR

spectrum of PPy-CS- TiO_2 nancomposite exhibits a broad band at cm^{-1} due to the N-H stretching of pyrrole and O-H stretching of chitosan. The typical peaks of polypyrrole at 1580 cm^{-1} (C=C benzoic form), 1420 cm^{-1} (C-N stretching) was confirmed (Li et al., 2006; Yoon & Jang, 2009). The peak at 1320 cm^{-1}, which is assigned to the –C–O stretching mode of $–CH_2–OH$ groups in CS, has shifted to lower wave numbers in Ppy-CS-TiO_2 nanocomposite film due to high intensity of TiO_2 similar with TiO_2 nanoparticles. A peak around 1006 cm^{-1} is related to the C–O stretching of CS, which has overlapped with Ppy. The peak at 2700 cm^{-1} for Ppy-CS-TiO_2 nanocomposite show high intensity peak which has shifted to lower wave numbers is due to high intensity with TiO_2 nanoparticles. The peaks at 1160 cm^{-1} (C-O stretching) and 1035 cm^{-1} (C-C stretching) confirm the formation of Ppy-CS- TiO2 nanocomposite doped with p-TS. The additional peaks at 902 cm^{-1}, 768 cm^{-1} and 670 cm^{-1} are due to the C-H out of plane deformation vibration of the ring. Some of the important FTIR spectra data shown in Table 5.

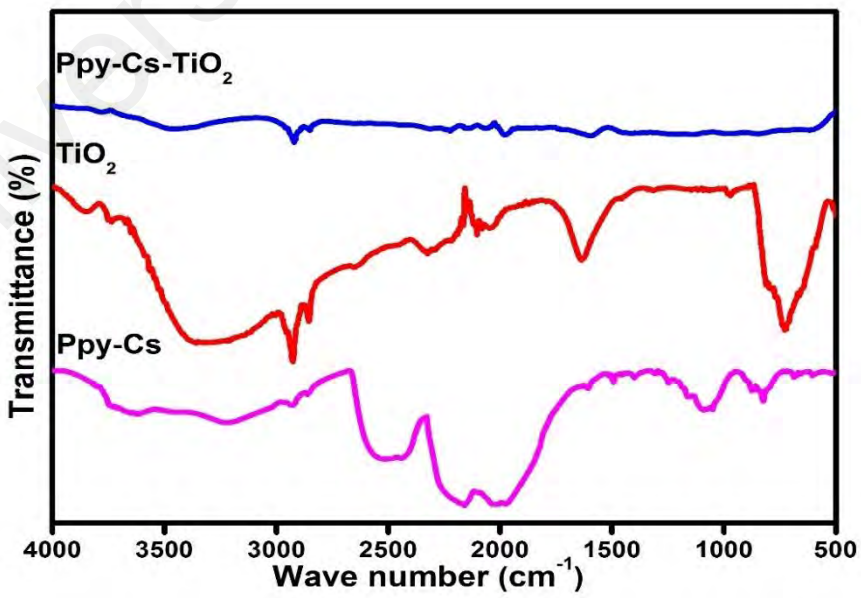

Figure 6.2: FTIR spectra of CS, Ppy and (PPy -CS- TiO_2/ITO) nanocomposite film.

Table 5: FTIR spectra data Ppy-CS-TiO_2 nanocomposite film.

Band Assignment	Peak position (cm^{-1})
–N–H and -O-H stretching vibration	3500
–C–H stretching vibration	3000
–C–N stretching mode in pyrrole ring	1420
–C–OH stretching angular deformation	1320
–C–N stretching mode in pyrrole ring	1580
–C–O stretching deformation	1006
–C–H in-plane deformation	1160
–C–H in-plane deformation	1035
–C–H out of plane deformation	902
–C–H waging vibration	768
-C-H vibration of the ring	670

6.3.2 XRD characterization of Ppy-CS-TiO_2 nanocomposites

The XRD peaks in wide angle range for nanocomposites ascertained that the peaks were in 27°, 31°, 37°, 51°could be attributed to crystalline structures of the anatase form of TiO_2-NPs. Figure. 6.3 shows the XRD pattern of Ppy-CS-TiO_2 nanocomposite film which shows a broad peak at ~ 27° indicating the amorphous structure for Ppy-CS-TiO_2 nanocomposite. The crystalline peaks of TiO_2 and the broad peak of polypyrrole have been found disappeared in this new broad peak in the Ppy-CS-TiO_2 nanocomposites at around 28°. The peak in 53° in the Ppy-CS-TiO_2 nanocomposite films shows an improvement of CS in the nanocomposite as seen in Figure 6.3.

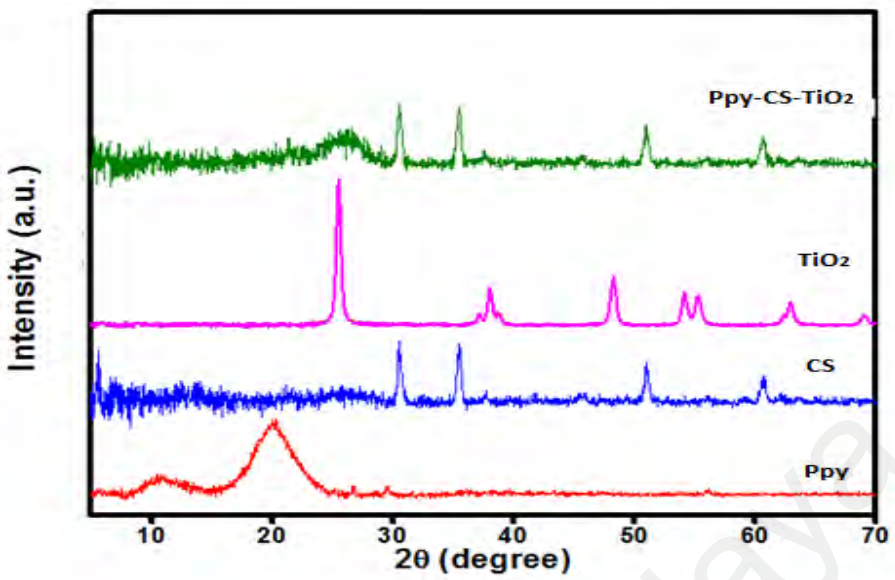

Figure 6.3: X-ray diffraction patterns of Ppy-CS-TiO_2 nanocomposite, Ppy and CS.

6.3.3 Morphology studies

FE-SEM micrographs confirmed the homogeneous distribution of TiO_2 at the surface of the Ppy-CS-TiO_2 nanocomposites film in Figure (6.4 a), which shows the white dots in color of the nanoparticles of TiO_2. The EDX analysis of Ppy-CS-TiO_2 nanocomposite shown in (Figure 6.4 b) clearly indicates the presence of (N, C, O, and Ti) components in the film. Based on the element analysis, it suggests that the TiO_2 nanoparticles are incorporated in Ppy-CS molecules.

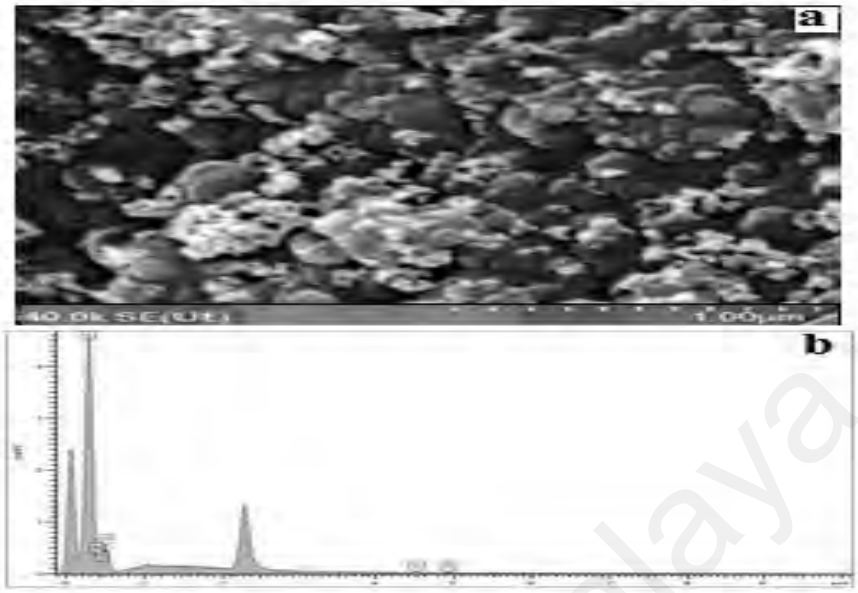

Figure 6.4: FE-SEM micrograph of (a) Ppy-CS- TiO_2, (b)The EDX analysis of Ppy-CS- TiO_2 nanocomposite /ITO.

The direct evidence for the immobilization of TiO_2 nanoparticles on the surface of CS- and polypyrrole was analyzed by HRTEM. The size and dispersion of TiO_2 nanoparticles and Py-CS-TiO_2 nanocomposites were measured by HR-TEM in Figure (6.5 a and b) respectively. Approximately spherical agglomerated particles were observed for Ppy-CS-TiO_2 nanocomposites and size ranging from 18 nm to 27 nm. The size of the particles in the nanocomposite was higher than that of the TiO_2 used (>20 nm). The TiO_2 nanoparticles were found to be spherical in shape in (Fig.6.5a) and the particle size distribution of TiO_2 nanoparticles was almost uniform distribution. The Py-CS-TiO_2 nanocomposites were found to have typical core shell structure (Fig. 6.5 b). The dark areas represent the crystalline TiO_2 nanoparticles, while the bright areas represent the amorphous CS. The interaction between CS and TiO_2 enhanced the properties of CS-TiO_2 nanocomposites.

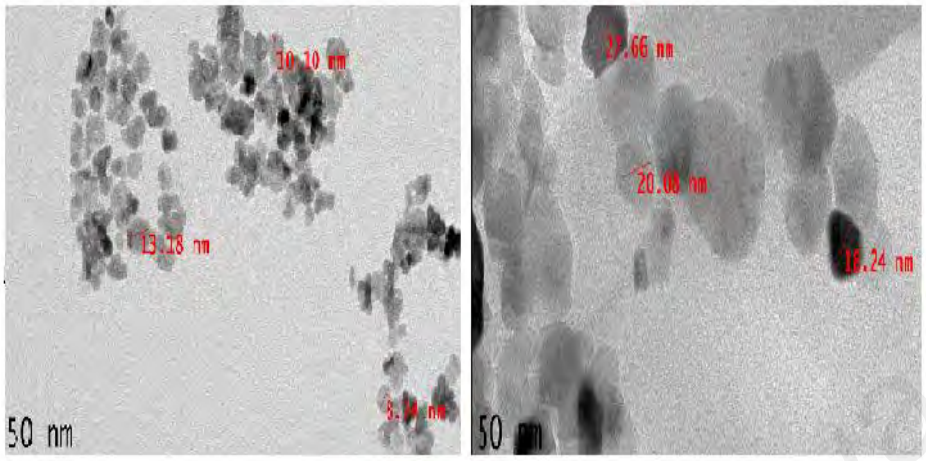

Figure 6.5: HR-TEM images of (a) TiO_2 and (b)Ppy-CS-TiO_2 nanocomposites film

6.3.4 XPS characterization of Ppy-CS-TiO_2 nanocomposites

The presence of TiO_2 nanoparticles in the nanocomposite films was confirmed by XPS. The XPS wide-scan spectra are presented in Figure 6.6 (a) and the XPS quantitative elemental analysis of narrow scan is presented in Figure 6.6 (b), (c), (d) and (e)) respectively. For pyrrole, C ls around (285) eV, N ls around (400) eV, O ls around (531) eV. The main carbon peak at 286.2 eV in chitosan corresponds to carbon bonded with both the hydroxyl group and nitrogen. In the carbon-related spectrum, two other significant peaks were appearing, which can be assigned to carbon to carbon single bonds (284.8) eV and carbonyl groups (approx. 287.8 eV), both are present in the chitosan structure. Moreover, the minor peak in the position of approximately (288.0) eV is noticeable. This peak can be observed as unreacted acidic acid hydroxyl groups (-COO) Figure 6.6 (b) (Lawrie, *et al.,* 2007). The high-resolution spectrum, however, exposes at least two chemically different nitrogen. The stronger peak at (399.8) eV can be assigned to neutral -N- whereas the higher binding energy peak at (401.0) eV is assigned to the oxidized -N^{+-} moieties. These values are considered for the conducting of Ppy associated well with the value obtained electrochemically in Figure 6.6 (e)

(Kang, *et al.,* 1993). The O1s peak for this nanocomposite appears with a split at 530.6 eV. Figure 6.6 (c) and represents the lattice oxygen. It is shifted slightly compared to database values (Wagner, *et al.,* 2003). It is expected that this shift is caused by the particle diameter of less than 20 nm. Another O1s peak shows at 532.5 eV and is due to the surface oxygen. In this case, the energy is higher compared to the bulk since there are open bonds. Since this material is of nanometer-size, it has a large specific surface area which increases the ratio of surface to bulk oxygen. It has been discussed that the ratio between the two peaks can be correlated to the surface area of the material (Jensen, *et al.,* 2014). In Figure 6.6 (d), the titanium atom shows two distinct peaks at 458.4 eV for the $Ti2p_{1/2}$ and at 459.2 eV for the $Ti2p_{3/2}$ showing the clear evidence of the element present in the surface of the Ppy-CS-TiO_2 nanocomposite films (Sathe, *et al.,* 2014).

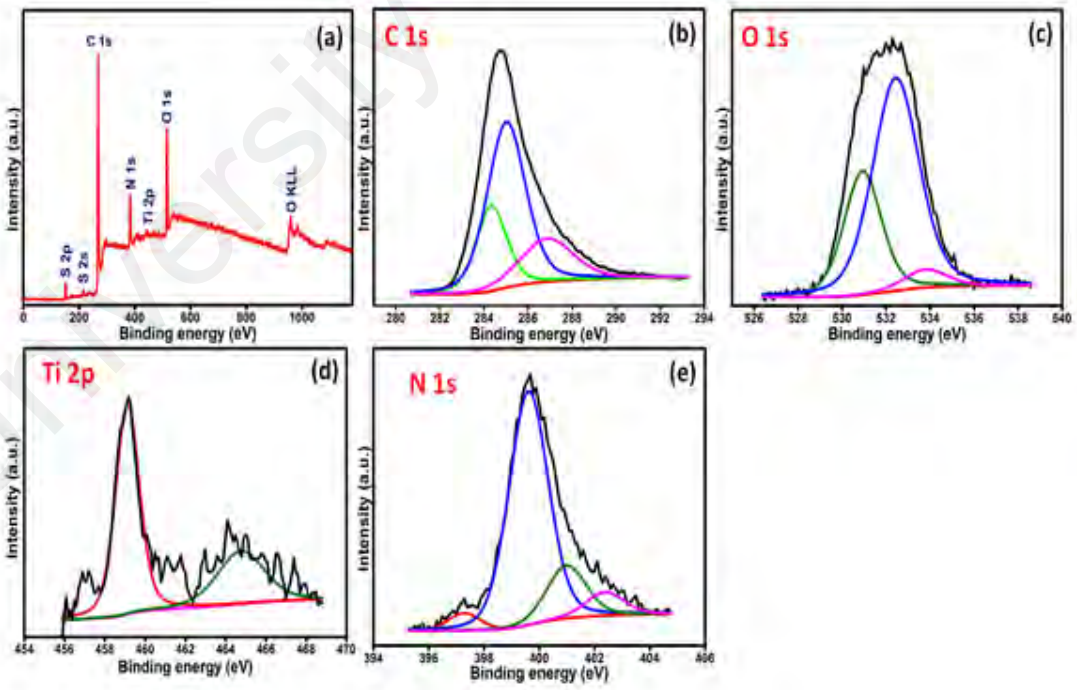

Figure 6.6: The XPS survey scan (a) and narrow scan (b, c, d, and e) of Ppy-CS-TiO_2 nanocomposite films.

6.4 Glucose sensing performance of Ppy–CS-TiO_2 nanocomposite films

The glucose sensing performances of Ppy-CS-TiO_2 nanocomposite /ITO was carefully found by cyclic voltammetry (CV) in Figure 6.7 with and without glucose in alkaline media (0.1M NaOH) at the scan rate of 50 mVs^{-1}. In presence of glucose the peak currents for Ppy-CS- TiO_2 nanocomposite/ITO electrode was observed much higher than without glucose. Thus, Ppy-CS- TiO_2 nanocomposite /ITO is acting as a good glucose sensor due to the glucose oxidation ability of Ppy-CS- TiO_2 nanocomposite

On the basis of the reported for glucose oxidation and our finding in this study, a possible catalytic of chemical equation for glucose oxidation at Ppy-CS-TiO_2 nanocomposite is proposed as follows:

$$2TiO_2 + C_6H_{12}O_6 \rightarrow 2TiOOH + C_6H_{10}O_6$$

glucose gluconolactone

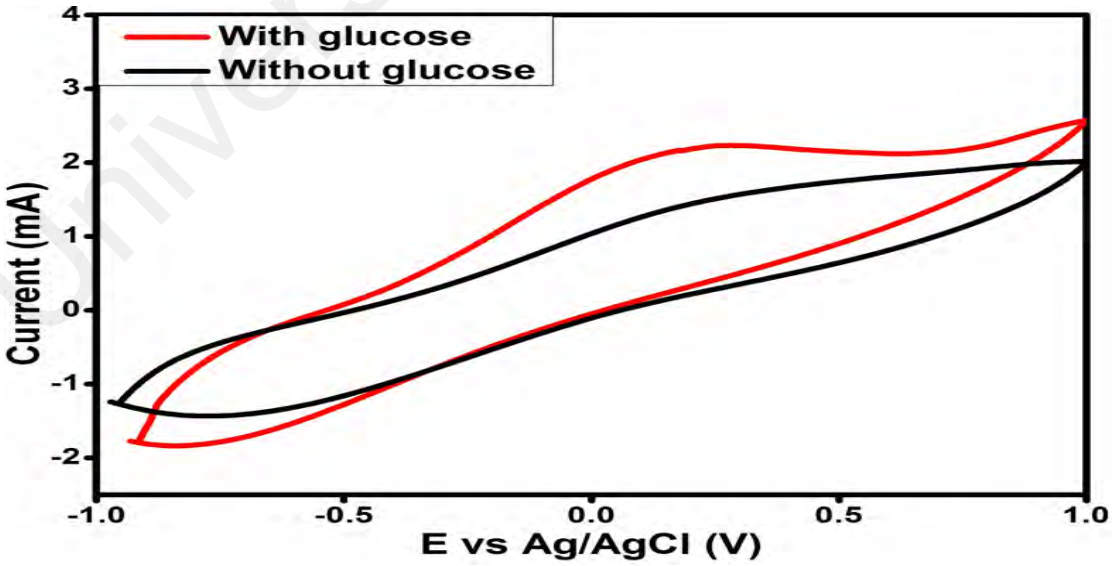

Figure 6.7: CV responses of Ppy-CS-TiO_2 /ITO in 0.1M NaOH electrolyte with 1mM glucose and without glucose at the scan rate of 50 mVs^{-1}.

6.4.1 Effect of TiO_2 content in Ppy–CS-TiO_2 nanocomposites film

The Ppy–CS-TiO_2 nanocomposite films were electrochemically deposited on the ITO electrode using different ratios of TiO_2 NP (0.5 %, 1%, 2%, and 3%) by cyclic voltammetry. The nanocomposite films were prepared at a scan rate of 50 mV s^{-1} using potential window from -1.0 to 1.2 V (vs Ag/AgCl/3MKCl). Figure 6.8 shows the linearly amperometric increased current response of the Ppy-CS- TiO_2 electrode examined with several additions of (1, 3, 5, 7, 9, 12, 14, 16) mM glucose (once every 50 s) spiked into 0.1 M NaOH solution into the cell. The current observed for the electrode of Ppy–CS-TiO_2 nanocomposite consisting of 1% TiO_2 was found higher than the current for all other electrodes of Ppy–CS-TiO_2 nanocomposite having different amounts of TiO_2 contents (0.5 %, 2%, and 3%) for the current response of glucose Figure 6.8 (b). The current response of the performance of glucose by the nanocomposite film containing the minimum amount of TiO_2 (0.5%) appears to be less due to the low content of TiO_2 NP. Increasing the amount of nanoparticles (2% and 3%) in the polymer composite make the polymer film surface heterogeneous and rough. This rough surface with high content of nanoparticles appears to be less effective in oxidation of glucose. The lower current response associated with the polymer nanocomposite electrodes containing 2% and 3 % TiO_2 for the oxidation of glucose can be seen in Figure (6.8 c and d). It can be noticed that the current response for the electrode containing 0.5% TiO_2 in the polymer composite is higher than the current response for the electrode containing of 2% and 3% TiO_2 in the polymer composite for the oxidation of glucose (Fig.6.8).

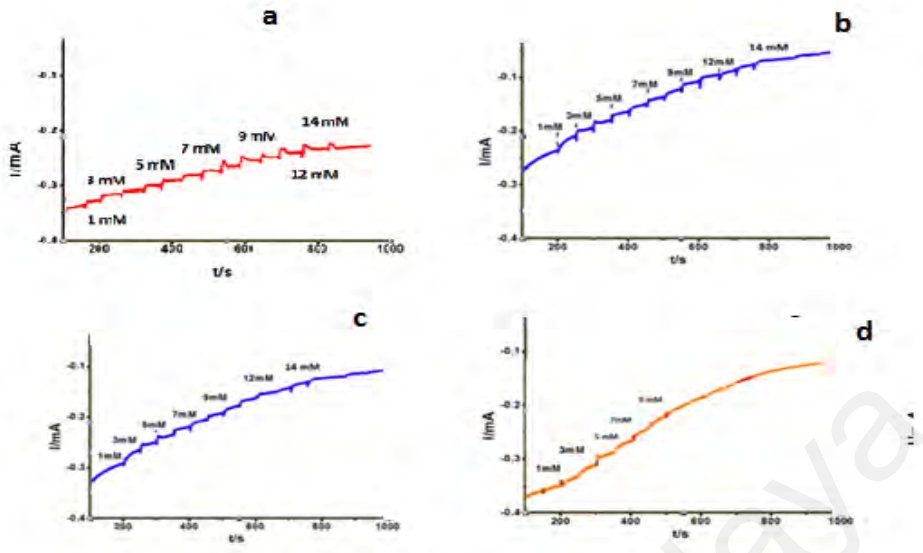

Figure 6.8: Amperometric response of examined of the TiO_2 NP, (a) 0.5 %, (b) 1%, (c) 2%, and (d) 3 % of Ppy-CS-TiO_2 electrode in 0.1 M NaOH with sequential additions of glucose concentration (1–16 mM) at scan rate of 50 mVs^{-1}.

Fig. 6.9 shows typical steady-state amperometric responses of Ppy-CS-TiO_2 nanocomposite /ITO (10 cycles) and Ppy-CS /ITO (10 cycles) on successively increasing glucose concentrations at an applied potential of +0.13 V (vs. Ag/AgCl). Ppy-CS-TiO_2 nanocomposite /ITO found linearly increased responses to the change of glucose concentrations while the current responses of Ppy-CS/ITO were much lower and only realized slight increase with the addition of glucose into the cell. The results are consistent with those obtained from cyclic voltammograms. The calibration curve for Ppy-CS-TiO_2 nanocomposite /ITO is presented in the inset of Fig. 6.8. The glucose sensors show linear dependence in the glucose concentration of dynamic range of 1 to 14 mM with a correlation coefficient of 0.989, a sensitivity of 0.008 μAcm^{-2} mM^{-1}, and a detection limit (LOD) of 614 µM at single of noise (S/N=3), and determination of quantification limit (LOQ) value was 2046 µM. This novel Ppy-CS-TiO_2

nanocomposite /ITO glucose sensor exhibits high sensitivity, low detection limit and fast response time in less than 3 second.

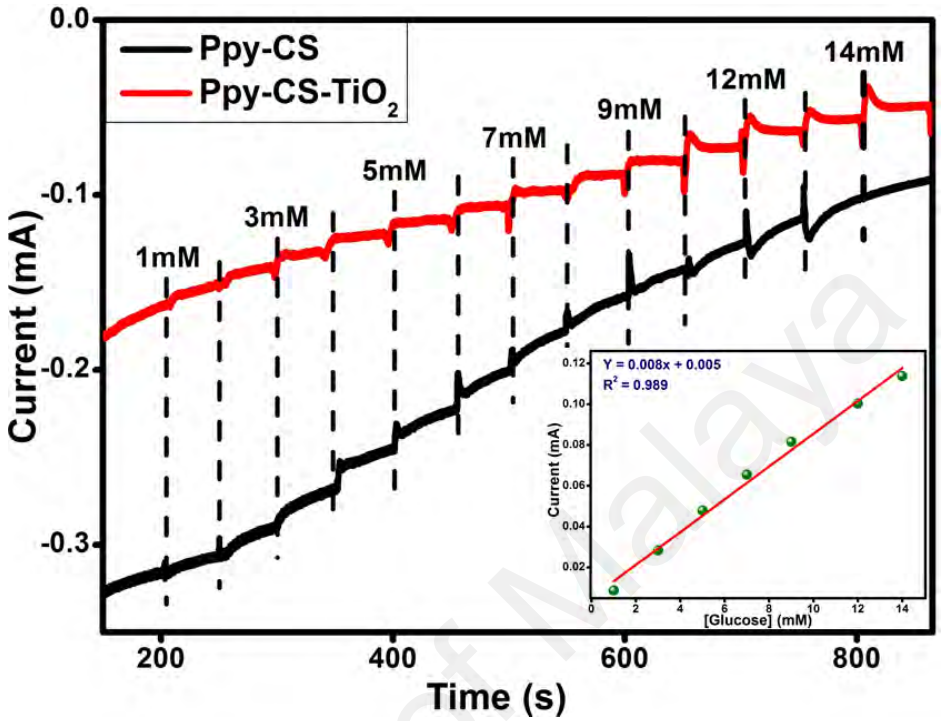

Figure 6.9: Amperometric responses to successive addition of glucose concentration in 0.1M NaOH solution at +0.13 V (vs. Ag/AgCl). The inset shows the steady-state calibration curve for the of Ppy-CS-TiO_2 nanocomposite /ITO electrode

6.4.2 Glucose sensing by the electrode prepared from various cycles

Figure 6.10 shows the linearly increased current responses with several additions of (1, 3, 5, 7, 9, 12, 14, and 16) mM glucose (once every 50 s) spiked into 0.1 M NaOH solution into the cell. The current observed in Figure 6.9 for the electrode of Ppy-CS-TiO_2 nanocomposite prepared by 10 cycles was found higher than the current for all other electrodes of Ppy-CS- TiO_2 nanocomposite prepared by multicycles (5, 15, and 20 cycles) for the oxidation response glucose Figure 6.10. In Figure 6.10 (a) the current response for the oxidation of glucose by the nanocomposite film prepared from 5 cycles appears to be lower due to the low content of thin deposition of the film. Increasing the multicycles (15 and 20 cycles) to produce the polymer composite, the film becomes thicker with little rough surface making it less effective for glucose oxidation. The

lower current response associated with the polymer nanocomposite electrodes prepared by 5, 15 and 20 cycles for the oxidation of glucose can be seen in Figure (6.10 a, b and c).

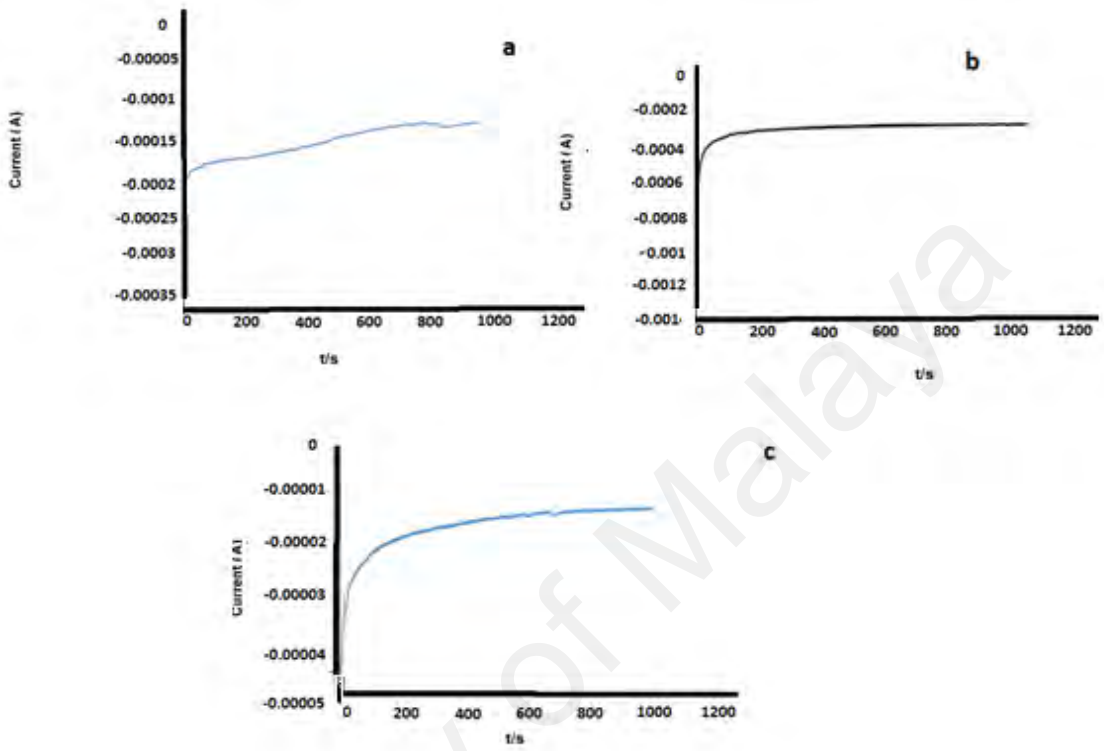

Figure 6.10: Amperometric response of the TiO_2 NP, (a).5 cycles, (b) 15 cycles (c) and 20 cycles of Ppy-CS-TiO_2 electrode in 0.1 M NaOH with sequential additions of glucose concentration (1–14 mM) at scan rate of 50 mVs^{-1}.

6.4.3 The stability study

The stability of the developed sensor was investigated by measuring its current response for glucose for 14 days. The prepared Ppy-CS-TiO_2 nanocomposite film on ITO was used to record the amparometric response for 1mM glucose on frequency of 2 days. Here, I_0 is the current response of fresh sensor and I_{14} is the current response after storage as shown in Figure 6.11. During the first 6 days, the current response did not change in a noticeable way, however on the last day (14^{th} day), the current response still

remained above 88 % of its initial response, revealing the excellent stability of the sensor.

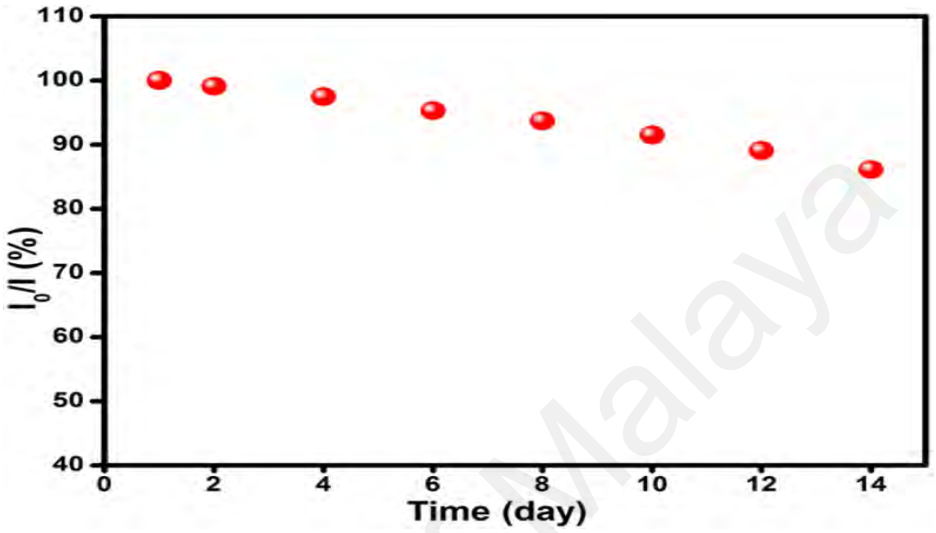

Figure 6.11: Stability of the sensor stored at ambient conditions over 14 days in 0.1 M NaOH glucose at potential of 0.13 V (vs. Ag/AgCl).

6.4.4 The interference study

The selectivity of the Ppy-CS-TiO_2 nanocomposite /ITO for the detection of glucose was examined by injecting three different interfering biomolecules, namely, uric acid (UA), ascorbic acid (AA) and cholesterol (CH) in the evenly stirred 0.1 M NaOH solution containing glucose. The current response was observed in Figure 6.12. It depicts the recorded amperometric response for the consecutive additions of glucose and interfering biomolecules. First, the successive injections of glucose (each of 1 mM) were used to record to the current response for two injections after every 50 sec. The clear response toward detection was observed. After those consecutive injections (each of 0.1 mM) of UA, AA and CH were added in the same stirred solution and shown there is no response observed. Again, we added 3 times of of (UA, AA, and CH) but there is no response following by three injections (each of 1 mM) of glucose were used (sample time of 50 s) to study the interference. It was found that, the addition of interfering

biomolecules did not contribute significant current response contrary to glucose which respond for each injection. These results revealed that the present sensor possesses a good selectivity and sensitivity towards the detection of glucose even in the presence of common physiological interfering biomolecules.

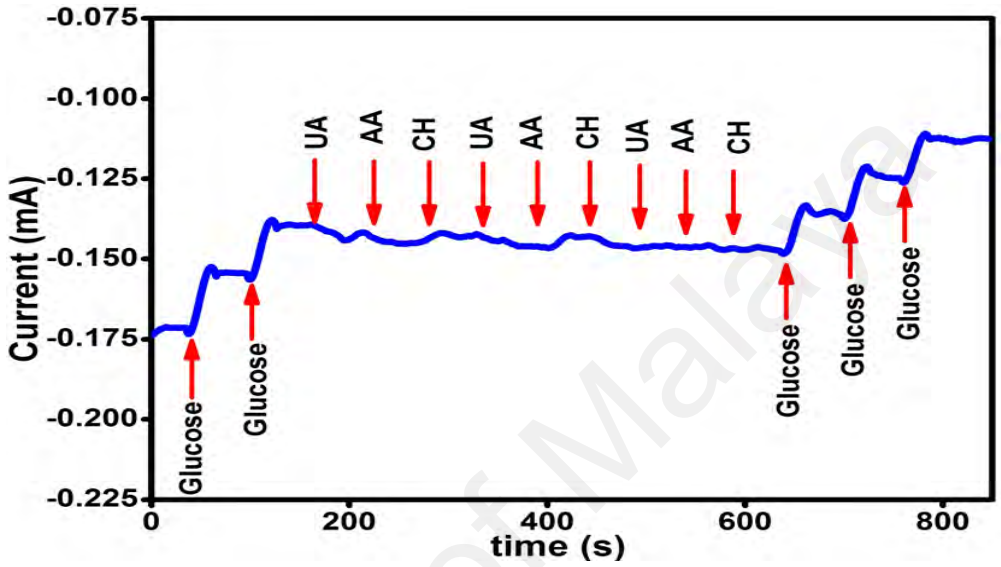

Figure 6.12: Amperometric responses obtained at successive addition of glucose and each of uric acid (UA), ascorbic acid(AA) and cholesterol (CH) in 0.1 M NaOH solution at +0.13 V (vs. Ag/AgCl) with regular interval of 50 s.

6.4.5 Electrochemistry of the redox marker $[Fe(CN)_6]^{3-/4-}$ and electrochemical impedance spectroscopy analysis

Fig. 6.13 describes the comparison of cyclic voltammetric responses obtained at the bare ITO, Ppy-CS composite and Ppy-CS-TiO_2 nanocomposites for 1 mM $K_3[Fe(CN)_6]$ in 0.1 M KCl at a scan rate of 50 mV s^{-1}. As known in previous chapters, the bare ITO electrode shows a reversible voltammetric characteristic for the one electron redox process of the $[Fe(CN)_6]^{3-/4-}$ couple with the peak-to peak separation of 80 mV at a scan rate of 50 mV s^{-1}. The Ppy-CS composite and Ppy-CS-TiO_2 nanocomposites electrode shows enhanced redox peak currents with a peak to peak separator of 124 mV and 137 mV respectively when compared to bare ITO. The high conductivity of Ppy made the electron transfer was more facilitated and presented a higher peak current of oxidation and reduction peaks values (480 µA and -500 µA) respectively for the Ppy-CS

composite electrode likewise (580 µA and -580 µA) for the nanocomposite electrode. It was noticeably found that the nanocomposite electrode performs as a new electrode surface; this is due to the effect of both TiO_2 and Ppy which increased the electrocatalytic activity and appeared as a good electrical communicator with the original electrode surface.

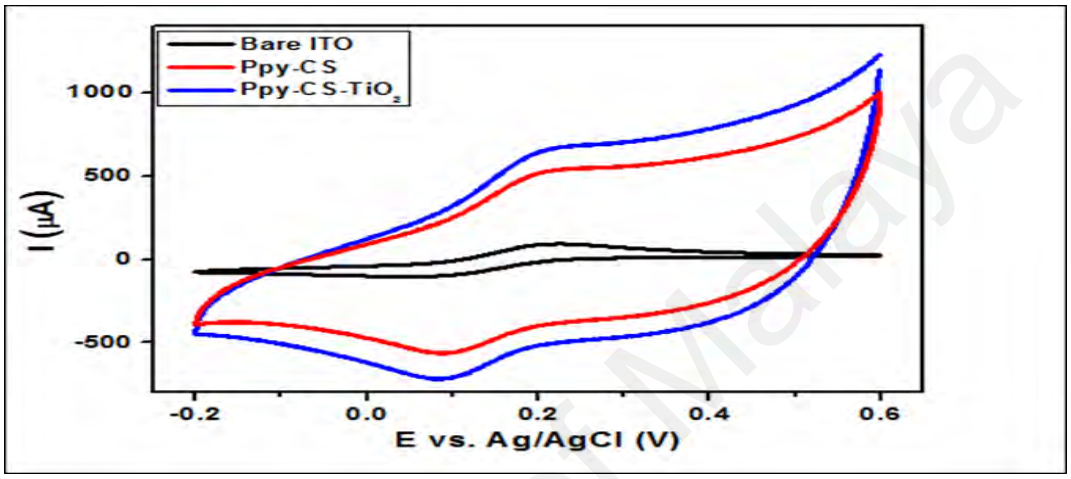

Figure 6.13: Cyclic voltammograms obtained for bare ITO, Ppy-CS composite and Ppy-CS-TiO_2 nanocomposites for 1 mM $K_3[Fe(CN)_6]$ in 0.1 MKCl at a scan rate of 50mVs^{-1}.

The interfacial properties of nanocomposites electrodes were considered by electrochemical impedance spectroscopy (EIS) and determined 1 mM $[Fe(CN)_6]^{3-/4-}$ in 0.1 M KCl with study the conducting behavior of the Ppy-CS-TiO_2 nanocomposite electrode in Figure. 6.14. The Nyquist diagram of the complex impedance shows that the bare ITO electrode has a semicircle-like shape Nyquist plot with a large diameter which recommends the hindrance to the electron-transfer kinetics at the electrode. The Ppy-CS-TiO_2 nanocomposites was no semi-circle observed which shows the higher electron transfer kinetics. Additionally, the composite and nanocomposite electrode presented only the linear portion at lower frequencies indicating the diffusion-limited process at the electrode- solution interface. The diffusion-limited process was much more facilitated at the nanocomposite electrode due to Ppy conducting performance and

magnetic present in the nanocomposite and Ppy composite. A perfect linear portion was observed at lower frequencies for the nanocomposite electrode when compared to bare ITO electrode. These results indicate that the Ppy-CS-TiO_2 nanocomposite was successfully designed and it facilitated a diffusion-limited process at the electrode-solution interface.

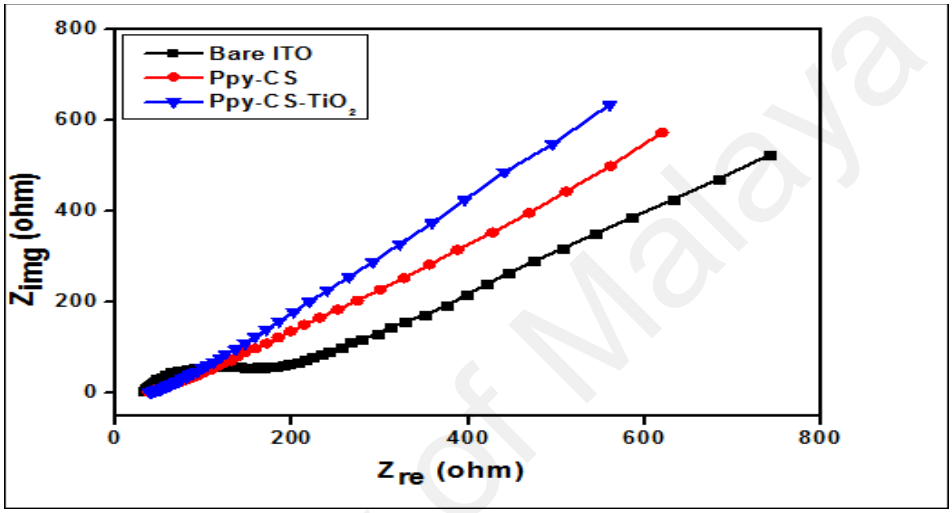

Figure 6.14: Nyquist plots obtained for bare ITO, Ppy-CS composite and Ppy-CS-TiO_2 nanocomposite electrodes for 1 Mm $K_3[Fe(CN)_6]$ in 0.1 M KCl.

Bode-phase plots of the nanocomposite electrodes were collected in the frequency range of 0.01–10 000 Hz (Fig.6.15). The phase peaks appeared at a frequency range of 100–10000 Hz correspond to the charge-transfer resistance of the nanocomposite electrodes. The shifting of peaks toward the low frequency region of 1– 0.01 Hz for composite and nanocomposite electrodes indicates the fast electron-transfer behavior of the nanocomposites. The conducting nature of Ppy present in the composite and nanocomposite electrode facilitates the peak shifting in the Bode plot. The Bode impedance plot of the nanocomposite electrode presented a lesser log Z value in a low frequency range of 1–100 Hz when compared to the composite electrodes (Fig.6.16).

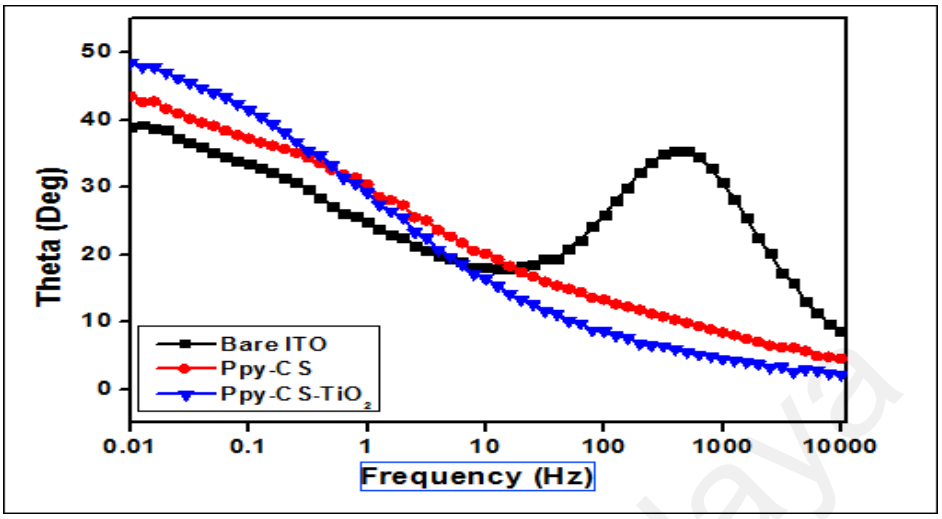

Figure 6.15: Bode phase plots obtained for bare ITO, Ppy-CS composite and Ppy-CS-TiO_2 nanocomposite for 1 x 10^{-3} M $K_3[Fe(CN)_6]$ in 0.1 M KCl.

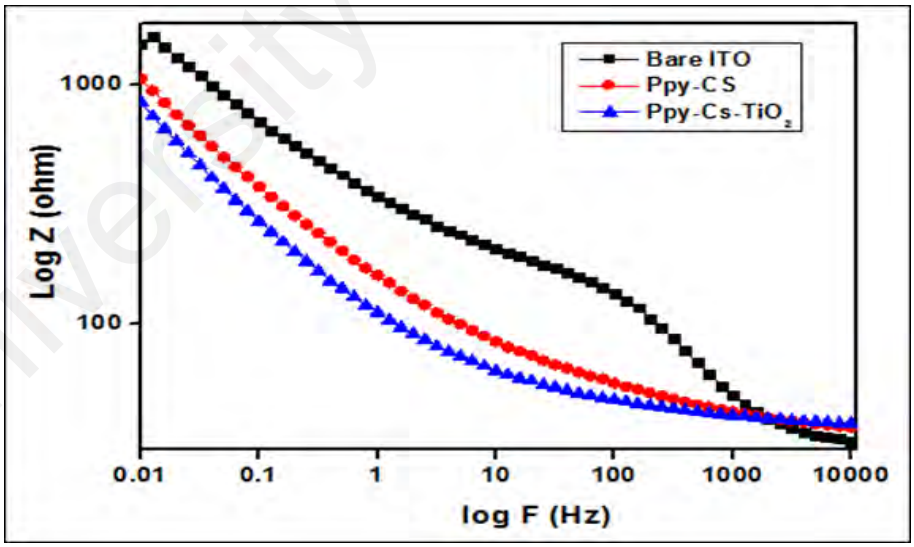

Figure 6.16: Bode impedance phase plots of log z obtained for bare ITO, Ppy-CS composite and Ppy-CS-TiO_2 nanocomposite for 1 x 10^{-3} M $K_3[Fe(CN)6]$ in 0.1 M KCl.

6.5 Conclusion

In this chapter, a novel non-enzyme glucose biosensor was fabricated by using PPy-CS-TiO_2 nanocomposite as a catalyst for the oxidation of glucose. It proved that Ppy-CS-TiO_2 nanocomposite showed excellent catalysis towards glucose in alkaline media and the sensor showed excellent performance, such as low detection limit, wide linear range, quick current response, high current and good stability. TiO_2 as a nanomaterial played a good role in glucose oxidation as has been well demonstrated by the polymer nanocomposite. The advantages of low-cost precursor and the simple preparation technique will make the material a promising economical candidate in glucose sensing.

CHAPTER 7: CONCLUSIONS AND FUTURE WORK

Non-enzymatic glucose biosensors based on polypyrrole conducting polymer, chitosan and metal oxides such as Fe_3O_4 and TiO_2 have been successfully fabricated by electrochemical technique. The films prepared from 1% solution of nanomaterial by cyclic voltammetry using 10 cycles appear to be the optimum process condition for preparing the nanocomposite films. In this one-step process, the nanomaterial is homogenously distributed in the polymer composite making it all through perfect for glucose sensing.

The formation of polypyrrole-chitosan-iron oxide (Ppy-CS-Fe_3O_4) and polypyrrole-chitosan-titanium dioxide (Ppy-CS- TiO_2) has been confirmed by various analytical tools such as FT-IR, XRD, EDX and XPS. The globular morphology of these films has been observed by FE-SEM and HR-TEM.

The glucose oxidation has been well realized by the nanomaterials incorporated in the polymer films. The increased current response by Ppy-CS-Fe_3O_4 and Ppy-CS-TiO_2 electrodes over Ppy-CS electrode for 0.1M glucose oxidation has been well observed in this present study suggesting that both the nanomaterials, Fe_3O_4 and TiO_2 are playing a good role on glucose oxidation. The low detection limits (LOD) of 234 μM and 614 μM, for Ppy-CS-Fe3O4 and Ppy-CS-TiO2 nanocomposites respectively with high sensitivity and good selectivity towards glucose sensing have been demonstrated.

In this non-enzymatic glucose sensor, Fe_3O_4 nanomaterial has been found superior in oxidizing glucose than TiO_2 nanomaterial as can be observed from the much higher current response for 0.1M glucose oxidation by Ppy-CS-Fe_3O_4 and Ppy-CS-TiO_2 nanocomposite electrodes. The present study shows that the alkaline medium favors the glucose oxidation.

EIS study shows that the high conductivity of Ppy made the electron transfer more facilitated and presented a higher peak current of oxidation and reduction peaks for both the Ppy-CS composite electrode and Ppy-CS-metal oxide nanocomposite electrode.

For the interference study, the chosen biomolecules such as ascorbic acid, uric acid, and cholesterol have been found to have no interference for the glucose detection by both Ppy-CS-Fe_3O_4 and Ppy-CS-TiO_2 nanocomposite electrodes. Ppy-CS-Fe_3O_4 and Ppy-CS-TiO_2 nanocomposite electrodes have been found to be stable in glucose sensing after a time period of more than 10 days.

The short response time and low detection limit have made Ppy-CS-Fe_3O_4 and Ppy-CS-TiO_2 nanocomposites as a unique material for non-enzymatic glucose sensor. The sizes of nanoparticles play a good role in glucose sensing performance. The superior glucose sensing performance of Fe_3O_4 nanoparticles over TiO_2 nanoparticles comes from the smaller nanoparticle size of Fe_3O_4.

Future work

The research study for future work can produce nanocomposite films from different metal oxides and combine these different metal oxides with different conducting polymers for non-enzymatic glucose biosensors.

The future work will explore the advantages of the nanomaterials in the field of glucose biosensors.

REFERENCES

Abdi M, Kassim A, Ekramul Mahmud HNM, Yunus WMM, Talib ZA. (2009). Physical, optical and electrical properties of a new conducting polymer. *Journal of Materials Science*.; 44:3682–3686.

Advani, S. G. (2007). *Processing and Poperties of Nanocomposites*: World Scientific.

Ajayan, P. M., Schadler, L. S., & Braun, P. V. (2006). *Nanocomposite Science and Technology*. John Wiley & Sons.

AL-Mokaram, A. M. A. A., Yahya, R., Abdi, M. M., & Mahmud, H. N. M. E. (2016). One-step electrochemical deposition of Polypyrrole–Chitosan–Iron oxide nanocomposite films for non-enzymatic glucose biosensor. *Materials Letters*, 183, 90-93.

Ameer, Q., & Adeloju, S. B. (2005). Polypyrrole-based electronic noses for environmental and industrial analysis. *Sensors and Actuators B: Chemical*,*106*(2), 541-552.

Ansari, R. (2006). Polypyrrole conducting electroactive polymers: synthesis and stability studies. *Journal of Chemistry, 3*(4), 186-201.

Bao, S. J., Li, C. M., Zang, J. F., Cui, X. Q., Qiao, Y., & Guo, J. (2008). New nanostructured TiO_2 for direct electrochemistry and glucose sensor applications. *Advanced Functional Materials*, *18*(4), 591-599.

Bodannes, R. S., & Chan, P. C. (1979). Ascorbic acid as a scavenger of singlet oxygen. *FEBS Letters*, *105*(2), 195-196.

Bockris, J. M., Piersma, B. J., & Gileadi, E. (1964). Anodic oxidation of cellulose and lower carbohydrates. *Electrochimica Acta*, *9*(10), 1329-1332.

Butterworth, M. D., Corradi, R., Johal, J., Lascelles, S. F., Maeda, S., & Armes, S. P. (1995). Zeta potential measurements on conducting polymer-inorganic oxide

nanocomposite particles. *Journal of Colloid and Interface Science*, *174*(2), 510-517.

Calvo, P., Remunan-Lopez, C., Vila-Jato, J. L., & Alonso, M. J. (1997). Novel hydrophilic chitosan-polyethylene oxide nanoparticles as protein carriers. *Journal of Applied Polymer Science*, *63*(1), 125-132.

Chen, A., & Chatterjee, S. (2013). Nanomaterials based electrochemical sensors for biomedical applications. *Chemical Society Reviews, 42(12)*, 5425-5438.

Chen, J., Xu, L., Xing, R., Song, J., Song, H., Liu, D., & Zhou, J. (2012). Electrospun three-dimensional porous CuO/TiO_2 hierarchical nanocomposites electrode for nonenzymatic glucose biosensing. *Electrochemistry Communications, 20*, 75-78.

Chen, J., Zhang, W. D., & Ye, J. S. (2008). Nonenzymatic electrochemical glucose sensor based on MnO 2/MWNTs nanocomposite. *Electrochemistry Communications*, *10*(9), 1268-1271.

Chen, X., Wu, G., Cai, Z., Oyama, M., & Chen, X. (2014). Advances in enzyme-free electrochemical sensors for hydrogen peroxide, glucose, and uric acid. *Microchimica Acta*, *181*(7-8), 689-705.

Cheng, F. Y., Su, C. H., Yang, Y. S., Yeh, C. S., Tsai, C. Y., Wu, C. L., ... & Shieh, D. B. (2005). Characterization of aqueous dispersions of Fe_3O_4 nanoparticles and their biomedical applications. *Biomaterials*, *26*(7), 729-738.

Clark, L. C., & Lyons, C. (1962). Electrode systems for continuous monitoring in cardiovascular surgery. *Annals of the New York Academy of Sciences*, *102*(1), 29-45.

Choi, H., Nahm, C., Kim, J., Moon, J., Nam, S., Jung, D. R., & Park, B. (2012). The effect of $TiCl_4$ - treated TiO_2 compact layer on the performance of dye-sensitized solar cell. *Current Applied Physics*, 12(3), 737-741.

Coronado, E., Galán-Mascarós, J. R., Gómez-García, C. J., & Laukhin, V. (2000). Coexistence of ferromagnetism and metallic conductivity in a molecule-based layered compound. *Nature*, *408*(6811), 447-449.

Crini, G. (2005). Recent developments in polysaccharide-based materials used as adsorbents in wastewater treatment. *Progress in Polymer Science*, *30*(1), 38-70.

Croce, F., Appetecchi, G. B., Persi, L., & Scrosati, B. (1998). Nanocomposite polymer electrolytes for lithium batteries. *Nature*, *394*(6692), 456-458.

Csoeregi, E., Schmidtke, D. W., & Heller, A. (1995). Design and optimization of a selective subcutaneously implantable glucose electrode based on" wired" glucose oxidase. *Analytical Chemistry*, *67*(7), 1240-1244.

Cui, C. X., & Kertesz, M. (1989). Two helical conformations of polythiophene, polypyrrole, and their derivatives. *Physical Review B*, *40*(14), 9661.

Cui, H. F., Ye, J. S., Zhang, W. D., Li, C. M., Luong, J. H., & Sheu, F. S. (2007). Selective and sensitive electrochemical detection of glucose in neutral solution using platinum–lead alloy nanoparticle/carbon nanotube nanocomposites. *Analytica Chimica Acta*, *594*(2), 175-183.

Cullity, B. D. and Graham, C. D. (2008). *Ferrimagnetism, in Introduction to Magnetic Materials,* Second Edition, John Wiley & Sons, Inc., Hoboken, NJ, USA.

Degani, Y., & Heller, A. (1987). Direct electrical communication between chemically modified enzymes and metal electrodes. I. Electron transfer from glucose oxidase to metal electrodes via electron relays, bound covalently to the enzyme. *Journal of Physical Chemistry*, *91*(6), 1285-1289.

Diaz, A., and Bargon, J. (1986). Electrochemical synthesis of conducting polymers. *Handbook of Conducting Polymers, 1*, 81-115.

Diaz, A., and Lacroix, J. (1988). Synthesis of electroactive/conductive polymer films: electrooxidation of heteroaromatic compounds. *New Journal of Chemistry, 12*(4), 171-180.

Diaz, A. F., Kanazawa, K. K., & Gardini, G. P. (1979). Electrochemical polymerization of pyrrole. *Journal of the Chemical Society, Chemical Communications*, (14), 635-636.

Epstein, A. J., & MacDiarmid, A. G. (1991). Novel concepts in electronic polymers: Polyaniline and its derivatives. In *Makromolekulare Chemie. Macromolecular Symposia* (Vol. 51, No. 1, pp. 217-234).

Esmaeili, C., Abdi, M. M., Mathew, A. P., Jonoobi, M., Oksman, K., & Rezayi, M. (2015). Synergy effect of nanocrystalline cellulose for the biosensing detection of glucose. *Sensors*, *15*(10), 24681-24697.

Feng, D., Wang, F., & Chen, Z. (2009). Electrochemical glucose sensor based on one-step construction of gold nanoparticle–chitosan composite film. *Sensors and Actuators B: Chemical*, *138*(2), 539-544.

Ferraris, R. P. (2001). Dietary and developmental regulation of intestinal sugar transport. *Biochemical Journal*, *360*(2), 265-276.

Fessenden, R. W., & Verma, N. C. (1978). A time-resolved electron spin resonance study of the oxidation of ascorbic acid by hydroxyl radical. *Biophysical Journal*, *24*(1), 93.

Freund, M. S., and Deore, B. (2007). *Self-doped conducting polymers*: Wiley Online Library.

Fujishima, A. (1972). Electrochemical photolysis of water at a semiconductor electrode. *Nature, 238,* 37-38.

Gailliot, M. T., Baumeister, R. F., DeWall, C. N., Maner, J. K., Plant, E. A., Tice, D. M., ... & Schmeichel, B. J. (2007). Self-control relies on glucose as a limited

energy source: willpower is more than a metaphor. *Journal of Personality and Social Psychology*, 92(2), 325.

Gailliot, M. T., & Baumeister, R. F. (2007). The physiology of willpower: Linking blood glucose to self-control. *Personality and Social Psychology Review*, 11(4), 303-327.

Gangopadhyay, R., De, A., and Ghosh, G. (2001). Polyaniline–poly (vinyl alcohol) conducting composite: material with easy processability and novel application potential. *Synthetic Metals, 123*(1), 21-31.

Gerard, M., Chaubey, A., & Malhotra, B. D. (2002). Application of conducting polymers to biosensors. *Biosensors and Bioelectronics*, *17*(5), 345-359.

George, P. M., Lyckman, A. W., LaVan, D. A., Hegde, A., Leung, Y., Avasare, R., ... & Sur, M. (2005). Fabrication and biocompatibility of polypyrrole implants suitable for neural prosthetics. *Biomaterials*, *26*(17), 3511-3519.

Ghosh, P., Siddhanta, S. K., and Chakrabarti, A. (1999). Characterization of poly (vinyl pyrrolidone) modified polyaniline prepared in stable aqueous medium. *European Polymer Journal, 35*(4), 699-710.

Gleiter, H. (1993). Nanostructured materials. In *Mechanical Properties and Deformation Behavior of Materials Having Ultra-Fine Microstructures* (pp. 3-35). Springer Netherlands.

González-Tejera, M. J., de la Blanca, E. S., & Carrillo, I. (2008). Polyfuran conducting polymers: synthesis, properties, and applications. *Synthetic Metals*, *158*(5), 165-189.

Gorski, W., & Kennedy, R. T. (1997). Electrocatalyst for non-enzymatic oxidation of glucose in neutral saline solutions. *Journal of Electroanalytical Chemistry*, *424*(1),43-48.

Gowariker, V. R., Gowariker, V. R., Viswanathan, N., and Sreedhar, J. (1986). *Polymer Science*: New Age International.

Griffiths, P. R., & De Haseth, J. A. (2007). *Fourier Transform Infrared Spectrometry*, Vol. 171. John Wiley & Sons.

Groenendaal, L., Jonas, F., Freitag, D., Pielartzik, H., & Reynolds, J. R. (2000). Poly (3,4-ethylenedioxythiophene) and its derivatives: past, present, and future. *Advanced Materials*, *12*(7), 481-494.

Guan B, Wu W, Ni, Z, Lai Y. (2009).Removal of Mn(II) and Zn(II) ions from flue gas desulfurization wastewater with water-soluble chitosan. *Separation and Purification Technology*.;65:269–274.

Guilbault, G. G., & Lubrano, G. J. (1973). An enzyme electrode for the amperometric determination of glucose. *Analytica Chimica Acta*, *64*(3), 439-455.

Gurrappa, I., & Binder, L. (2016). Electrodeposition of nanostructured coatings and their characterization-a review. *Science and Technology of Advanced Materials*.

Hadziioannou, G., and Malliaras, G. G. (2006). *Semiconducting Polymers: Chemistry,* Physics and Engineering: Wiley.

Hajji, P., David, L., Gerard, J. F., Pascault, J. P., & Vigier, G. (1999). Synthesis, structure, and morphology of polymer–silica hybrid nanocomposites based on hydroxyethyl methacrylate. *Journal of Polymer Science Part B: Polymer Physics*, *37*(22), 3172-3187.

Hatchett, D. W., & Josowicz, M. (2008). Composites of intrinsically conducting polymers as sensing nanomaterials. *Chemical Reviews, 108(2)*, 746-769.

He, Z., Gudavarthy, R. V., Koza, J. A., & Switzer, J. A. (2011). Room-temperature electrochemical reduction of epitaxial magnetite films to epitaxial iron films. *Journal of the American Chemical Society*, *133*(32), 12358-12361.

Heller, A., & Feldman, B. (2008). Electrochemical glucose sensors and their applications in diabetes management. *Chemical Reviews*, *108*(7), 2482-2505.

Henry, C. (1998). Getting under the skin: implantable glucose sensors. *Analytical Chemistry*, *70*(17), 594A-598A.

Hou, C., Xu, Q., Yin, L., & Hu, X. (2012). Metal–organic framework templated synthesis of Co_3O_4 nanoparticles for direct glucose and H_2O_2 detection. *Analyst*, *137*(24), 5803-5808.

Huang, W. S., Humphrey, B. D., & MacDiarmid, A. G. (1986). Polyaniline, a novel conducting polymer. Morphology and chemistry of its oxidation and reduction in aqueous electrolytes. *Journal of the Chemical Society, Faraday Transactions 1: Physical Chemistry in Condensed Phases*, *82*(8), 2385-2400.

Huang, L., Guo, Y., Peng, Z., & Porter, A. L. (2011). Characterising a technology development at the stage of early emerging applications: nanomaterial-enhanced biosensors. *Technology Analysis & Strategic Management*, *23*(5), 527-544.

Iroh, J. O., and Levine, K. (2002). Electrochemical synthesis of polypyrrole/polyimide conducting composite using a polyamic acid precursor. *European Polymer Journal, 38*(8), 1547-1550.

JanČa, J., Moinard, D., JanČová, E., and Gospodinova, N. (2001). Characterization of Polyaniline and Poly (m-toluidine)-based Nanoparticles of Ultranarrow Particle Size Distribution. *International Journal of Polymer Analysis and Characterization, 6*(1-2), 213-228.

Jensen, H., Soloviev, A., Li, Z., & Søgaard, E. G. (2005). XPS and FTIR investigation of the surface properties of different prepared titania nano-powders. *Applied Surface Science*, *246*(1), 239-249.

Jin, S., Cong, S. H, Xue, G., Xiong, H., Mansdorf, B., & Cheng, S. Z. (2002). Anisotropic polythiophene films with high conductivity and good mechanical

properties via a new electrochemical synthesis. *Advanced Materials*, *14*(20), 1492-1496.

Joly, C., Smaihi, M., Porcar, L., & Noble, R. D. (1999). Polyimide-silica composite materials: How does silica influence their microstructure and gas permeation properties. *Chemistry of Materials*, *11*(9), 2331-2338.

Kang, E. T., Neoh, K. G., & Tan, K. L. (1993). X-ray photoelectron spectroscopic studies of electroactive polymers. *In Polymer Characteristics* (pp. 135-190). Springer Berlin Heidelberg.

Karaca, E., Şatır, M., Kazan, S., Açıkgöz, M., Öztürk, E., Gürdağ, G., & Ulutaş, D. (2015). Synthesis, characterization and magnetic properties of Fe_3O_4 doped chitosan polymer. *Journal of Magnetism and Magnetic Materials*, *373*, 53-59.

Karyakin, A. A., Vuki, M., Lukachova, L. V., Karyakina, E. E., Orlov, A. V., Karpachova, G. P., & Wang, J. (1999). Processible polyaniline as an advanced potentiometric pH transducer. Application to biosensors. *Analytical Chemistry*, *71*(13), 2534-2540.

Kassim, A., Basar, Z. B., and Mahmud, H. N. E. (2002). Effects of preparation temperature on the conductivity of polypyrrole conducting polymer. *Journal of Chemical Sciences, 114*(2), 155-162.

Kassim A, Block H, Davis FJ, Mitchell GR. (1992). Anisotropic films of polypyrrole formed electrochemically using a non-planar dopant. *Journal of Material Chemistry*, 2:987–988.

Kaur, G., Adhikari, R., Cass, P., Bown, M., & Gunatillake, P. (2015). Electrically conductive polymers and composites for biomedical applications.*RSC Advances*, *5*(47), 37553-37567.

Kaushik, A., Khan, R., Solanki, P. R., Pandey, P., Alam, J., Ahmad, S., & Malhotra, B. D. (2008). Iron oxide nanoparticles–chitosan composite based glucose biosensor. *Biosensors and Bioelectronics*, *24*(4), 676-683.

Kiani, M. A., Tehrani, M. A., & Sayahi, H. (2014). Reusable and robust high sensitive non-enzymatic glucose sensor based on $Ni(OH)_2$ nanoparticles.*Analytica Chimica Acta*, *839*, 26-33.

Koschwanez, H. E., & Reichert, W. M. (2007). In vitro, in vivo and post explantation testing of glucose-detecting biosensors: current methods and recommendations. *Biomaterials*, *28*(25), 3687-3703.

Krajewska, B. (2004). Application of chitin-and chitosan-based materials for enzyme immobilizations: a review. *Enzyme and Microbial Technology, 35*(2), 126-139.

Kung, H. H. (1989). *Transition metal oxides: Surface Chemistry and Catalysis* (Vol. 45). Elsevier.

Kurniawan, F., Tsakova, V., & Mirsky, V. M. (2006). Gold nanoparticles in nonenzymatic electrochemical detection of sugars. *Electroanalysis*, *18*(19-20), 1937-1942.

Lawrie, G., Keen, I., Drew, B., Chandler-Temple, A., Rintoul, L., Fredericks, P., & Grøndahl, L. (2007). Interactions between alginate and chitosan biopolymers characterized using FTIR and XPS. *Biomacromolecules*, *8*(8), 2533-2541.

Lee, C., Lee, M. H., Kang, Y. K., Moon, B. S., & Rhee, S. B. (1993). The preparation of polypyrrole and polythiophene in the presence of ferrocene derivatives. *Synthetic Metals*, *55*(2), 1119-1122.

Li, S., Chen, M., He, L., Xu, F., & Zhao, G. (2009). Preparation and characterization of polypyrrole/TiO_2 nanocomposite and its photocatalytic activity under visible light irradiation. *Journal of Materials Research*, *24*(08), 2547-2554.

Li X, Wan MM, Wei Y, Shen, JZ. Chen. (2006). Electromagnetic functionalised and core shell micro/nanostructured polypyrrole composites, *Journal of Physics and Chemistry B*. 11 14623-146260.

Loeb, W. (1909). Sugar decomposition III. Electrolysis of dextrose. *Biochemische Zeitschrift Biochemistry*, 132-144.

Ma, Y., Di, J., Yan, X., Zhao, M., Lu, Z., & Tu, Y. (2009). Direct electrodeposition of gold nanoparticles on indium tin oxide surface and its application. *Biosensors and Bioelectronics*, *24*(5), 1480-1483.

MacDiarmid, A. G. (2001). "Synthetic metals": A novel role for organic polymers (Nobel lecture). *Angewandte Chemie International Edition*, *40*(14), 2581-2590.

Maclean, W., Harnly, J., Chen, J., Chevassus-Agnes, S., Gilani, G., Livesey, G., & Warwick, P. (2003). Food energy–Methods of analysis and conversion factors. In *Food and Agriculture Organization of the United Nations Technical* Workshop Report, Vol. 77.

Mahmud, H., Kassim, A., Zainal, Z., and Yunus, W. M. M. (2006). Fourier transform infrared study of polypyrrole–poly (vinyl alcohol) conducting polymer composite films: Evidence of film formation and characterization. *Journal of Applied Polymer Science, 100*(5), 4107-4113.

Maksymiuk, K. (2006). Chemical reactivity of polypyrrole and its relevance to polypyrrole based electrochemical sensors. *Electroanalysis*, *18*(16), 1537-1551.

Marie, E., Landfester, K., and Antonietti, M. (2002). Synthesis of chitosan-stabilized polymer dispersions, capsules, and chitosan grafting products via miniemulsion. *Biomacromolecules, 3*(3), 475-481.

Martinek, P. G. (1970). Quaternary ammonium compound toxicity in chicken. *Journal of American Medical Technology*, *32*, 233.

Masoomi-Godarzi, S., Khodadadi, A. A., Vesali-Naseh, M., & Mortazavi, Y. (2014). Highly stable and selective non-enzymatic glucose biosensor using carbon nanotubes decorated by Fe_3O_4 nanoparticles. *Journal of The Electrochemical Society*, *161*(1), B19-B25.

Matyjaszewski, K. (2002). General concepts and history of living radical polymerization. *Handbook of Radical Polymerization*, 361-406.

Meisner, D., Pringle, J., and Mezei, M. (1989). Liposomal ophthalmic drug delivery. III. Pharmacodynamic and biodisposition studies of atropine. *International Journal of Pharmaceutics, 55*(2), 105-113.

Merkel, T. C., Freeman, B. D., Spontak, R. J., He, Z., Pinnau, I., Meakin, P., & Hill, A. J.(2002). Ultrapermeable, reverse-selective nanocomposite membranes. *Science*, *296*(5567), 519-522.

McQuade, D. T., Pullen, A. E., & Swager, T. M. (2000). Conjugated polymer-based chemical sensors. *Chemical Reviews,* 100(7), 2537-2574.

Mitchell GR, Geri A. (1987). Molecular organisation of electrochemically prepared conducting polypyrrole films. *Journal of Physical Applied Physics*; 20:1346–1353.

Mitzi, D. B. (2001). Thin-film deposition of organic-inorganic hybrid materials.*Chemistry of Materials*, *13*(10), 3283-3298.

Mortimer, R. J., Dyer, A. L., & Reynolds, J. R. (2006). Electrochromic organic and polymeric materials for display applications. *Displays*, *27*(1), 2-18.

Muzzarelli, R. A. (1983). Chitin and its derivatives: new trends of applied research. *Carbohydrate Polymers*, *3*(1), 53-75.

Muzzarelli, R. A. (1973). Natural chelating polymers; alginic acid, chitin and chitosan. In *Natural Chelating Polymers; Alginic Acid, Chitin and Chitosan*. Pergamon Press.

Myung, Y., Jang, D. M., Cho, Y. J., Kim, H. S., Park, J., Kim, J. U., ... & Lee, C. J. (2009). Nonenzymatic amperometric glucose sensing of platinum, copper sulfide, and tin oxide nanoparticle-carbon nanotube hybrid nanostructures. *The Journal of Physical Chemistry C*, *113*(4), 1251-1259.

Nagy, L., Nagy, G., & Hajós, P. (2001). Copper electrode based amperometric detector cell for sugar and organic acid measurements. *Sensors and Actuators B: Chemical*, *76*(1), 494-499.

Nylander, C., Armgarth, M., & Lundström, I. (1983). An ammonia detector based on a conducting polymer. *International Annual Chemistry Symposium.* Vol. 17, pp. (203-207).

Noguera, C. (1996). *Physics and Chemistry at Oxide Surfaces*. Cambridge University Press.

Ohara, T. J., Rajagopalan, R., & Heller, A. (1994). " Wired" Enzyme Electrodes for Amperometric Determination of Glucose or Lactate in the Presence of Interfering Substances. *Analytical Chemistry*, *66*(15), 2451-2457.

Park, S., Boo, H., & Chung, T. D. (2006). Electrochemical non-enzymatic glucose sensors. *Analytica Chimica Acta*, *556*(1), 46-57.

Peterkofsky, B., & Prather, W. (1977). Cytotoxicity of ascorbate and other reducing agents towards cultured fibroblasts as a result of hydrogen peroxide formation. *Journal of Cellular Physiology*, *90*(1), 61-70.

Portes, E., Gardrat, C., Castellan, A., & Coma, V. (2009). Environmentally friendly films based on chitosan and tetrahydrocurcuminoid derivatives exhibiting antibacterial and antioxidative properties. *Carbohydrate Polymers*, *76*(4), 578-584.

Rahman, M. M., Ahammad, A. J., Jin, J. H., Ahn, S. J., & Lee, J. J. (2010). A comprehensive review of glucose biosensors based on nanostructured metal-oxides. *Sensors*, *10*(5), 4855-4886

Ramanavicius, A., Kausaite, A., Ramanaviciene, A., Acaite, J., & Malinauskas, A. (2006). Redox enzyme–glucose oxidase–initiated synthesis of polypyrrole. *Synthetic Metals*, *156*(5), 409-413.

Rao, A. P., Robin, A. I., & Komarneni, S. (1996). Bismuth titanate from nanocomposite and sol-gel processes. *Materials Letters*, *28*(4-6), 469-473.

Rodriguez-Mozaz, S., de Alda, M. J. L., & Barceló, D. (2006). Biosensors as useful tools for environmental analysis and monitoring. *Analytical and Bioanalytical Chemistry*, *386*(4), 1025-1041.

Roth, S., & Carroll, D. (2015). One-dimensional Metals: *Conjugated Polymers, Organic Crystals, Carbon Nanotubes and Graphene.* John Wiley & Sons.

Rinaudo, M. (2006). Chitin and chitosan: properties and applications. *Progress in Polymer Science*, *31*(7), 603-632.

Rodriguez, J. A., Liu, G., Jirsak, T., & Hrbek, C. (2002). Z.; Dvorak, J.; Maiti, A. *Journal of American Chemical Society, 124*, 5247.

Rubio-Retama, J., Hernando, J., Lopez-Ruiz, B., Härtl, A., Steinmüller, D., Stutzmann, M., ... & Antonio Garrido, J. (2006). Synthetic nanocrystalline diamond as a third-generation biosensor support. *Langmuir,* 22(13), 5837-5842.

Sadki, S., Schottland, P., Brodie, N., and Sabouraud, G. (2000). The mechanisms of pyrrole electropolymerization. *Chemical Socity Review ., 29*(5), 283-293.

Šafařík, I., & Šafaříková, M. (2002). Magnetic nanoparticles and biosciences. *In Nanostructured Materials*, 1-23, Springer Vienna,

Sangawar, V. S., & Moharil, N. A. (2012). Study of electrical, thermal and optical behavior of polypyrrole filled PVC: PMMA thin film thermoelectrets. *Chemical Science Transactions*, *1*(2), 447-455.

Sanford, P. A., & Hutchings, G. P. (1987). Chitosan--a natural, cationic biopolymer: commercial applications. *Progress in Biotechnology*.

Sanchez, C., Soler-Illia, G. D. A., Ribot, F., Lalot, T., Mayer, C. R., & Cabuil, V. (2001). Designed hybrid organic-inorganic nanocomposites from functional nanobuilding blocks. *Chemistry of Materials*, *13*(10), 3061-3083.

Sathe, A., Peck, M. A., Balasanthiran, C., Langell, M. A., Rioux, R. M., & Hoefelmeyer, J. D. (2014). X-ray photoelectron spectroscopy of transition metal ions attached to the surface of rod-shape anatase TiO_2 nanocrystals. *Inorganica Chimica Acta*, *422*, 8-13.

Saxena, V., & Malhotra, B. D. (2003). Prospects of conducting polymers in molecular electronics. *Current Applied Physics*, *3*(2), 293-305.

Scavetta, E., Guadagnini, L., Mignani, A., & Tonelli, D. (2008). Anti-Interferent Properties of Oxidized Nickel Based on Layered Double Hydroxide in Glucose Amperometric Biosensors. *Electroanalysis*, *20*(20), 2199-2204.

Schmidtke, D. W., Freeland, A. C., Heller, A., & Bonnecaze, R. T. (1998). Measurement and modeling of the transient difference between blood and subcutaneous glucose concentrations in the rat after injection of insulin. *Proceedings of the National Academy of Sciences*, *95*(1), 294-299.

Shrivastava, A., & Gupta, V. B. (2011). Methods for the determination of limit of detection and limit of quantitation of the analytical methods. *Chronicles of Young Scientists*, *2*(1), 21.

Sidorov, S. N., Volkov, I. V., Davankov, V. A., Tsyurupa, M. P., Valetsky, P. M., Bronstein, L. M., ... & Lakina, N. V. (2001). Platinum-containing hyper-cross-

linked polystyrene as a modifier-free selective catalyst for L-sorbose oxidation. *Journal of the American Chemical Society*, *123*(43), 10502-10510.

Skotheim, T. A. (Ed.). (1997). *Handbook of Conducting Polymers*. CRC press.

Song, S., Xu, H., & Fan, C. (2006). Potential diagnostic applications of biosensors: current and future directions. *International Journal of Nanomedicine*, *1*(4), 433.

Street, G., Clarke, T., Geiss, R., Lee, V., Nazzal, A., Pfluger, P., et al. (1983). Characterization of polypyrrole. *Le Journal de Physique Colloques*, *44*(C3), 3-3.

Street, G., Clarke, T., Krounbi, M., Kanazawa, K., Lee, V., Pfluger, P., et al. (1982). Preparation and characterization of neutral and oxidized polypyrrole films. *Molecular Crystals and Liquid Crystals*, *83*(1), 253-264.

Street, G., Lindsey, S., Nazzal, A., and Wynne, K. (1985). The structure and mechanical properties of polypyrrole. *Molecular Crystals and Liquid Crystals*, *118*(1), 137-148.

Subramanian, V., Karki, A., Gnanasekar, K. I., Eddy, F. P., & Rambabu, B. (2006). Nanocrystalline TiO_2 (anatase) for Li-ion batteries. *Journal of Power Sources, 159(1)*, 186-192.

Suh, J. K. F., & Matthew, H. W. (2000). Application of chitosan-based polysaccharide biomaterials in cartilage tissue engineering: a review. *Biomaterials*, *21*(24), 2589-2598.

Surareungchai, W., Deepunya, W., & Tasakorn, P. (2001). Quadruple-pulsed amperometric detection for simultaneous flow injection determination of glucose and fructose. *Analytica Chimica Acta*, *448*(1), 215-220.

Tabata, Y., & Ikada, Y. (1998). Protein release from gelatin matrices. *Advanced Drug Delivery Reviews*, *31*(3), 287-301.

Thévenot, D. R., Toth, K., Durst, R. A., & Wilson, G. S. (2001). Electrochemical biosensors: recommended definitions and classification. *Biosensors and Bioelectronics*, *16*(1), 121-131.

Tian, Y., Cuneo, M. J., Changela, A., Höcker, B., Beese, L. S., & Hellinga, H. W. (2007). Structure-based design of robust glucose biosensors using a Thermotoga maritima periplasmic glucose-binding protein. *Protein Science*, *16*(10), 2240-2250.

Timmer, B., Olthuis, W., & Van Den Berg, A. (2005). Ammonia sensors and their applications—a review. *Sensors and Actuators B: Chemical*, *107*(2), 666-677.

Toghill, K. E., & Compton, R. G. (2010). Electrochemical non-enzymatic glucose sensors: a perspective and an evaluation. *International Journal of Electrochemistry Science* ,*5*(9), 1246-1301.

Tsai, Y. C., Li, S. C., & Liao, S. W. (2006). Electrodeposition of polypyrrole-multiwalled carbon nanotube-glucose oxidase nanobiocomposite film for the detection of glucose. *Biosensors and Bioelectronics*, *22*(4), 495-500.

Valden, M., Lai, X., & Goodman, D. W. (1998). Onset of catalytic activity of gold clusters on titania with the appearance of nonmetallic properties. *Science*, *281*(5383), 1647-1650.

Vassilyev, Y. B., Khazova, O. A., & Nikolaeva, N. N. (1985). Kinetics and mechanism of glucose electrooxidation on different electrode-catalysts: Part I. Adsorption and oxidation on platinum. *Journal of Electroanalytical Chemistry and Interfacial Electrochemistry*, *196*(1), 105-125.

Vieira, D. F., & Pawlicka, A. (2010). Optimization of performances of gelatin/LiBF 4-based polymer electrolytes by plasticizing effects. *Electrochimica Acta*, *55*(4), 1489-1494.

Vincent, B., & Waterson, J. (1990). Colloidal dispersions of electrically-conducting, spherical polyaniline particles. *Journal of the Chemical Society, Chemical Communications*, (9), 683-684.

Wagner, C. D., Naumkin, A. V., Kraut-Vass, A., Allison, J. W., Powell, C. J., & Rumble Jr, J. R. (2003). *NIST X-ray Photoelectron Spectroscopy Database*, NIST Standard Reference Database 20, Version 3.4. *U. S.* Department of Commerce.

Wang, L., Rocci-Lane, M., Brazis, P., Kannewurf, C. R., Kim, Y.-I., Lee, W., et al. (2000). α-RuCl3/Polymer Nanocomposites: The First Group of Intercalative Nanocomposites with Transition Metal Halides. *Journal of the American Chemical Society, 122*(28), 6629-6640.

Wang, Y., & Jing, X. (2005). Intrinsically conducting polymers for electromagnetic interference shielding. *Polymers for Advanced Technologies*,*16*(4), 344-351.

Wang, H. L., Toppare, L., and Fernandez, J. E. (1990). Conducting polymer blends: polythiophene and polypyrrole blends with polystyrene and poly (bisphenol A carbonate). *Macromolecules, 23*(4), 1053-1059.

Wang X, Du Y, Liu H. (2004). Preparation, characterization and antimicrobial activity of chitosan–Zn complex. *Carbohydrate Polymer*.;56:21–26.

Wang, R., Hashimoto, K., Fujishima, A., Chikuni, M., Kojima, E., Kitamura, A., ... & Watanabe, T. (1997). Light-induced amphiphilic surfaces. *Nature,388,* 431-432.

Wei, H., & Wang, E. (2008). Fe_3O_4 magnetic nanoparticles as peroxidase mimetics and their applications in H_2O_2 and glucose detection. *Analytical Chemistry*, *80*(6), 2250-2254.

Welch, C. M., & Compton, R. G. (2006). The use of nanoparticles in electroanalysis: a review. *Analytical and Bioanalytical Chemistry*, *384*(3), 601-619.

Willner, I., & Willner, B. (2002). Functional nanoparticle architectures for sensoric, optoelectronic, and bioelectronic applications. *Pure and Applied Chemistry*, *74*(9), 1773-1783.

Wilson, R., & Turner, A. P. F. (1992). Glucose oxidase: an ideal enzyme. *Biosensors and Bioelectronics*, *7*(3), 165-185.

Wooten, M., Shim, J. H., & Gorski, W. (2010). Amperometric determination of glucose at conventional vs. nanostructured gold electrodes in neutral solutions. *Electroanalysis*, *22*(12), 1275-1277.

Wroblowa, H., Piersma, B. J., & Bockris, J. O. M. (1963). Studies of the mechanism of the anodic oxidation of ethylene in acid and alkaline media. *Journal of Electroanalytical Chemistry*, *6*(5), 401-416.

Wu, N. L., Wang, S. Y., & Rusakova, I. A. (1999). Inhibition of crystallite growth in the sol-gel synthesis of nanocrystalline metal oxides. *Science*,*285*(5432), 1375-1377.

Xia, L., Wei, Z., & Wan, M. (2010). Conducting polymer nanostructures and their application in biosensors. *Journal of Colloid and Interface Science*,*341*(1), 1-11.

Xiao, X., Li, H., Pan, Y., & Si, P. (2014). Non-enzymatic glucose sensors based on controllable nanoporous gold/copper oxide nanohybrids. *Talanta*,*125*, 366-371.

Xie, L., Xu, H., Niu, B., Ji, X., Chen, J., Li, Z. M., ... & Zhong, G. J. (2014). Unprecedented access to strong and ductile poly (lactic acid) by introducing in situ nanofibrillar poly (butylene succinate) for green packaging.*Biomacromolecules, 15(11),* 4054-4064.

Xiong, H. M., Wang, Z. D., Liu, D. P., Chen, J. S., Wang, Y. G., & Xia, Y. Y. (2005). Bonding polyether onto ZnO nanoparticles: an effective method for preparing polymer nanocomposites with tunable luminescence and stable conductivity. *Advanced Functional Materials*, *15*(11), 1751-1756.

Yamashita, T., & Hayes, P. (2008). Analysis of XPS spectra of Fe 2+ and Fe 3+ ions in oxide materials. *Applied Surface Science*, *254*(8), 2441-2449.

Yang, M., Yang, Y., Liu, Y., Shen, G., & Yu, R. (2006). Platinum nanoparticles-doped sol–gel/carbon nanotubes composite electrochemical sensors and biosensors. *Biosensors and Bioelectronics*, *21*(7), 1125-1131.

Yang, M., Yang, Y., Yang, H., Shen, G., & Yu, R. (2006). Layer-by-layer self-assembled multilayer films of carbon nanotubes and platinum nanoparticles with polyelectrolyte for the fabrication of biosensors. *Biomaterials*, *27*(2), 246-255.

Yang, S., Tirmizi, S. A., Burns, A., Barney, A. A., and Risen, W. M. (1989). Chitaline materials: soluble chitosan-polyaniline copolymers and their conductive doped forms. *Synthetic Metals, 32*(2), 191-200.

Yang, S., Ge, H., Hu, Y., Jiang, X., and Yang, C. (2000). Formation of positively charged poly (butyl cyanoacrylate) nanoparticles stabilized with chitosan. *Colloid & Polymer Science, 278*(4), 285-292.

Yi, Q., Yu, W., & Niu, F. (2010). Novel Nanoporous Binary AuRu Electrocatalysts for Glucose Oxidation. *Electroanalysis*, *22*(5), 556-563.

Yoon, H., & Jang, J. (2009). Conducting-polymer nanomaterials for high-performance sensor applications: issues and challenges. *Advanced Functional Materials*, *19*(10), 1567-1576.

Zakaria, M. B., Muda, M. W., & Abdullah, M. P. (Eds.). (1995). *Chitin and chitosan: the versatile environmentally friendly modern materials*. Penerbit Universiti Kebangsaan Malaysia.

Zhang, H., Zhong, X., Xu, J. J., & Chen, H. Y. (2008). Fe_3O_4/polypyrrole/Au nanocomposites with core/shell/shell structure: synthesis, characterization, and their electrochemical properties. *Langmuir*, *24*(23), 13748-13752.

Zhang, J., Ma, J., Zhang, S., Wang, W., & Chen, Z. (2015). A highly sensitive nonenzymatic glucose sensor based on CuO nanoparticles decorated carbon spheres. *Sensors and Actuators B: Chemical*, *211*, 385-391.

Zhitomirsky, I. (2006). Electrophoretic deposition of organic-inorganic nanocomposites. *Journal of Materials Science*, *41*(24), 8186-8195.

http://www.geocities.jp/ohba_lab_ob_page/structure6.html

LIST OF PUBLICATIONS AND PAPERS PRESENTED

- Ali M. A. Abdul Amir AL-Mokaram, RosiyahYahya, Mahnaz M.Abdi, Habibun Nabi Muhammad Ekramul Mahmud. One-step electrochemical deposition of Polypyrrole–Chitosan–Iron oxide nanocomposite films for non-enzymatic glucose biosensor. *Materials Letters* 183 (2016) 90–93.